NASA CR- 143711

BOEING

[redacted]

(NASA-CR-143711) RADIATION AND SHIELDING STUDY FOR THE INTERNATIONAL ULTRAVIOLET EXPLORER Final Report (Boeing Aerospace Co., Seattle, Wash.) 153 p HC $6.25 CSCL 22B G3/15

N75-21329

Unclas 18628

REV LTR

THE BOEING COMPANY

CODE IDENT. NO. 81205

NUMBER D180-18486-1

TITLE: Radiation and Shielding Study for The International Ultraviolet Explorer: Final Report

ORIGINAL RELEASE DATE 11/8/74 FOR THE RELEASE DATE OF SUBSEQUENT REVISIONS, SEE THE REVISIONS SHEET. FOR LIMITATIONS IMPOSED ON THE DISTRIBUTION AND USE OF INFORMATION CONTAINED IN THIS DOCUMENT, SEE THE LIMITATIONS SHEET.

MODEL

ISSUE NO.

ISSUE TO

PREPARED UNDER:

☐ CONTRACT NO. NAS5-20038

☐ IR&D

☐ OTHER

PREPARED BY Paul R Measel
P. R. Measel

SUPERVISED BY K.D. Friddell
K.D. Friddell

APPROVED BY P.A. Gomes
P.A. Gomes

APPROVED BY

SHEET

FINAL REPORT
RADIATION AND SHIELDING STUDY FOR THE INTERNATIONAL ULTRAVIOLET EXPLORER (IUE)

D180-18486-1

OCTOBER 1974

FOR

NATIONAL AERONAUTICS AND SPACE ADMINISTRATION
GODDARD SPACE FLIGHT CENTER
GREENBELT, MARYLAND

FROM

THE BOEING AEROSPACE COMPANY
BALLISTICS MISSILE DIVISION
SEATTLE, WASHINGTON

1. Report No.	2. Government Accession No.	3. Recipient's Catalog No.
D180-18486-1		

4. Title and Subtitle	5. Report Date
Radiation and Shielding Study for the International Ultraviolet Explorer Final Report	October 1974
	6. Performing Organization Code
7. Author(s) M. Baze, R. H. Firminhac, W. E. Horne R. C. Kennedy, P. R. Measel, L.L. Sivo, M.C. Wilkinson	8. Performing Organization Report No.
9. Performing Organization Name and Address The Boeing Aerospace Co. P. O. Box 3999 Seattle, Washington 98124	10. Work Unit No.
	11. Contract or Grant No.
	13. Type of Report and Period Covered
12. Sponsoring Agency Name and Address National Aeronautics and Space Administration Goddard Space Flight Center Greenbelt Road Greenbelt, Maryland 20771	14. Sponsoring Agency Code

15. Supplementary Notes

16. Abstract

The Radiation and Shielding Study for the IUE provides technical advisory services to ensure integrity of parts and material exposed to energetic particle radiation for the IUE scientific instruments, spacecraft, and subsystems.

A significant potential for interference, degradation, or failure for unprotected or sensitive items was found. Vulnerable items were identified, and appropriate tests, changes, and shields were defined.

17. Key Words (Selected by Author(s))		18. Distribution Statement
electron	radiation	
interface	satellite	
material	semiconductor	
optics	shielding	
proton		

19. Security Classif. (of this report)	20. Security Classif. (of this page)	21. No. of Pages	
uncl.	uncl.	152	

CONTENTS

LIST OF FIGURES

LIST OF TABLES

1.0 INTRODUCTION

The natural-radiation environment for the IUE orbit is sufficiently severe to cause a significant possibility of interference, degradation, or failure for unprotected or sensitive items. Consequently, the Radiation and Shielding Study for the IUE was performed to provide technical advisory services to ensure integrity of parts and material exposed to energetic particle radiation for the IUE scientific instruments, spacecraft, and subsystems.

1.1 IUE SPACECRAFT, MISSION, AND ORBIT

The International Ultraviolet Explorer is intended to fill the need for an ultraviolet astronomical observatory for use primarily as a national and international research facility (Reference 1). Its general characteristics are:

- Delta Launch
- 45-cm UV telescope with echelle spectrograph
- Three-to-five-year lifetime
- Eccentric synchronous orbit
- Three-axis control with one-arc-sec pointing
- International guest observer facility

The scientific aims of the IUE are as follows:

- To obtain high-resolution spectra of stars of all spectral types in order to determine more precisely the physical characteristics of these stars.

- To study gas streams in and around some binary systems.

1.1 (Continued)

- To observe at low-resolution faint stars, galaxies, and quasars, and to interpret these spectra by reference to high-resolution spectra.

- To observe the spectra of planets and comets as these objects become accessible.

- To make repeated observations of objects which show variable spectra.

- To define more precisely the modifications of starlight caused by interstellar dust and gas.

The IUE spacecraft is made up of the following subsystems:

- Mechanical subsystems
- Communications subsystem
- Command subsystem
- Data-handling subsystem
- Power subsystem
- Stabilization and controls subsystem
- Scientific instrument subsystem

The basic configuration of the spacecraft is shown in Figure 1-1. Most of the electrical subsystems are mounted on the main platform and upper platform. The scientific instrument subsystem includes the spectrograph, telescope and the experimental electronics. Some characteristics of the scientific instrument are shown in Table 1-1. A view of the spectrograph assembly is shown in Figure 1-2. The locations of the various cameras are shown in Figure 1-3.

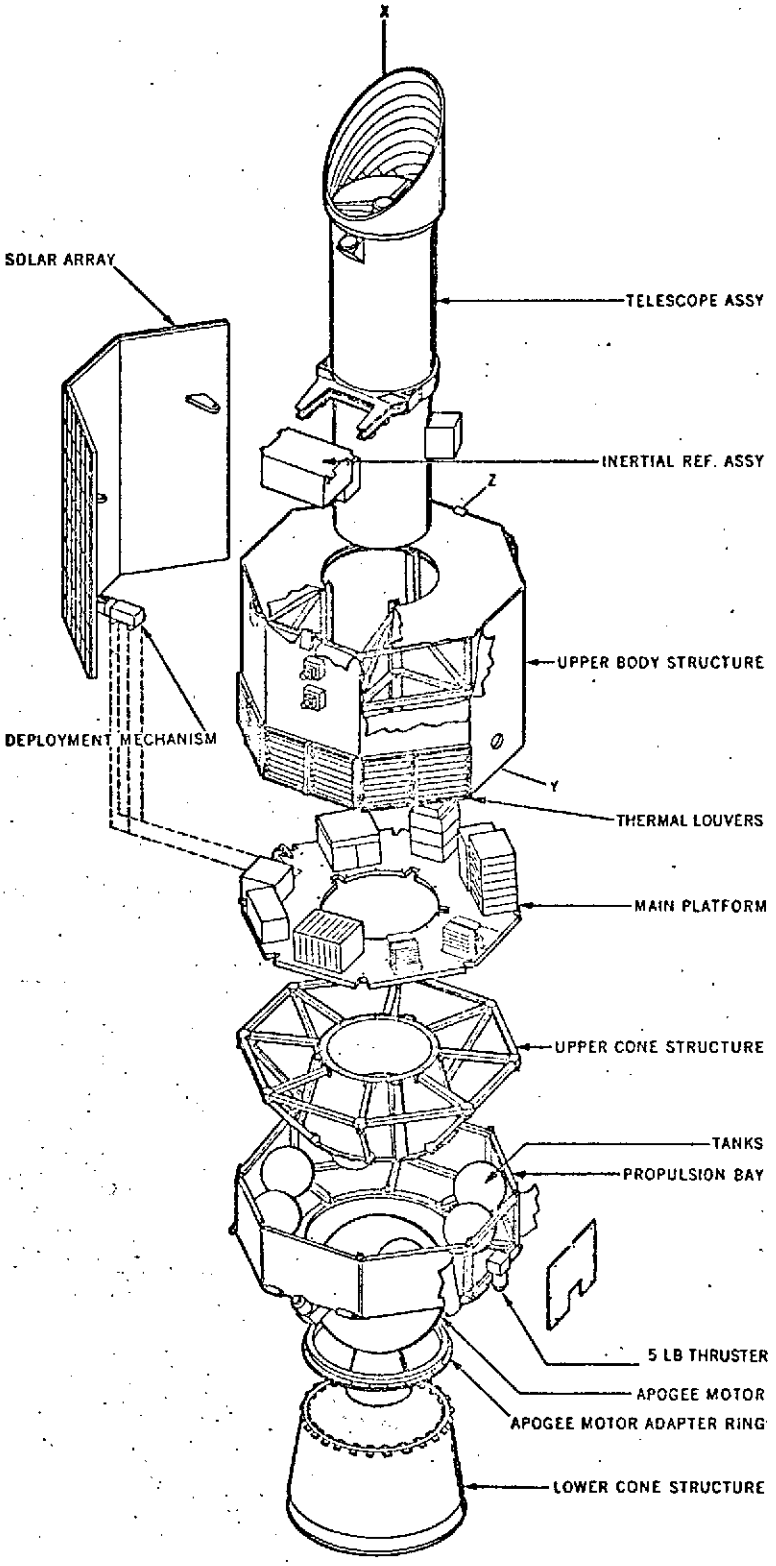

FIGURE 1-1 IUE EXPLODED VIEW

TABLE 1-1 IUE SCIENTIFIC INSTRUMENT

TELESCOPE		
Type	Ritchey Chretien	
Aperture	45 cm	
Focal Ratio	F/15	
Image Quality	1 arc-sec	
Acquisition Field	10 arc-min diameter	
SPECTROGRAPHS		
Type	Echelle	
Detector	Proximity focussed converter plus SEC vidicon camera	
	Camera 1	Camera 2
Entrance Apertures	3 & 10 arc-sec	3 & 10 arc-sec
High Dispersion		
• Wavelength range	1180-1990Å	1860-3005Å
• Resolving power	10^4	1.5×10^4
• Limiting magnitude*	7	7
Low Dispersion		
• Wavelength range	1120-2160Å	1750-3250Å
• Resolution	6Å	6Å
• Limiting magnitude*	12	12

*Limiting magnitudes estimated for 30 minutes exposure on a BOV star.

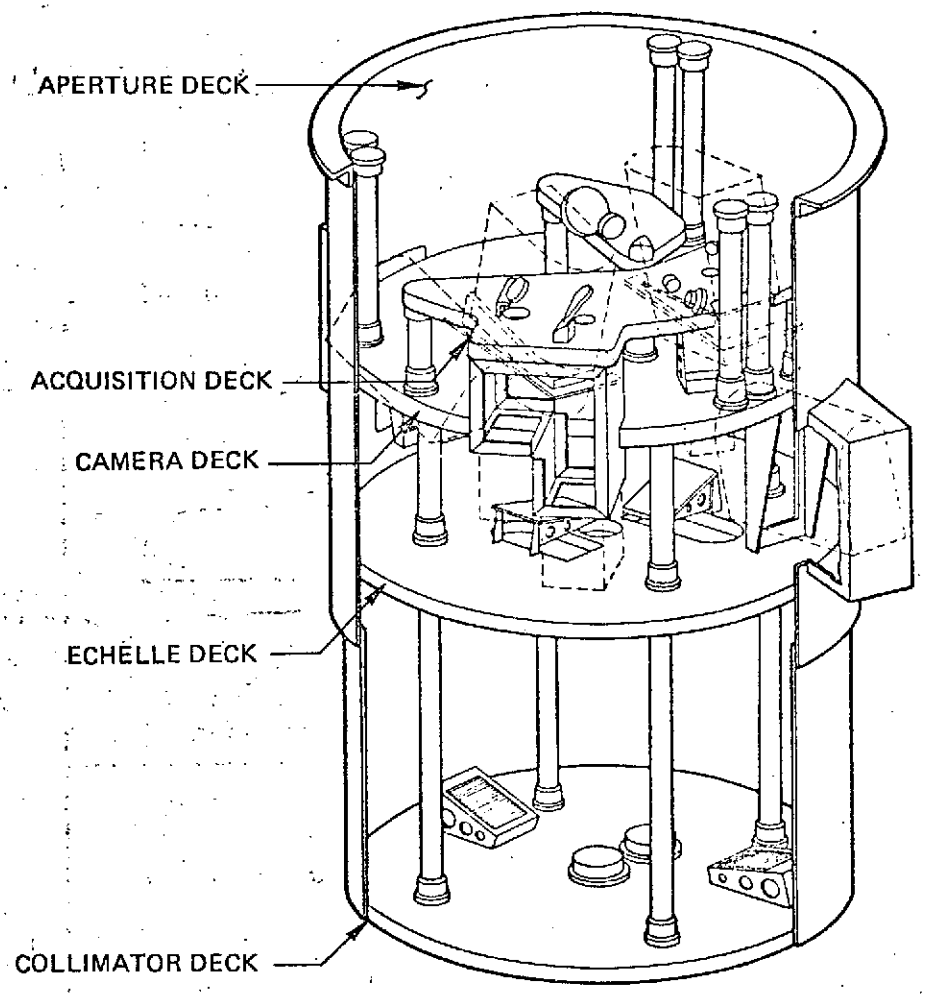

FIGURE 1-2 CUTAWAY VIEW OF SPECTROGRAPH ASSEMBLY (CAMERAS SHOWN BY DOTTED LINES)

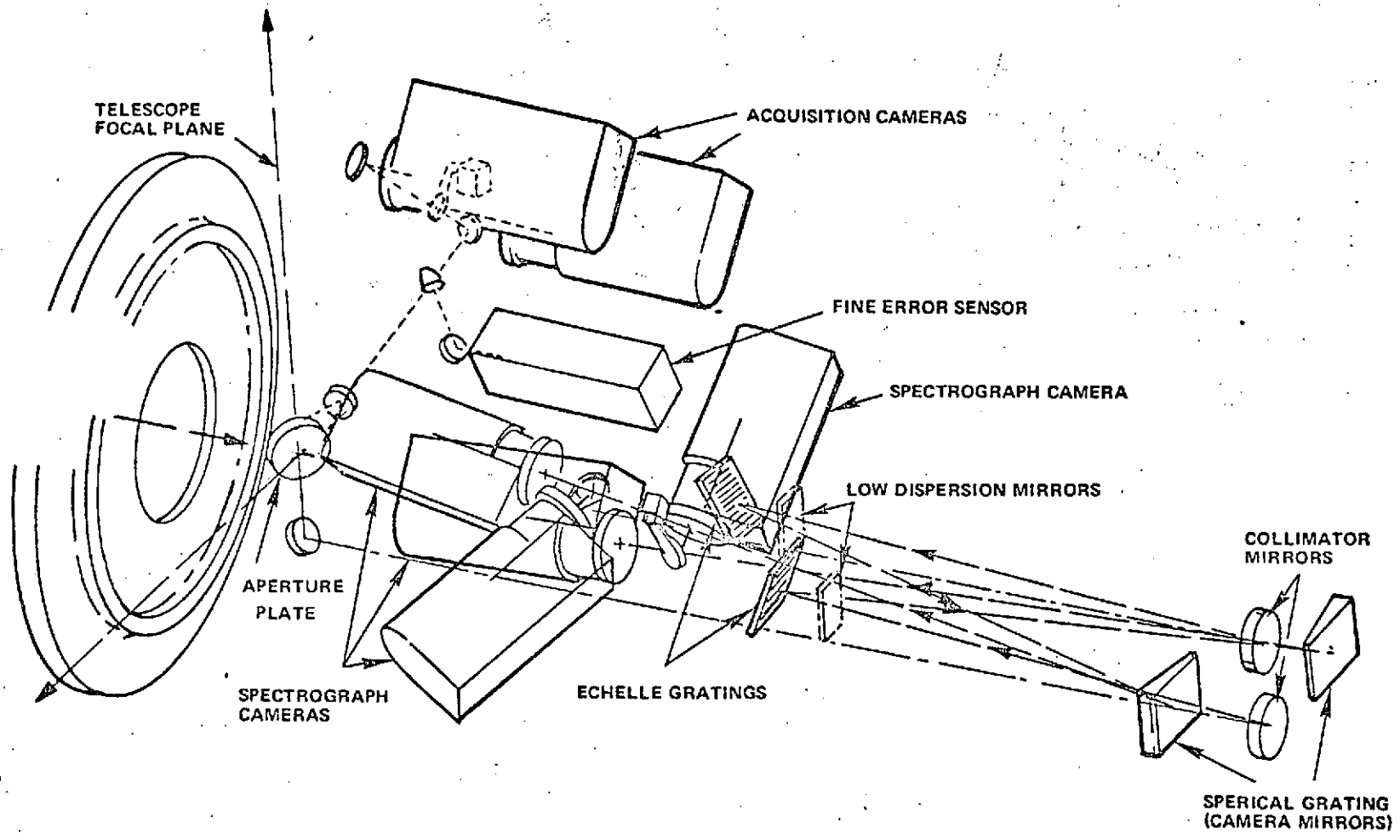

FIGURE 1-3 IUE SPECTROGRAPHS MAJOR COMPONENT LAYOUT

1.1 (Continued)

The figures discussed above are not revised to show the design changes; however, they illustrate the general spacecraft configuration.

An eccentric synchronous orbit was chosen for the IUE (Reference 2). This orbit provides a weight advantage of 62 pounds over the fully circularized inclined synchronous orbit to permit a spacecraft weight of 809 pounds. Parameters of this orbit are given in Table 1-2.

A comparison of the earth's magnetic flux lines in relationship to the eccentric orbit and a circular orbit is shown in Figure 1-4. The magnetic L-shells relate to the trapped particle radiation intensity.

TABLE 1-2 NOMINAL ESO PARAMETERS (MISSION ORBIT)

APOGEE HEIGHT, h_a	= 45,600 km (24,625 nmi)
PERIGEE HEIGHT, h_p	= 25,970 km (14,025 nmi)
SEMI-MAJOR AXIS, a	= 42,164 km
ECCENTRICITY, e	= 0.233
INCLINATION, i	= 28.7 DEGREES
PERIOD, T	= 23,93 HOURS
NODE	= DEPENDS ON MISSION CONSTRAINTS
ARGUMENT OF PERIGEE	= DEPENDS ON MISSION CONSTRAINTS
NODAL REGRESSION	= -4.8 DEGREES PER YEAR
ARGUMENT OF PERIGEE RATE	= +7.8 DEGREES PER YEAR
GROUND TRACK (TENTATIVE)	= TEARDROP SHAPED, TILTED TOWARD NORTHWEST; NORTH-BOUND EQUATOR CROSSING AT +47°W, SOUTH-BOUND AT +88°W

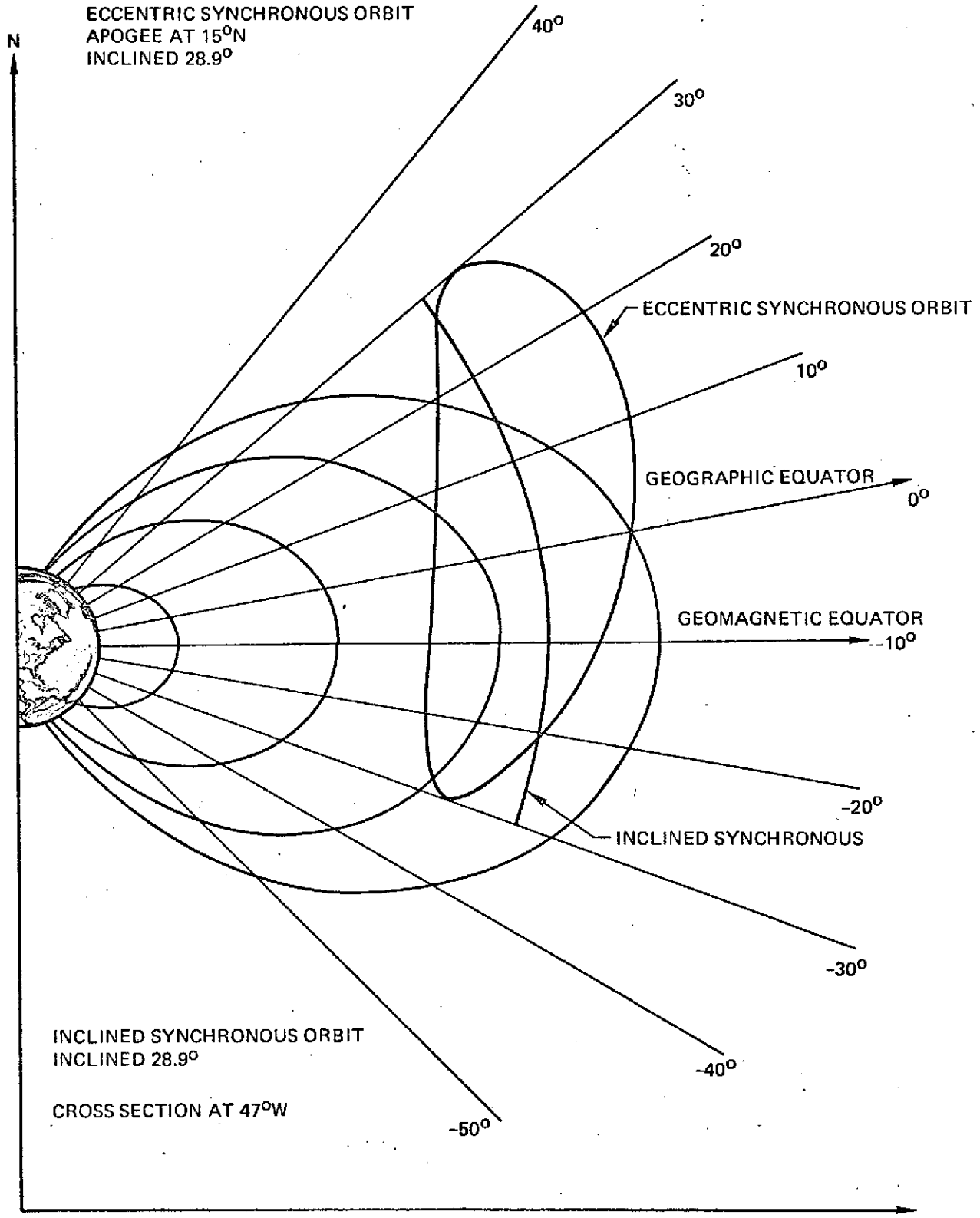

FIGURE 1-4 IUE ORBITS IN GEOGRAPHIC AND GEOMAGNETIC COORDINATES

1.2 RADIATION ANALYSIS METHOD

The tasks in the IUE Radiation and Shielding Study were to:

- Provide radiation degradation assessment on all parts and materials and advise on their acceptability for the IUE mission.
- Identify those critical parts and materials requiring radiation testing and provide test plans and parameters.
- Conduct shielding surveys of scientific instruments, spacecraft, and subsystems design configurations and advise on shielding requirements for radiation-sensitive parts and materials.
- Provide on-call quick advice over entire 18-month term of the contract.

Additional effort was expended to perform a detailed shielding analysis to determine and justify shielding-material thickness requirements for each side of every subsystem component or component stack. Data from previous satellite experience also was analyzed to provide baseline data for particularly sensitive IUE parts.

The salient features of the radiation analysis were:

- Evaluation of IUE environment
- Evaluation of material and piece-part degradation
- Evaluation of optical sensor degradation and interference rates

1.2 (Continued)

- o Application of results of these evaluations to the prediction of the IUE spacecraft system performance degradation, preparation of test requirements, and determination of shielding requirements

Inputs used for this study program were the spacecraft description, design information, and trajectory definition. The following tasks were performed: radiation environment levels were defined in terms suitable for vulnerability analysis; screening was performed to identify those materials and components that are not significantly degraded by the radiation environment; the remaining materials and components were analyzed in greater detail. The performance of detailed circuit analysis was not within the scope of this program.

The task of determining the necessary data for the probably degraded parts and materials included selection of appropriate test data from existing test results; determination of degradation or failure thresholds from test data and damage equations; estimation of degradation to the extent possible for types of parts and materials having no test data; and definition, in cooperation with Goddard, of relevant system-related failure criteria.

The cases for which test data were inadequate were identified and tests proposed.

The classes of items receiving analysis emphasis because of their expected radiation sensitivity were semiconductor devices, optical sensors, and materials. The IUE semiconductors were organized by subsystem and component into categories and problem areas associated with each category were identified. Optical sensors were analyzed for

1.2 (Continued)

degradation of critical elements and interference. The spacecraft construction materials were classified by generic failure thresholds and the application and general location of the materials were examined to facilitate identification of the possibility of problem areas.

Failure thresholds for the various generic categories of piece parts and materials were used as a basis for establishing permissible internal-environment levels for the associated spacecraft component. Potential exceptions to the categorization were defined to the extent possible, and appropriate recommendations were made. The existing shielding was determined, and the additional shielding to provide the required internal environment was calculated.

2.0 RADIATION ENVIRONMENT

Energetic electrons and protons of the earth's radiation belts, and solar protons comprise the penetrating radiation environment of principal concern for the IUE spacecraft. Solar ultraviolet radiation, in conjunction with solar x-ray activity increases total ionization, but is of concern only for spacecraft surface effects.

The intensity and energy of trapped protons and electrons are described in a series of publications by J. I. Vette and Co-workers (Reference 3). Solar and galactic cosmic ray intensities and particle types to be expected during the IUE mission are estimated in Reference 4, 5, and 6. The solar UV and x-ray intensity are given in Reference 7. The actual particle flux and fluence incident on the spacecraft depends on the trajectory of the spacecraft in the earth's magnetic field. An estimate of these environments is obtained by the use of several computer code systems (Reference 8 and 9). The penetrating energy spectra, energy deposition, and displacement profiles in materials are then calculated by appropriate radiation transport codes for the incident particles. This calculation procedure is described in the following section.

2.1 RADIATION ENVIRONMENTAL CALCULATION METHODS

The two orbits examined in this study were a circular, synchronous altitude mission inclined at 28.7^{o} with a parking longitude of $47^{o}W$, and an eccentric synchronous orbit with a perigee of 25,970 km, apogee of 45,600 km, inclination of 28.7^{o}, initial perigee at -15^{o} longitude, and an geographic equatorial crossing point of $47^{o}W$. These trajectory parameters are then combined with the trapped radiation models in computer code systems which evaluate the flux and fluence

2.1 (Continued)

of particles incident on the spacecraft during the mission. Stassinopoulous (Reference 9) has used the Goddard Space Flight Center computer system UNIFLUX to analyze the circular inclined synchronous orbit and an orbit similar to the eccentric synchronous orbit in some detail. This study used his results, where possible and the Boeing SPARES computer to evaluate the differences between the eccentric synchronous orbits studied by Stassinopoulous and the current IUE eccentric synchronous orbit. Peak flux values per orbit were obtained from trajectory analysis results of UNIFLUX and SPARES, and AE-4 electron model environment. The long-term average integral electron energy spectra for the inclined circular and eccentric synchronous orbits are shown in Figure 2-1. Also shown is the long-term average integral spectrum encountered at the spacecraft deepest penetration in the earth's magnetic field on the eccentric synchronous orbit, which is near L = 5.0 at the geomagnetic equator. Long-term averaged orbit-integrated flux values are used for the mission total electron dose calculations, while appropriate fluxes at each point along the orbit are used for interference calculations. As the actual electron flux at any point along the IUE trajectory is strongly time dependent, varying with both local time and solar activity, the 90% flux values taken from the AE-4 model environment were used. This means that 90% of the time the interference will be less than calculated. Similar considerations hold for trapped proton fluxes but their energy is low enough to result only in near surface ionization dose.

Radiation transport calculations required to describe electron and proton penetration characteristics are done with codes from the SPARES system, the electron Monte Carlo code ELMCD and the proton

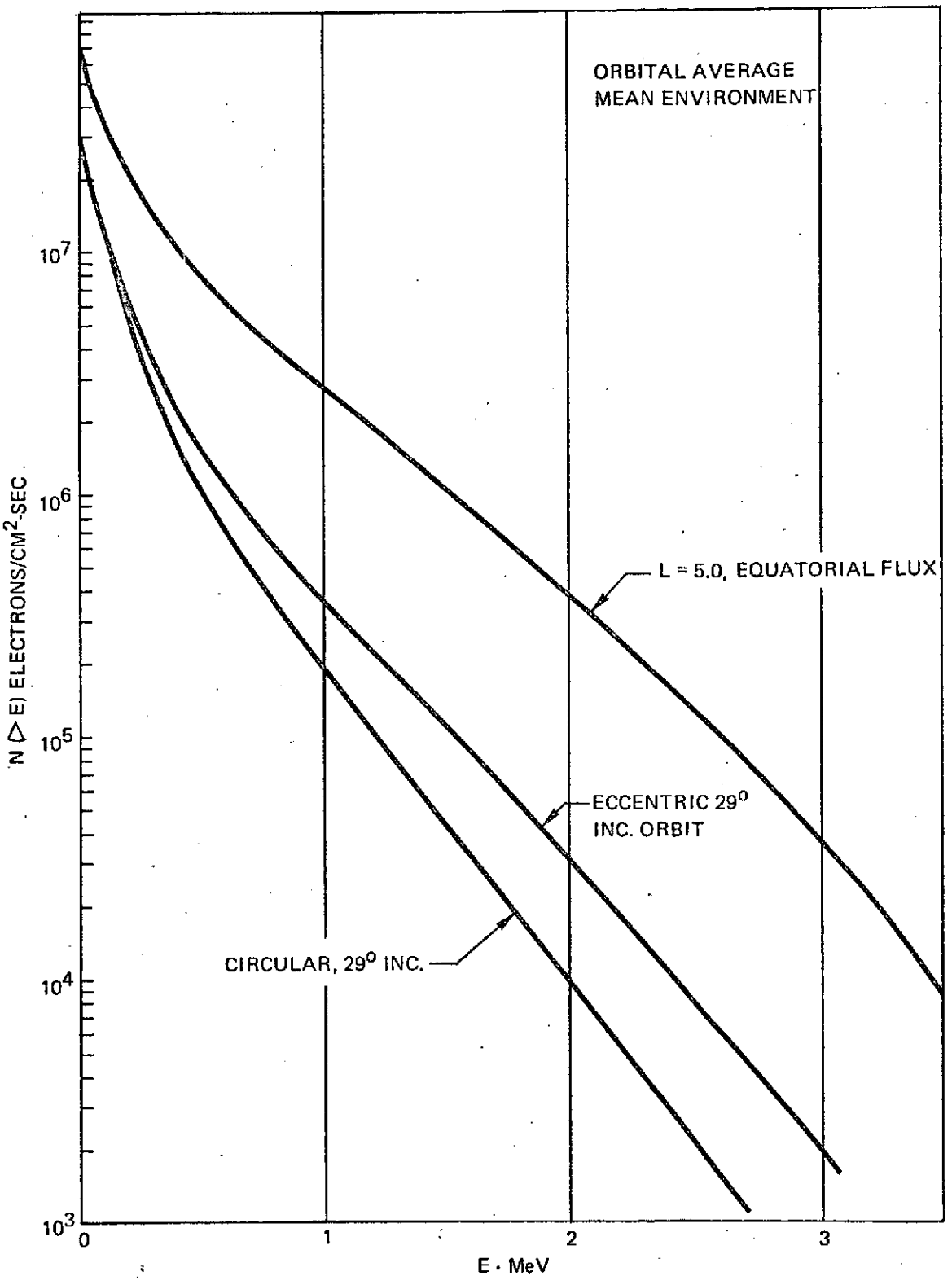

FIGURE 2-1 ELECTRON FLUX AT SYNCHRONOUS, ECCENTRIC SYNCHRONOUS AND L = 5.0 EQUATORIAL

2.1 (Continued)

penetration code HEVPEN. The calculational methods used in these codes are discussed in detail in Reference 8. Basically, the incident electron or proton differential energy spectrum is transformed into the energy and angle dependent flux at various depths in the shield material. The penetrating spectrum can then be used to calculate absorbed dose, displacement damage, or any other energy-dependent parameter of interest.

2.2 TRAPPED PARTICLE ENVIRONMENT

2.2.1 Electron Dose

The yearly electron dose behind aluminum or magnesium shields of various thickness has been calculated by ELMCD for the circular and eccentric synchronous orbits. The ESO curve is shown in Figure 2-2. The spherical value is the dose calculated at the center of a sphere of the indicated thickness, while the slab value is the dose under a slab of the indicated thickness, with the incident flux taken as isotropic in the half space. Calculations are made using 1000 incident electron histories sampled from the appropriate energy spectrum with a uniform distribution, and the curves given are smoothed from the Monte Carlo results. These yearly doses are calculated from the long-term average flux, and the actual dose rate at any time depends on the orbital position of the satellite, the local time, and the previous level of solar activity and resulting trapped electron flux variations.

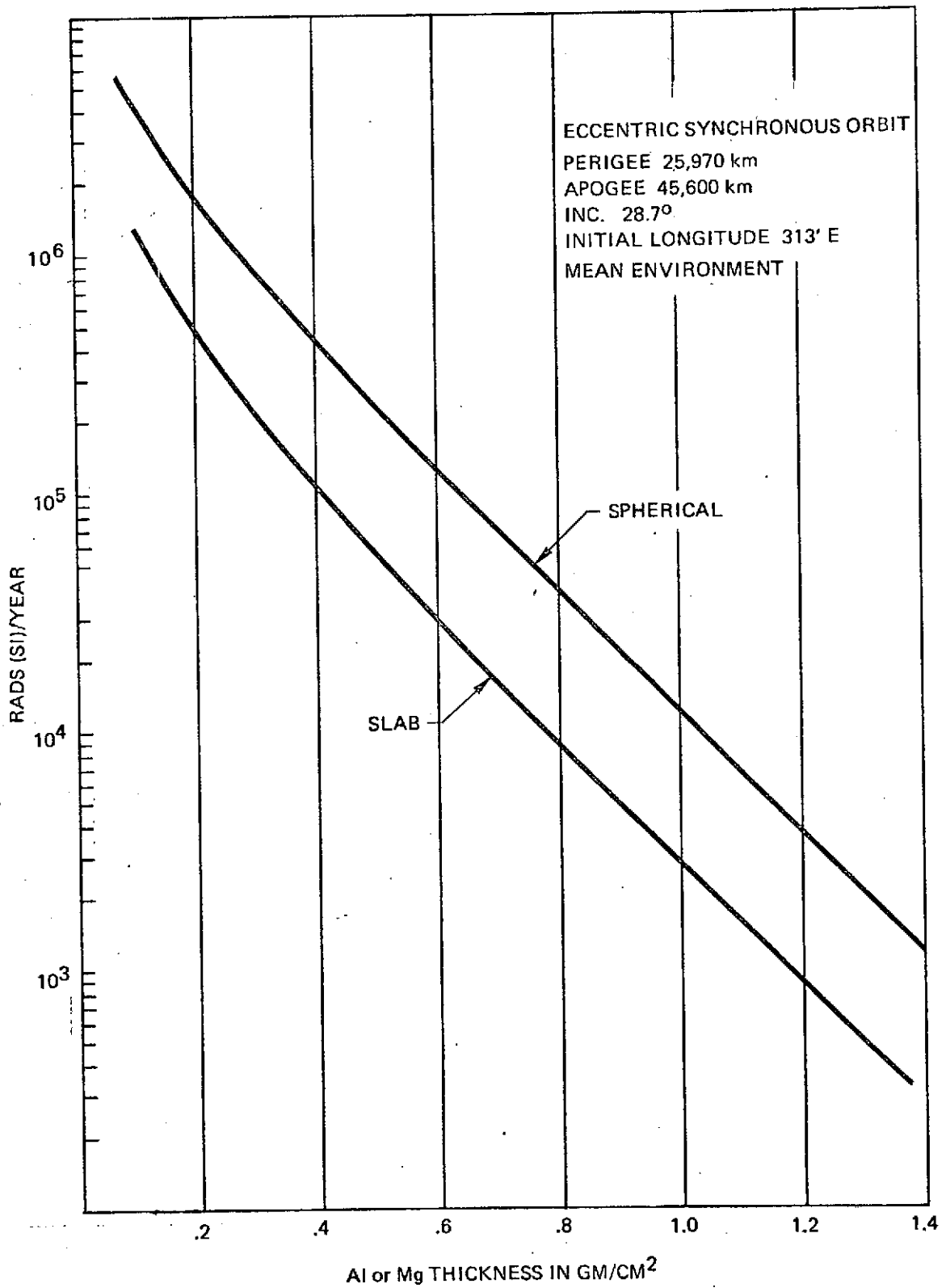

FIGURE 2-2 TRAPPED ELECTRON YEARLY DOSE, ECCENTRIC SYNCHRONOUS ORBIT

2.2.2 Electron Flux

Electron penetration calculations were required for the evaluation of interference levels in the cameras and fine error sensor. For these calculations the ELMCD code was used to determine the penetrating number and energy spectrum of the electrons through MgF_2 and mu metal, as well as the backscattered spectrum from SiO_2. These results are shown in Figures 2-3 through 2-6. For these calculations it was necessary to account for the change in intensity and spectral shape as a function of orbital position.

2.2.3 Trapped Protons

The trapped protons are of such low energy in the circular or eccentric synchronous orbits that their dose contribution is of concern only for spacecraft surface effects. Figure 2-7 shows the dose contributions from trapped proton, trapped electron, solar UV and X-rays in thin layers of material. These values are of interest for materials effects.

2.3 SOLAR PROTON ENVIRONMENT

2.3.1 Solar Proton Criteria

The annual solar proton environment anticipated during the maximum of the next solar cycle, Cycle 21, is given in Reference 6.

Considering the length of the IUE mission, 3 to 5 years, and considering the possibility of a large solar proton event, such as the August 1972 event, it is appropriate that a solar proton environment of 10 times the annual mean environment be used so that this

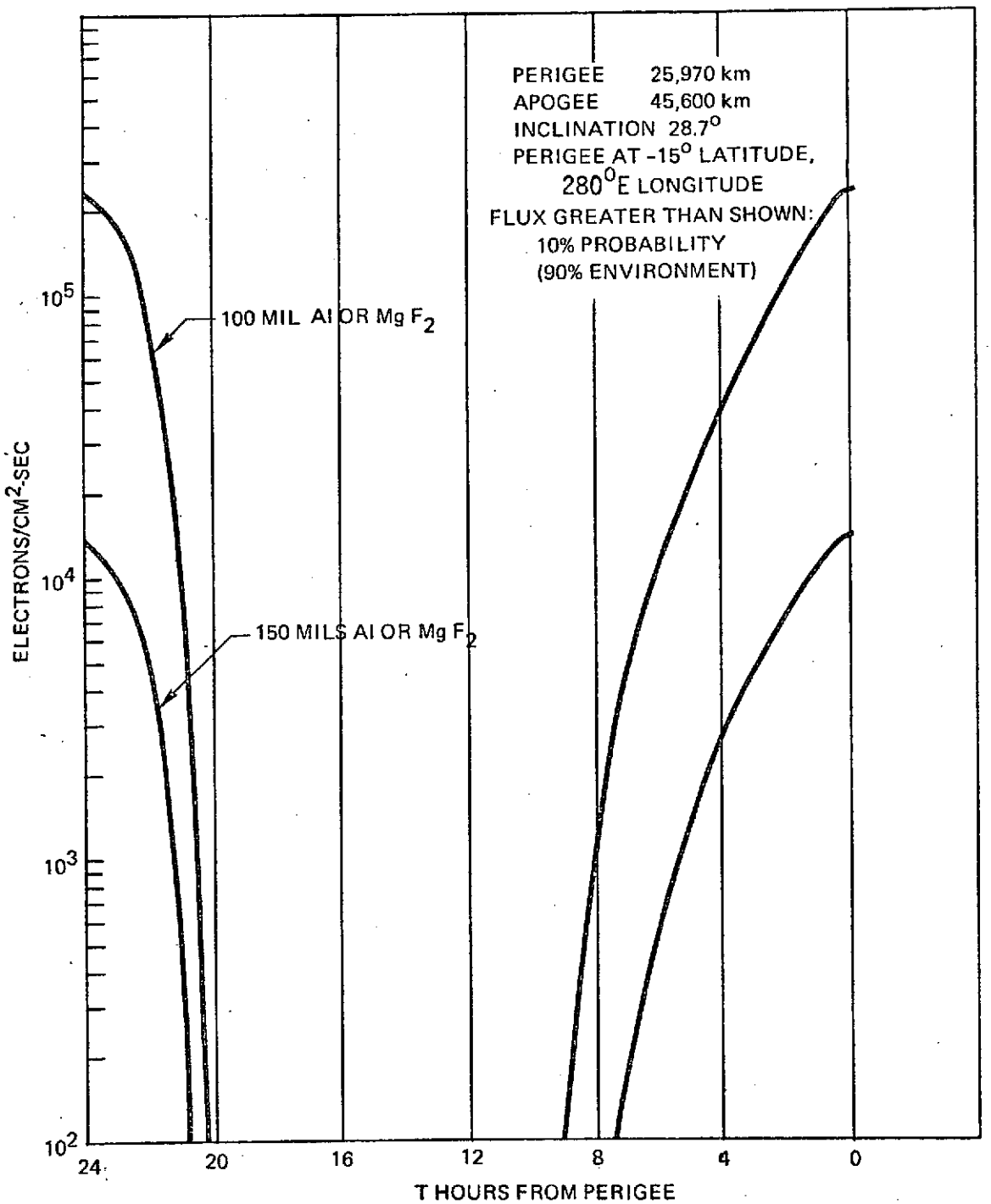

FIGURE 2-3 MgF_2 WINDOW PENETRATION RATE, ECCENTRIC SYNCHRONOUS ORBIT

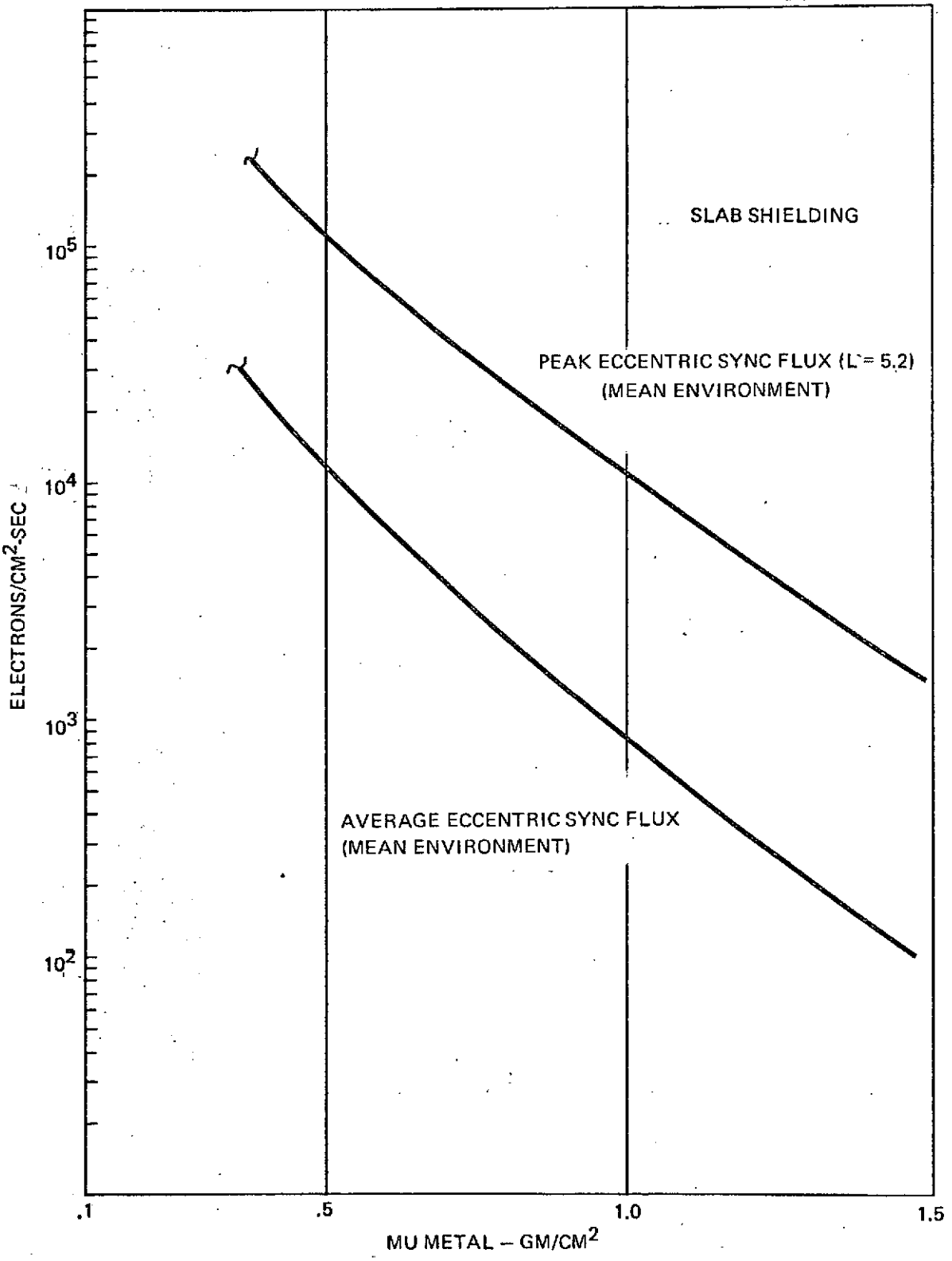

FIGURE 2-4 AVERAGE AND PEAK PENETRATION RATES

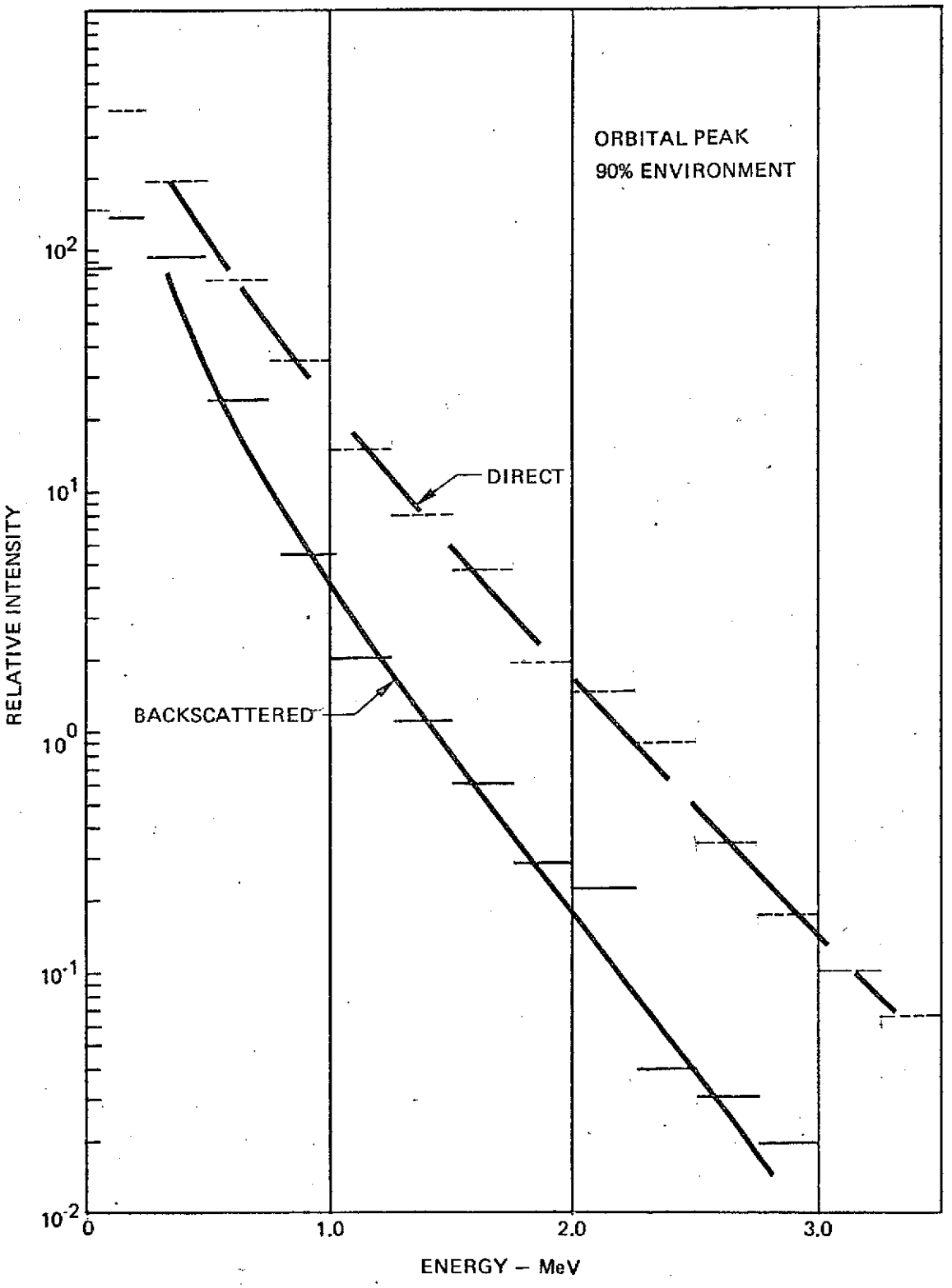

FIGURE 2-5 DIRECT AND BACKSCATTERED ELECTRON SPECTRUM FROM SiO_2 ECCENTRIC SYNCHRONOUS SPECTRUM

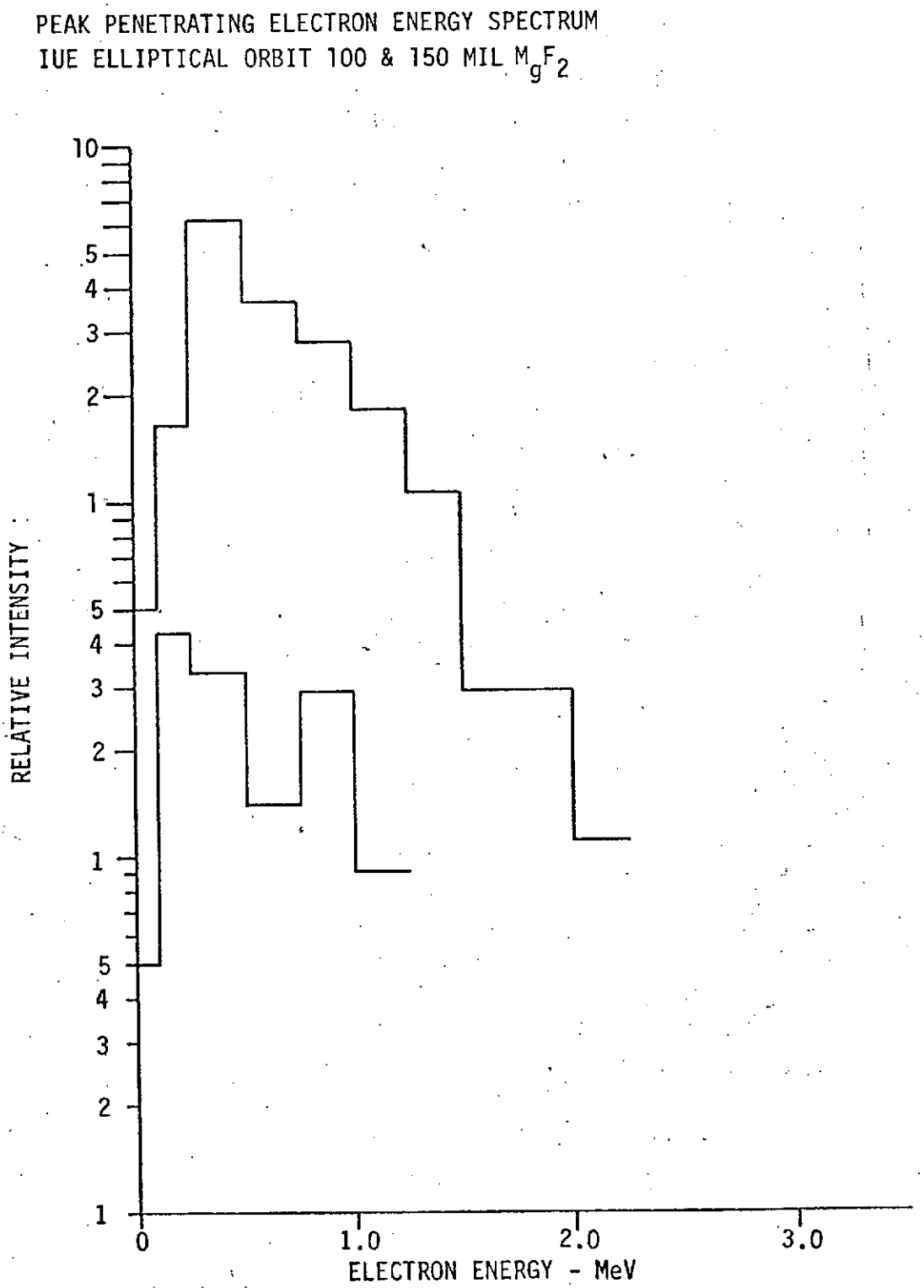

FIGURE 2-6 PEAK PENETRATING ELECTRON ENERGY SPECTRUM

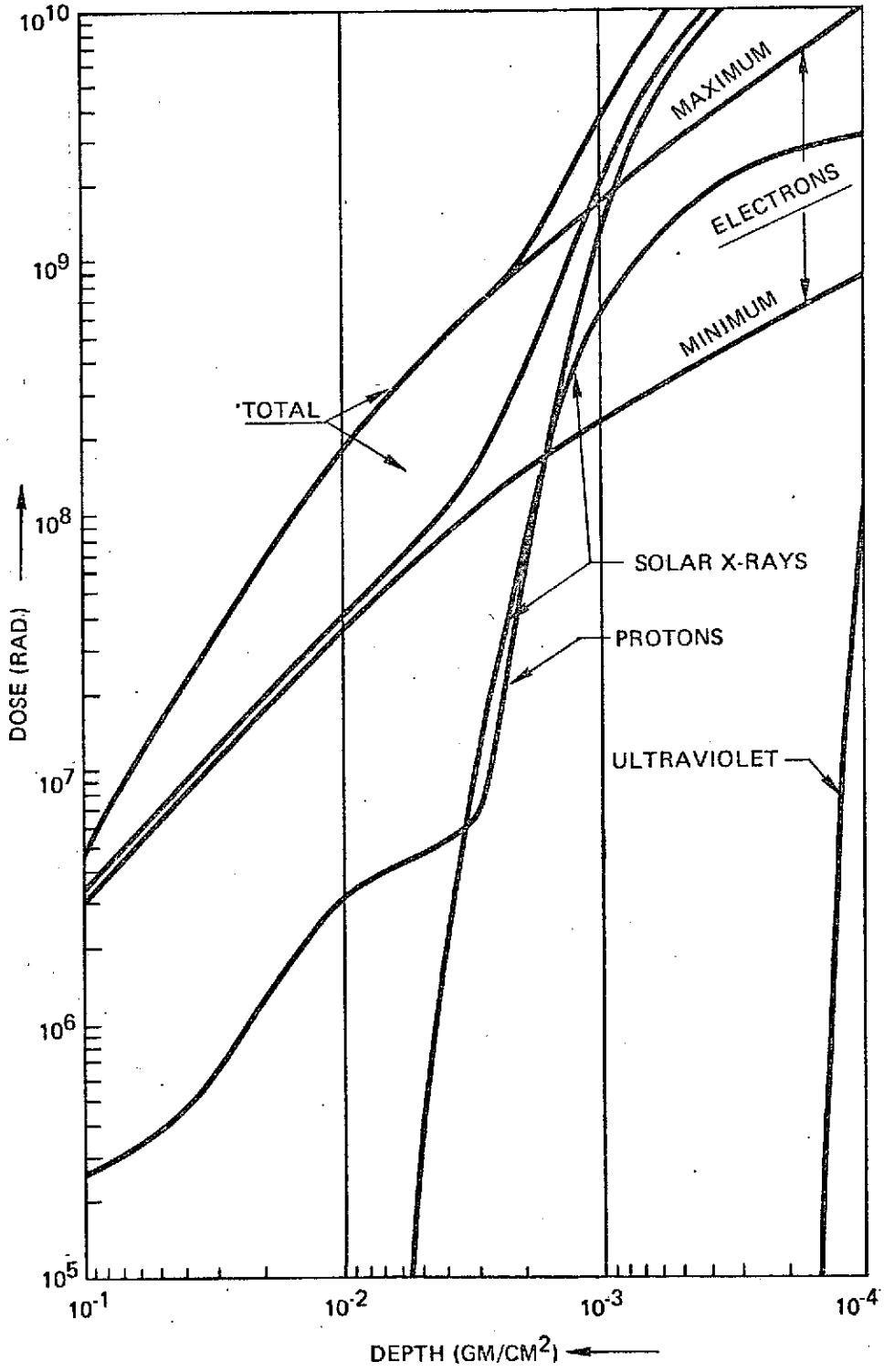

FIGURE 2-7 DOSE DEPTH PROFILE IN CARBON-EPOXY DURING TWO YEAR GEOSTATIONARY MISSIONS

2.3.1 (Continued)

environment will result in approximately 95% confidence for not exceeding the solar proton criteria during a 3-year mission, using the prediction method of J. King (Reference 4) for the flux greater than 30 MeV.

2.3.2 Solar Proton Damage Evaluation

The absorbed dose and displacement damage from the annual and criteria solar proton spectra are calculated by the use of the proton transport code HEVPEN. Figures 2-8 and 2-9 show dose and displacement values for aluminum spherical and slab shielding. The absorbed dose is given for a silicon absorber, while the 20 MeV equivalent proton fluence is calculated by a product integration of the penetrating proton energy spectrum and the energy dependent displacement cross section, and then presenting the displacement damage in terms of a 20 MeV proton fluence. The displacement cross section used was taken from the work of Baicker (Reference 10).

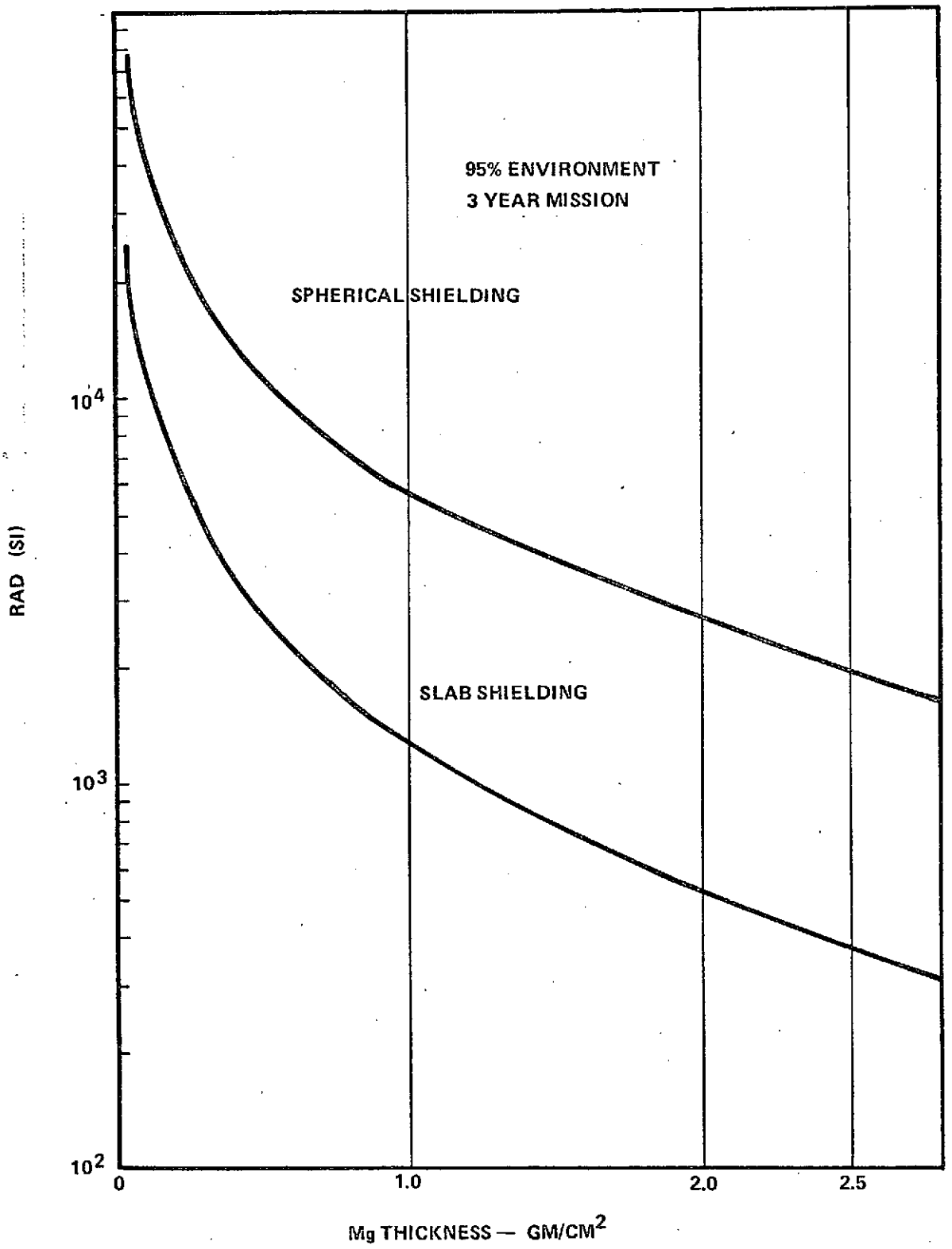

FIGURE 2-8 SOLAR PROTON DOSE (MISSION)

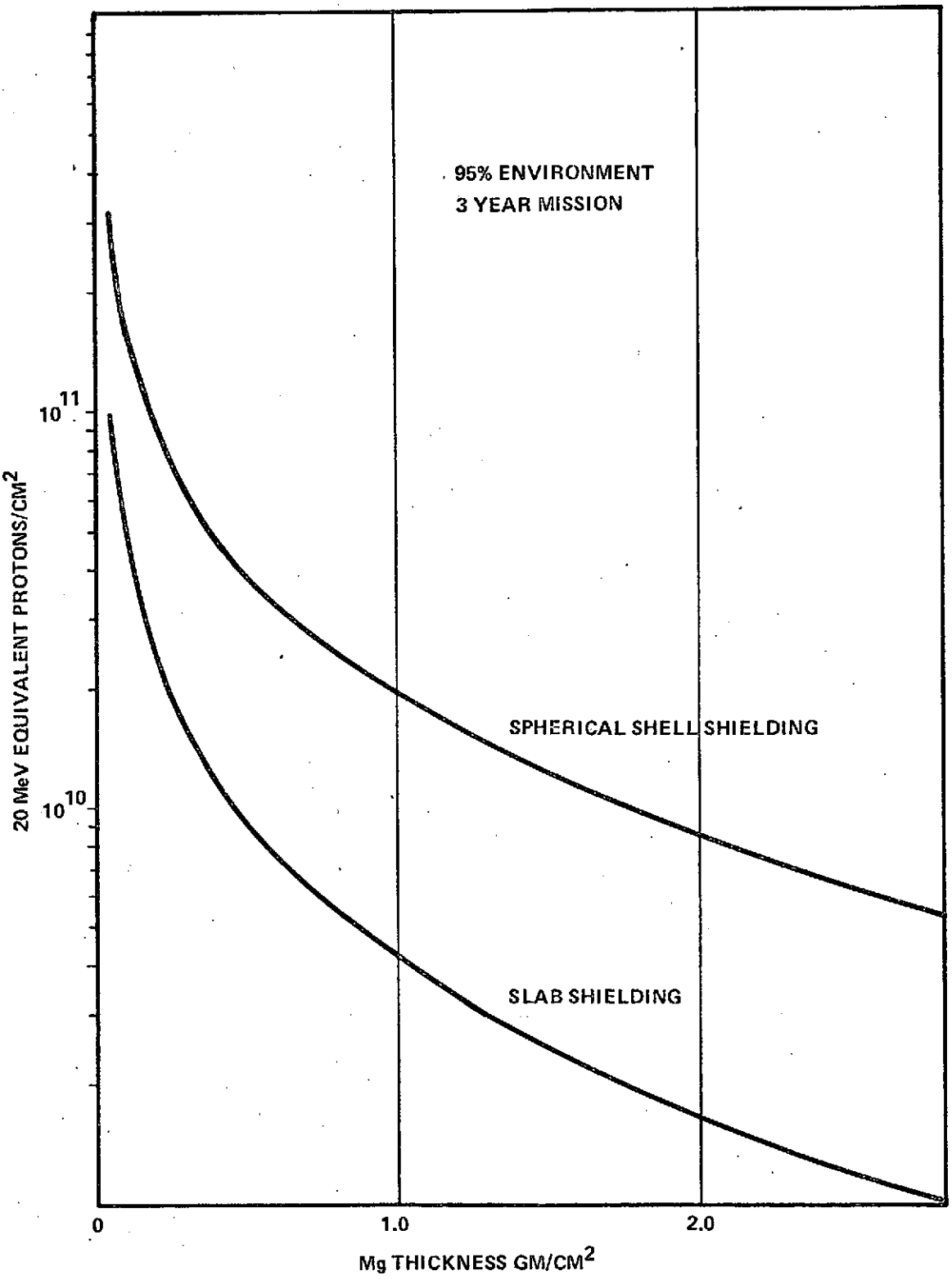

FIGURE 2-9 SOLAR PROTON DISPLACEMENT DAMAGE (MISSION)

3.0 MATERIALS ANALYSIS

3.1 MATERIALS SURVEY

The IUE materials list, dated 29 May 1974, has been studied to identify materials which might suffer unacceptable radiation damage. In making such an assessment, certain generalizations must necessarily be made because test data may only be available on generically similar materials (Reference 11 and 12). The damage thresholds cited in the graphs below are generally the radiation level at which changes are first observed. Usually the change is in one of the important physical properties, such as tensile strength. Electrical properties usually change more slowly than physical properties (in the initial stages at least). In several organic insulators, the loss tangent changes more rapidly than the resistivity. Obviously a judgment as to which property is the most important cannot be made on the basis of a materials list alone. It is also necessary to make an engineering judgment on the consequences of small changes in properties. For example, a small change in α/Σ of a thermal-control coating is much more serious than a small change in the mechanical properties of wire insulation.

There might be secondary consequences of some kinds of degradation caused by radiation or heat. Irradiated teflon produces fluorine and fluorine compounds, and polyvinyl chloride produced hydrogen chloride, for example. It seems likely that the lack of moisture, the vacuum environment, and the slow release of corrosive gases should prevent corrosion of the electronics or the optics in a satellite, but there is no information on this subject.

3.1 (Continued)

A few materials, specifically teflon and nylon, exhibit markedly improved stability to radiation in vacuum or a nonoxidizing atmosphere. As much as two orders of magnitude improvement has been reported. In the tabulation of damage thresholds, a more conservative improvement of one order of magnitude has been taken.

Fillers and reinforcing materials usually improve the radiation resistance of organic polymers, but this is not always true. Titanium oxide is reported to decrease the radiation resistance of nitrocellulose lacquers, whereas carbon black increased the resistance of the otherwise identical formulation. Nitrocellulose may be unique because it is relatively unstable, but it should be observed that the damage level shown below for paints is that of the generic organic base because references have not been found to the radiation effects on the specific paints listed for the IUE.

Therefore, materials have been grouped by generic types and a range of dose given for the threshold of damage, moderate damage and severe damage.

Material damage thresholds for the various categories have been defined as follows: Category 1 -- greater than 10^{10} rad (C); Category 2 -- greater than 10^{8} rad (C); Category 3 -- between 10^{7} and 10^{8} rad (C); Category 4 -- less than 10^{7} rad (C).

Metals and ceramics have been placed in the first category. The damage thresholds for these materials are so high, greater than 10^{10} rad (C), that no further analysis is necessary. Other materials are placed in this category because they serve no function after launch. Marking ink and wire labels are examples.

3.1 (Continued)

In the second category, materials have been identified which have damage thresholds of greater than 10^8 rad (C). These materials would be completely satisfactory if shielded by 5 mils of aluminum (of the order of .03 gm/cm^2) and probably of low risk if shielded by 1 to 3 mils of aluminum. In this group are polyolefines, polyimides, filled epoxies, polyurethanes, and polyalkenes. The range of damage to these materials is shown graphically below. Generally, reinforcement and fillers, such as fibre glass, improve the resistance of these materials significantly.

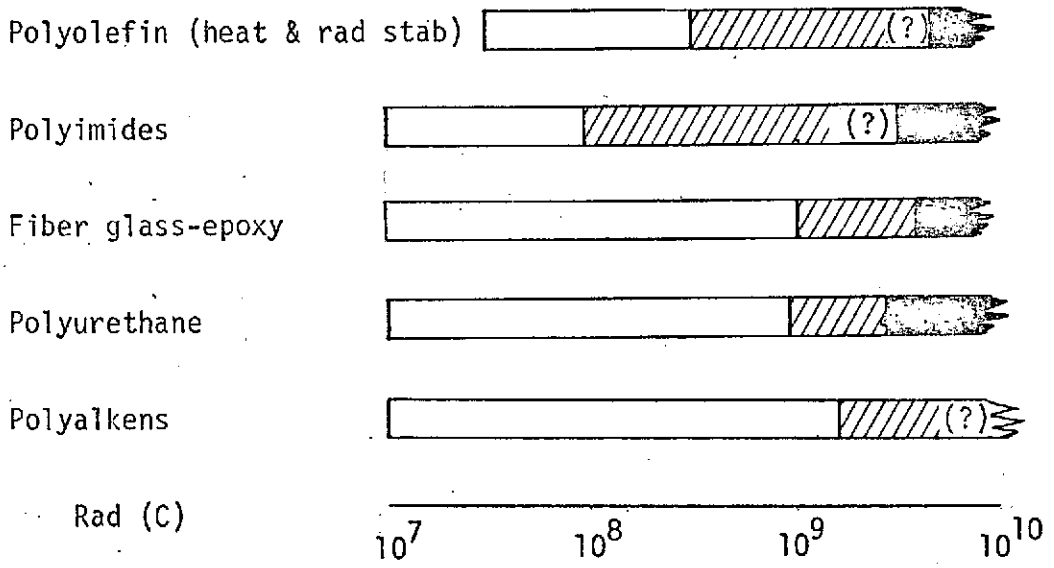

Incipient to mild.

Mild to moderate. Often satisfactory.

Moderate to severe. Limited use.

3.1 (Continued)

In the third category are those materials with a damage threshold between 10^7 and 10^8 rad (C). These materials are nylon, unfilled epoxies, and oriented polyesters such as mylar. Materials in this category should certainly survive behind shielding >.012 inches of aluminum (.08 gm/cm^2).

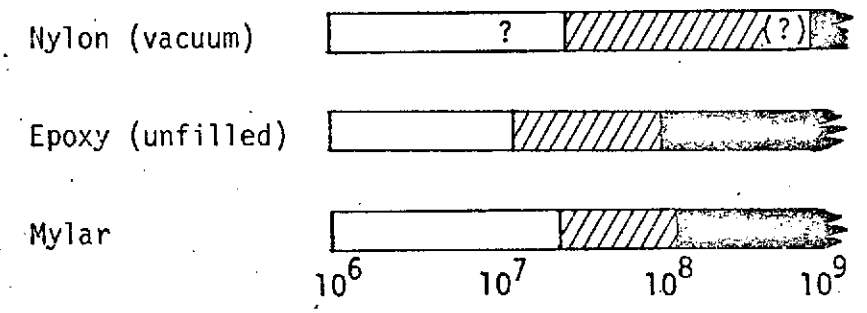

Nylon was somewhat uncertainly placed in Category 3 above because it, along with teflon, which is the fourth category, shows improved resistance to radiation in an oxygen-free environment. There are some contradictions in the published resistance to radiation for nylon and teflon.

Teflon (TFE-type), silicone elastomers, and acrylics are the least radiation-resistant materials on the list, and have been placed in the fourth category. The threshold of damage for these materials is 5 x 10^6 rad (C) or less. They would be certainly safe behind .040 inches of aluminum (.28 gm/cm^2) shielding.

3.1 (Continued)

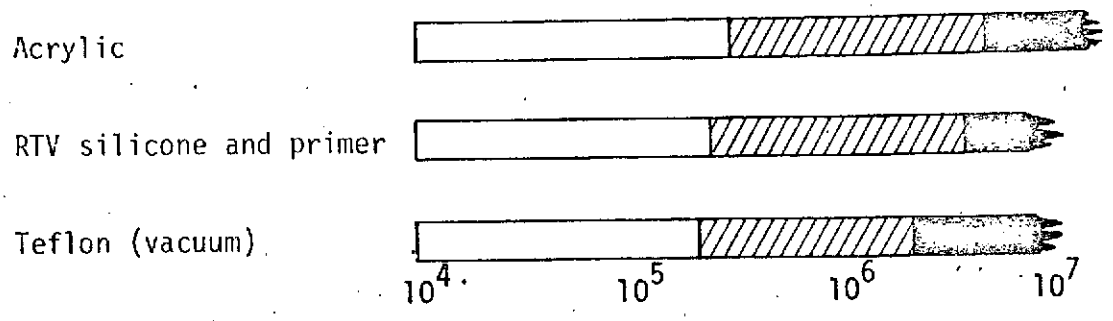

TFE teflon is one of the least radiation-tolerant materials in general use. In air, it shows significant damage well below 10^5 rad (C), but is reported to be approximately two orders of magnitude more resistant in an oxygen-free environment.

Severely damaged teflon is still a good electrical insulator if there is no mechanical stress. For example, a teflon insulated wire, irradiated to a high dose in a vacuum chamber auxilliary to an accelerator, retained good electrical insulation until an attempt was made to move the wire slightly, at which time the teflon crumbled into a powder. The stresses to which acrylics and RTV silicones are subjected should be reexamined. Of relevance is the fact that the adhesive on tapes and other materials are acrylics.

The cement for the solar cell covers is a possible problem. Recent work by L. Fogdall, at The Boeing Aerospace Company, indicates that the RTV 500 series cements tend to creep slowly over the surface of

3.1 (Continued)

the covers where they are evidently polymerized by radiation and, on long missions of one or more years, might decrease the solar cell power output by as much as 10 percent. It is expected that the other silicone elastomers would perform similarly.

The acrylics, elastomers, and teflon are considered possibly susceptible only if operated under a large, long-term mechanical load where cracking, separation, or crumbling could cause a critical failure. In addition, the heat dump resistor adhesive may merit testing in a radiation environment because of its exposed position.

The particular IUE materials classified in the fourth category are: the Scotch #5, Permacell EE7240, and Macbond 0200 (9626) tapes which use acrylic adhesives; the Ben Hur 1062-C sleeving, RTV-566 with SS-4155, Stycast 265111, and RTV 3116 which are silicon elastomer compounds; and the many clearly identified items using teflon.

Engineering judgment is that all the materials except possibly those in the fourth category will survive the mission because they will be subject to fairly mild stresses, both electrical and mechanical. There is significant shielding outside of most materials to reduce the expected dose to near damage threshold and in most cases the materials themselves provide at least some additional self-shielding because of their thickness.

3.2 ANALYSIS OF SELECTED MATERIALS

3.2.1 Transmission Optics

The coloring of glass, usually browning, by ionizing radiation is well recognized, but the relative sensitivity of various glasses to discoloration by radiation covers several orders of magnitude. The basic composition of glass and impurities or minor constituents all are important factors in determining the degree of discoloration by radiation. Much of the work on radiation coloring of glasses up to 1966 is discussed in Reference 13. Several authors, (Reference 14, 15, and 16) have observed severe darkening in several optical quality glasses at doses from 10^4 to 10^6 rad. Stabilized glasses are available, however, in a good range of optical specifications. These are usually stabilized by the addition of cerium, which seems to be quite generally applicable as a stabilizing agent. Kleinpeter and Clare (Reference 14) describe radiation tests on several compound lenses and optical glasses which show that improvement of radiation resistance of 10^3 to 10^4 times that of noncerium doped glasses is obtainable and useful transmission (~50 percent) was observed after 10^9 to 10^{10} rad doses on stabilized glasses.

Apparently the six-digit number and the Mil. G 174 specification only specify the optical properties of optical glass and these specifications can be met by various compositions. It is, therefore, not possible to determine the radiation response from these specifications. There are, however, Mil. Spec. cerium stabilized radiation-resistant glasses. Table 3-1 shows cerium stabilized glass that optically corresponds to unhardened six-digit and Military Specifications glasses. This table does not cover all IUE glasses. It is recommended that radiation resistant transmission optics be specified for the IUE. However, it should be noted that changes in the refractive index of cerium stabilized glass have been observed (Reference 17). A Δn of

TABLE 3-1 OPTICAL GLASSES

INDUSTRY 6 DIGIT	MIL G 174	MIL SPEC CE STABILIZED
573-574	BAK 1	BAK1G12
517-642	BK 7	BK7G14
517-642	BK 7	BK7G25
603-364	F2	F2G12
636-353	F6	FG20
691-547	LAKN9	LAK9G15
578-416	LF 4	F4 G34
581-409	LF 5	LF 5G15
717-295	SF 1	SF1G7
689-312	SF 8	SF8G7
646-341	SF 16	SF16G12
667-330	SF 19	SF19G7
623-569	SK 10	SK10G10
613-586	SK 4	SK4G13

3.2.1 (Continued)

about $+5 \times 10^{-5}$ in the region of 0.5 μ, after a dose of 10^6 rad(Si) from a cobalt source (C060) plus $10^{15} e/cm^2$ of 2 MeV ($\sim 3 \times 10^7$ rad), was reported. This change may be significant for high resolution optics.

3.2.2 Metallized FEP Teflon

The data on changes in the solar absorption in metallized FEP teflon are summarized in Reference 18 to late 1970, and newer data are given by References 19, 20, and 21. Considering that these data represent a fair variety of experiental conditions for space simulation as well as flight data, the agreement between observations is good. It is reasonable to conclude from these data that the worst case absorptance, α, for a fluence of several times 10^{16} particles/cm^2, whether the particles are protons or electrons, would be $\sim$0.20 and that a more probable α is 0.17, for aluminized teflon. The initial α reported for approximately equal thicknesses of teflon by various sources varies from 0.08 to 0.135 and change in absorptance, $\delta\alpha$, from 0.04 to 0.13. From this it would seem that there are inconsistencies in measurement and/or product, but if thermal analysis of the satellite shows that a final α of 0.17 to 0.20 does not cause serious trouble, aluminized FEP teflon is an acceptable material. In any case, no satisfactory substitute seems to be available.

3.2.3 Hydrazine System

3.2.3.1 Hydrazine Decomposition

Hydrazine is decomposed by ionizing radiation into hydrogen and nitrogen. The yield at STP is reported to be of the order of 0.1 ml/M

3.2.3.1 (Continued)

rad per gram H_4N_2, Reference 22 and 23.

The volume of the IUE hydrazine tanks was estimated to be approximately 7600 ml and from the sketches, they are assumed to be 1/2 full containing approximately 3800 ml = 3800 gm. Thus one Megarad would produce a maximum of 380 ml of gas, which would add little to the pressure in the tanks. This volume of gas is an upper limit since many of the electrons and protons penetrating the tank walls would have ranges much less than the full thickness of hydrazine and the expected total dose would be well below 10^6 rad in much of the volume.

3.2.3.2 Hydrazine Tank Diaphragm

The diaphragms in the hydrazine tanks may become somewhat degraded. No specific data has been found on radiation damage to the ethylene-propylene copolymer, but both polythylene and polypropylene suffer undesirable changes in mechanical properties in the 10^7 to 10^8 rad (C) region. At 8.9×10^7 rad (C) polypropylene is reported to have become brittle, lost all of its elongation and most of its tensile strength. Polyethylene loses only about 25 percent of its strength at the same dose. It is not known whether the copolymer would be better or worse. The expected dose to the diaphragms is of the order of 2×10^6 rad (C), and the acceptability of small changes in diaphragm properties is not given. In view of the importance of this part to the success of the mission, it is suggested that the specific polymer to be used be tested to at least 10^7 rad (C) if small changes in properties are significant.

4.0 SEMICONDUCTORS

4.1 PIECE-PARTS

4.1.1 Electronics Survey

The assessment of the IUE electronics is based on piece-parts vulnerability. Detailed circuit analysis to determine specific margins and electrical-failure criteria for each circuit application of the piece-parts is beyond the scope of this analysis effort. This effort involved no testing.

Piece-part types were categorized according to the types of construction which bear some relationship to their general response to radiation. These categories are shown in Table 4-1. Wide variability in radiation response within part types reduces accuracy of such a categorization. The intent of the categorization is to permit establishment of a reasonable lower limits on the environment levels which could cause failure for each piece-part category. Hence the categories of piece-parts used in particular system components provide the basis for setting reasonable values for the vulnerability threshold of those components. Shielding thicknesses were determined that reduce component internal-environment levels to values less than these threshold levels.

Semiconductor parts lists were abstracted from the available system component parts lists supplied by NASA and categorized. The result is summarized in Table 4-1.

The vulnerability thresholds for the various piece-part categories were set using as much test information for the specific piece-parts

TABLE 4-1 ELECTRONICS SCREENING SUMMARY

SUBSYSTEM/COMPONENT	BIPOLAR TRANSISTOR	BIPOLAR LINEAR I.C.	BIPOLAR DIGITAL I.C.	MOS DIGITAL I.C.	SCR, UJT	OPTICAL SENSOR	NOTES	SHIELDING LEVEL
COMMUNICATIONS SUBSYSTEM:								
S BAND TRANSMITTER #1	X						a, f	1
S BAND TRANSMITTER #2	X						a, f	1
VHF TRANSPONDER #1	X						a	1
VHF TRANSPONDER #2	X						a	1
COMMAND SUBSYSTEM:								
COMMAND RELAY	X			X	X			1, 4
COMMAND DECODER #1	X	X		X				1
COMMAND DECODER #2	X	X		X				1
DATA HANDLING SUBSYSTEM:								
MULTIPLEXER:								
CONVERTER (PRIME)	X	X						1
CONVERTER (BACKUP)	X	X						1
DATAPLEXER (PRIME)		X		X			e	1
DATAPLEXER (BACKUP)		X		X			e	1
SUBPLEXER #1		X		X			e	1
SUBPLEXER #2		X		X			e	1
SUBPLEXER #3		X		X			e	1
SUBPLEXER #4		X		X			e	1

TABLE 4-1 ELECTRONICS SCREENING SUMMARY (CONTINUED)

SUBSYSTEM/COMPONENT	BIPOLAR TRANSISTOR	BIPOLAR LINEAR I.C.	BIPOLAR DIGITAL I.C.	MOS DIGITAL I.C.	SCR, UJT	OPTICAL SENSOR	NOTES	SHIELDING LEVEL
COMPUTER:								
POWER CONVERTER #1							a, f	1
POWER CONVERTER #2							a, f	1
CPM #1			X				b	3
CPM #2			X				b	3
MEMORY:								
MEMORY #1	X						a	1
MEMORY #2	X						a	1
MEMORY #3	X						a	1
POWER SUBSYSTEM:								
POWER MODULES (2TOT)	X	X					a	1
MISSION ADAPTOR	X	X		X				1
STABILIZATION & CONTROLS SUBSYSTEM:								
INERTIAL REFERENCE ASSY.								
IRA SENSOR				X			f	1
IRA ELECTRONICS							f	1
NUTATION SENSOR ASSY	X						f	N.R.
CONTROL ELECTRONICS ASSY	X	X		X	X			1, 4
WHEEL DRIVE ASSY	X	X	X	X				1

TABLE 4-1 ELECTRONICS SCREENING SUMMARY (CONTINUED)

SUBSYSTEM/COMPONENT	BIPOLAR TRANSISTOR	BIPOLAR LINEAR I.C.	BIPOLAR DIGITAL I.C.	MOS DIGITAL I.C.	SCR, UJT	OPTICAL SENSOR	NOTES	SHIELDING LEVEL
SUN SENSORS AND PAS						X		N.R.
SUN SENSOR & PAS ELECTRONICS	X	X	X					1
SCIENTIFIC INSTRUMENT SUBSYSTEM:								
EXP. MECH MOUNTED ELECTRONICS:								
SELECTORS							c	NR
MODE SELECT MECH EL	X	X					a	2
SHUTTER MECH EL		X					a	2
FOCUS MECH EL	X						a, d	2
EXPERIMENT ELECTRONICS ASSY	X	X		X	X			1, 4
CAMERA ELECTRONICS BOX	X	X	X					1
ACQUISITION CHM (2 TOTAL)				X		X	f	1,4
SPECTROGRAPH CHM (4 TOTAL)				X		X	f	1, 4
FES HM						X	a, f	1, 4
FES ELECTRONICS	X	X	X	X				1
SUN SHUTTER SENSOR						X		NR

NOTES:
a) ALL BIPOLAR
b) ALL TTL
c) DIODES ONLY
d) LVDT
e) AMI PMOS
f) NO PARTS LIST AVAILABLE

1) 5×10^3 RAD (Si) ELECTRON DOSE
2) 5×10^4 RAD (Si) ELECTRON DOSE
3) 10^7 RAD (Si)
4) SEE APPLICABLE ANALYSIS, OPTICS OR 4-LAYER

4.1.1 (Continued)

as available, supplemented to a considerable extent by test data on similar piece-part types. The vulnerability thresholds should be set as high as possible to minimize shield weight, balanced against risk. The establishment of vulnerability thresholds by this approach necessarily involves engineering judgment, and the assumption of small, but non-zero risk. To minimize the risk involved in the use of a generalized vulnerability threshold for the determination of requirements on internal environment levels, appropriate radiation test data is necessary. Test data is desirable on every potentially vulnerable semiconductor piece-part type used in the system, on at least a sampling basis, to identify particularly vulnerable piece-part types. Such types can then be replaced, or spot shielded to lower environment levels.

The vulnerability thresholds established for the semiconductor categories are summarized below. The bases for these thresholds are developed in later sections of this report. Piece-part testing and screening are also discussed.

For bipolar transistors particularly sensitive device types have been observed to degrade significantly at doses as low as 10^3 rad (Si). A level of 10^4 rad (Si) is below roughly 95 percent of the device-type failure levels, and may be used as the threshold level provided the extremely vulnerable types are identified by test. Further, 10^4 rad (Si) is also a reasonable threshold for both the bipolar linear ICs and the MOS digital ICs. The bipolar digital ICs of the general type used in the IUE have failure thresholds in excess of 10^7 rad (Si). The silicon controlled rectifiers have extremely variable total-dose

4.1.1 (Continued)

response from part type to part type, and particular types can safely be used only after radiation tests have demonstrated acceptable thresholds.

Predicted displacement (proton) degradation for bipolar transistors is given in Section 4.1.3. Displacement damage is not considered to be significant for the other semiconductor categories, except for unijunction transistors.

For the IUE environment, the vulnerability thresholds of diodes (Reference 24) and passive piece-parts are sufficiently high so that these piece-parts are not of concern.

4.1.2 Total Dose Effects

4.1.2.1 Total Dose Response Summary

Total dose response of semiconductor piece-parts has been surveyed for the purpose of: 1) establishing minimum total dose hardness levels for each semiconductor category or device type; 2) examination of methods for identification of the most sensitive piece-parts of a batch of parts of a particular type. Item 1 can be carried out by using historical data, or better by using sample groups for radiation tests. However, Item 2 methods involve radiation tests of all the particular devices in question.

The radiation sensitivities of the various device categories listed below can be expressed as probability plots as shown in the sketch.

4.1.2.1 (Continued)

These curves are approximate and are presented to illustrate the relative sensitivities of these categories to total dose.

Device Categories	No. of Types in Each
1. Low-power bipolars	11
2. Medium power bipolars	14
3. Power bipolars	13
4. Linear bipolar ICs	17
5. Digital bipolar ICs	17
6. JFT	2
7. P MOS digital ICs	14
8. CMOS digital ICs	56
9. CMOS Linear ICs	0
10. 4-Layer devices: SCRs, etc.	2
11. Diodes	NR

4.1.2.1 (Continued)

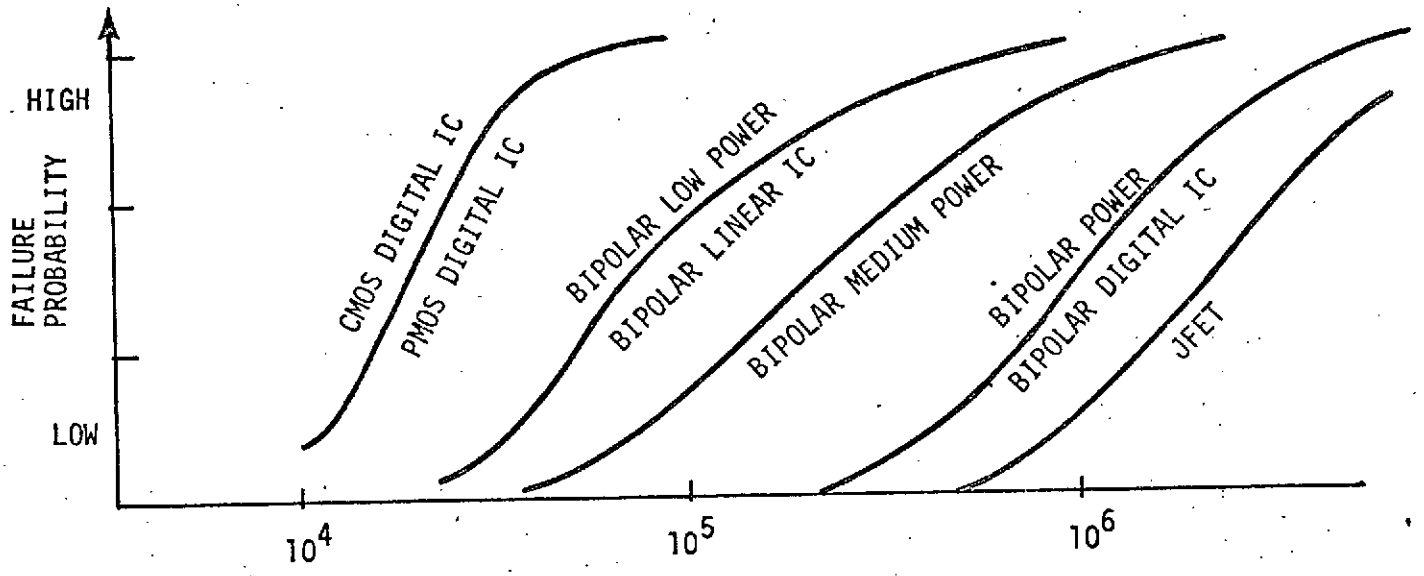

Notes on preceding sketch:

a. CMOS curve reflects the latest test data on the RCA devices by Sandia.

b. PMOS curve reflects the Goddard test data on their own devices. Corresponding data on AMI PMOS will be generated later by Goddard.

c. Each of the bipolar curves represent the average of many types of devices with an expected large scattering among the various types.

d. All curves represent worst-case bias conditions.

4.1.2.1 (Continued)

A small sample (5 to 10) of devices from a particular parts type is useful in defining the relative radiation vulnerability of that part type. A log normal failure distribution can be assumed, and a lower limit established for a given confidence and population proportion as an indicator of a safe dose level for that part type. Particular parts types which have an inadequate safety margin may not be reasonably replaced or spot shielded. If these parts types have their mean failure level above the internal environment level, a screening technique to select the particular units of a device type which are adequately hard may be useful. Total dose screening is difficult because of the lack of suitable electrical parameters that correlate well with total dose damage. Recent research has established 100 percent irradiate and anneal (IRAN) as a possible technique. One-hundred-percent IRAN involves irradiating all of the units of a particular type to the specification level, performing electrical measurements of critical parameters on all units, rejecting the units to recover their performance, and using the annealed units in the system. This technique is reasonably effective, but is expensive, and reliability effects remain to be determined.

Several total-dose test-program concepts are outlined below. They vary in the level of detail and, consequently, the level of risk varies accordingly.

Level-C Program--Small sample irradiation test representative device types from MOS, linear, and four-layer device categories. These devices should be the overall spacecraft shielding to provide the desired hardness margin.

4.1.2.1 (Continued)

Level-B Program--Perform Level-C testing. Also perform small sample irradiation tests (no bias) on all other device types except bipolar digital, JFET types, and diodes; then small sample irradiation retest (worst-case bias) device types which do not have a large hardness margin. Perform a trade study between adjusting overall shielding, adding spot shielding, and replacing device types.

Level-A Program--Perform Level-B testing, and complete Level-B trade study. Then 100-percent IRAN all device types with minimal margin. Since 100-percent IRAN is planned for marginal types, a higher internal-environment criterion may be possible.

4.1.2.2 Total-Dose Effects in Bipolar Transistors

Establishing total-dose thresholds for electronic systems containing bipolar transistors is a difficult problem because of the erratic nature of the total-dose-induced surface effect. Consequently, devices within a given batch show a wide scatter in total-dose response. The spread between devices of different batches and different device types is even greater (spanning orders of magnitude). The situation is further complicated by the fact that the total-dose response is also a function of bias or operating condition of the transistor during irradiation.

To establish the level of total-dose exposure below which no failures are likely to occur in a system, it is necessary to know the details of the circuit applications of each device type and the radiation-response data for each device type (from the batch to be used) at each operating condition within the circuit.

4.1.2.2 (Continued)

However, in many applications such detailed analysis as discussed above is not practical and complete data do not exist. The discussion that follows presents an approach to proper perspective. Data have been accumulated and analyzed for a large number of bipolar device types both from Boeing test data and from other related published data. These data include both npn and pnp transistors. Some of the devices were operated actively during irradiation, while other types were passive; however, the data have been treated without regard to operating condition or construction. The only restriction placed on the data is that the device type be a low-power silicon transistor. All the device types fell within the range 300-mW to 800-mW power dissipation. This approach is reasonable in that devices within a large system will consist of both npn and pnp types operating in a variety of conditions. Generally, the tests reported included groups of five to 20 devices. The mean failure level for the group is the value considered in this analysis.

The results of this analysis for three different gain degradation levels are tabulated in Table 4-2 and are plotted on a log-normal distribution in Figure 4-1. The current of 1 mA was chosen as being reasonable for the IUE circuitry. It should be noted that a reduced current would reduce the dose level required for failure, while generally an increase in current level increases the dose required to produce failure.

The results indicate no apparent threshold for total-dose effects. That is, failures may occur at doses of the order of 10^3 rad (Si) or less. It should be noted that as the gain margin is increased, the lower end of the curve is not changed significantly. The slope of

TABLE 4-2 TOTAL DOSE FAILURE LEVELS FOR SEVERAL DEVICE TYPES

DEVICE		TOTAL DOSE LEVEL FOR $\beta = 0.75\,\beta_o$ Rad (Si)
2N2487		2.2×10^3
2N2369		5.0×10^3
2N2222		1.1×10^4
2N1613	①	1.3×10^4
2N2946		2.0×10^4
2N930	③	2.2×10^4
2N3347		3.0×10^4
2N930[2]	②	3.0×10^4
2N1613	②	4.0×10^4
2N930	①	4.0×10^4
2N2219		4.5×10^4
FS7966		5.0×10^4
2N2920		7.0×10^4
2N1893		1.1×10^5
2N2605		1.5×10^5
2N1132		4.5×10^5
2N743		No Failure

DEVICE	TOTAL DOSE LEVEL FOR $\beta = 0.25\beta_o$ Rad (Si)
2N2484	3.0×10^4
2N930	2.3×10^5
2N2222	4.0×10^5
2N2605	6.0×10^5
2N2920	3.0×10^6
2N1132	1.0×10^7
2N3347	1.4×10^7
2N1613	3.5×10^7
2n743	No Failure

DEVICE		TOTAL DOSE LEVEL FOR $\beta = 0.5\,\beta_o$ Rad. (Si)
2N2484		6×10^3
2N2369		8×10^3
2N2222		5×10^4
2N1613	②	5×10^4
2N2946		5×10^4
2N930	②	6×10^4
2N930	①	8×10^4
2N930	③	1×10^5
FS7966		1.2×10^5
2N2920		2.5×10^5
2N2219		3.0×10^5
2N1613	①	3.0×10^5
2N2605		3.0×10^5
2N3347		4.0×10^5
2N1893		1.0×10^6
2N708		2.0×10^6
2N1132		3.0×10^6
2N743		No Failure

NOTE: Flagged types represent data from different experimenters on different batches of devices of the same type.

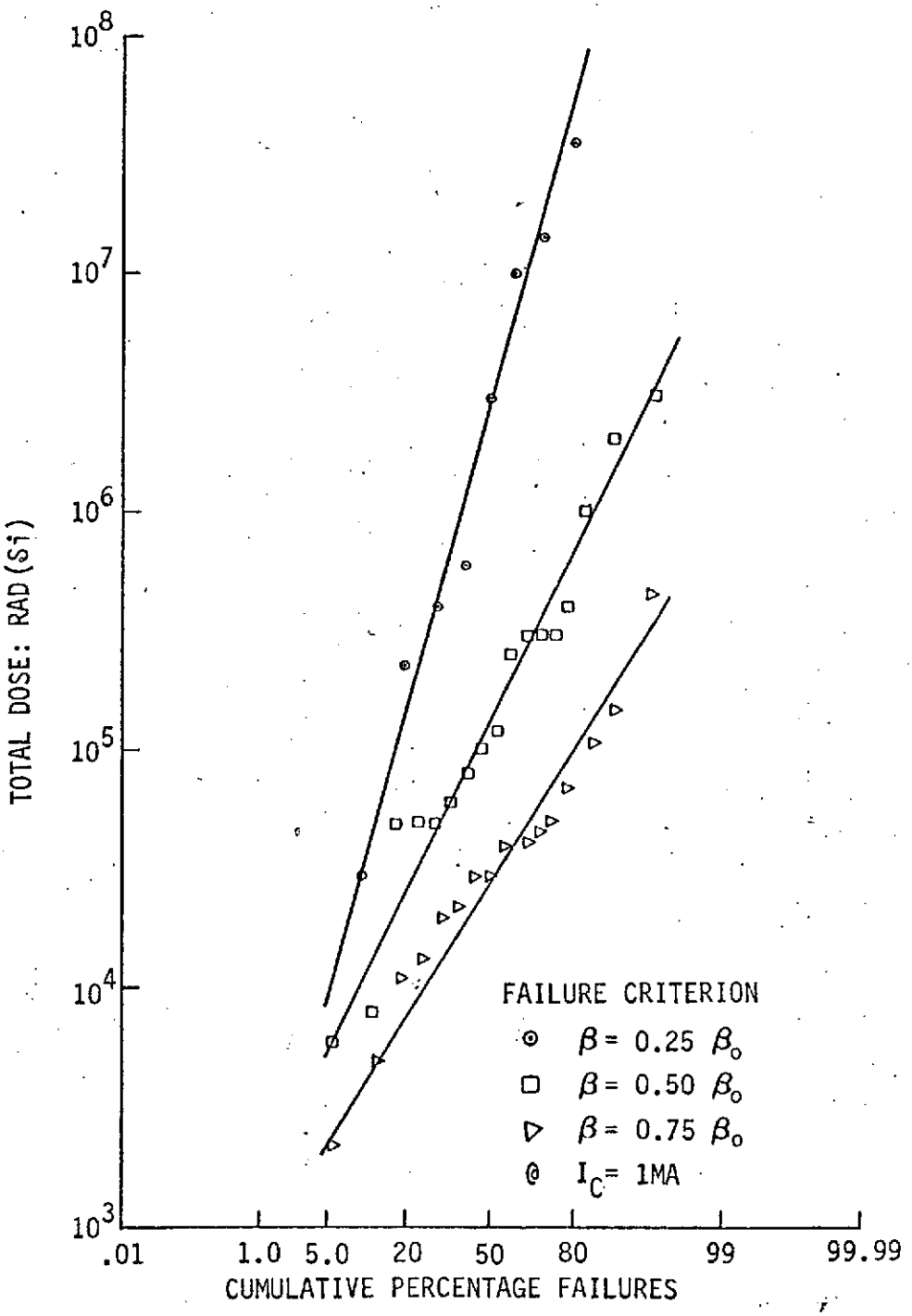

FIGURE 4-1 DISTRIBUTIONS OF BIPOLAR DEVICE-TYPE FAILURE LEVELS FOR TOTAL DOSE

4.1.2.2 (Continued)

the line changes but the probability of failure at low-total dose is not improved very much. This observation reflects the nonlinearity of the total-dose effect in transistors. That is, as total dose is increased, the gain degradation from surface effects is initially rapid, then saturates (shows small increase in damage) at higher dose levels. The change in slope of the plots in Figure 4-1 reflects this saturation; however, the softer devices apparently reach failure for $\beta/\beta_0 = 0.25$ before saturation commences and, hence, the dose range over which failure occurs for the three criteria is not large (as is the case for harder devices for which the damage saturates at a lower level). It is important to note that the graph shows cumulative percentage failures among different device types, rather than for units within a particular type. Assuming the device types used are representative, these data indicate that one percent of the device types within a system are likely to be vulnerable at 10^3 rad (Si), apparently independent of failure criteria. At 10^4 rad (Si), 5 percent of the device types within a system are likely to be vulnerable for a failure criterion of 25 percent remaining gain. Table 4-2 indicates that a system can be hardened to levels greater than 10^5 rad (Si) by parts-type selection. However, total-dose hardening must also accommodate the significant variability in the degradation of units within a particular device type. Even so, the benefits of minimal radiation testing and parts-type selection are considerable.

The bipolar transistors known to be used on IUE are listed in Table 4-3 with the associated test data where available. It is recommended that the low-power devices (under one watt) be screened for total-dose susceptibility by sample testing under active bias. The circuit

TABLE 4-3 TOTAL DOSE FOR IUE TRANSISTORS

DEVICE NUMBER	DEVICE TYPE	RATING (WATTS)	f_t MHz	β_0	DOSE FOR $\beta/\beta_0=0.75$	DOSE FOR $\beta/\beta_0=0.5$	DOSE FOR $\beta/\beta_0=0.25$	REMARKS
2N918	NPN Si	0.2	600	20				It is recommended that these devices (Power <1W) be screened for total dose susceptibility.
2N3350(a)	PNP Si Dual	0.2	60	150				
2N3838	NPN-PNP Si Dual	0.25	200	100				
2N2920(a)	NPN Si Dual	0.30	60	300	8.0×10^4	2.6×10^5	1.2×10^7	Applied physics lab data 1965
2N2848(b)	NPN Si	0.36	15	175	2.2×10^3	6.0×10^3	3.0×10^4	August 1974 Boeing test data
2N3811(a)	PNP Si Dual	0.50	100	300				
2N2060	NPN Si Dual	0.50	50	50				
2N2222A	NPN Si	0.50	300	100	2.8×10^4	8.5×10^4	8.0×10^5	Applied physics lab data 1965
					1.1×10^4	5.0×10^4	4.0×10^5	August 1974 Boeing test data
2N5338	NPN Si	0.60	30	30				
2N2605	PNP Si	0.60	200	100	6.0×10^4	1.5×10^5	8.0×10^5	August 1974 Boeing test data
2N2905A	PNP Si	0.60	200	100	105	No Data	No Data	Boeing test data (active) 1970
2N2219	NPN Si	0.80	300	100	4.5×10^4	3.0×10^5	10^6	1967 Boeing test data
2N2219A	NPN Si	0.80	300	100				
2N3019	NPN Si	0.85	100	100				
2N2854-2 (a)	NPN Si	0.85	30	100				
MSC4003 MSC4000	Microwave Devices							Should be tested: Electrons, Protons

TABLE 4-3 TOTAL DOSE FOR IUE TRANSISTORS (CONTINUED)

DEVICE NUMBER	DEVICE TYPE	RATING (WATTS)	f_t MHz		DOSE FOR β/β_0=0.75	DOSE FOR β/β_0=0.5	DOSE FOR β/β_0=0.25	REMARKS
2N3636	PNP Si	1.0	150	50				In general, power devices, if used in a power application (that is high-current) are relatively immune to total dose degradation (i.e., 4×10^5 Rad(Si)). However, if they are used in low-current modes, they can be softer to total dose than low-power high-gain devices. Based on these considerations the circuit applications of these devices should be examined.
2N3720	PNP Si	1.0	60	20				
2N4236(b)	PNP Si	1.0	3	40				
2N3468	PNP Si	1.0	150	25				
2N3444	NPN Si	1.0	175	20				
2N3635	PNP Si	1.0	150	50	Boeing Test Data 1970			
2N3501	NPN Si	1.0	150	100	1.0×10^5	No Data	No Data	
2N2658	NPN Si	1.25	20	40				
2N1724/1 (a)	NPN Si	3.0	10	30				
2N4863	NPN Si	4.0	50	50				
2N2034C (b)	NPN Si	5.0	1	20				
2N4150(a)	NPN Si	5.0	15	40				
2N3375	NPN Si	11.6	500	10				
2N1486(b)	PNP Si	25.0	1.2	35				
2N3741(b)	PNP Si	25.0	3	40				
2N3749(c)	NPN Hi Freq	30.0						
2N491B(b)	NPN Si	UJT						
2N2814(a)	NPN Si	70.0	15	40				
2N5539-5 (c)	NPN Si	100.0	20	25				

(a) Significant proton damage likely.
(b) Severe proton damage likely
(c) If multiple emitter, should be tested for dose.

4.1.2.2 (Continued)

application of the power devices should be examined to determine if any device is operating at current levels significantly less than the gain peak. If so, those particular power devices also should be tested.

4.1.2.3 Total-Dose Effects on Microcircuits

The microcircuits can be classified as MOS logic, bipolar logic, and bipolar linear. There were no MOS linear microcircuits found to be used on IUE.

The MOS logic circuits used on IUE consist of RCA CMOS, AMI PMOS, and some NMOS used in the vidicon electronics.

A survey of the pertinent literature, References 25 through 38, indicates that in general, small changes in device parameters begin to occur at a level of 10^4 rad (Si), with failure at considerable higher levels in some cases. However, the most recent data, for RCA CMOS, indicate functional failure in the neighborhood of 3×10^4 rad (Si). J. Novelo (Reference 39) found failure at 3×10^4 rad (Si) for the CD4011AK/1. R. Burghard (Sandia) tested CD4061 and CD4011 devices from RCA Findlay. These devices failed at 3×10^4 rad (Si). J. W. Spaniol (JPL) tested a CMOS memory system made up of CD4000 series devices, and reports a 55 percent power increase at 2.2×10^4 rad (Si) and complete failure at 5.3×10^4 rad (Si). It seems generally accepted that there has been a process change that has reduced the failure of the RCA devices. D. Lokerson (NASA Goddard) has found the prototype PMOS devices failing in the neighborhood of 3×10^4 rad (Si), also. No annealing of the PMOS was found. Tests

4.1.2.3 (Continued)

of the production AMI PMOS devices are recommended. Tests of the NMOS devices in the cameras are recommended also.

Based on the preceeding data, a failure threshold of 10^4 rad (Si) for the CMOS seems reasonable.

A basis for total dose testing the RCA CMOS is given in Table 4-4. The device types listed were selected to be the most representative of all the types used in the IUE. The types listed are prioritized to indicate the device types to be tested first. If variations in failure levels between device types are small (within range of statistical variation for a device type), only the priority AA and A devices need be tested. Specific electrical test and measurement details depend on the particular application of each device type.

The bipolar logic circuitry in the IUE is the 5400 series TTL type. Reference 40, and Reference 41, which survey failure dose levels for a wide variety of bipolar logic circuits, report failure levels in excess of 10^7 rad (Si). Reference 41 shows failure levels of 4.5×10^8 rad (Si) for T^2 L epitaxial NAND gates and 2×10^7 rad (Si) for T^2L RS flip flops. The piece-part package plus a nominal housing thickness (0.040Al) is sufficient to reduce the dose level to less than 10^6 rad (Si).

Bipolar linear circuits tend to show more variability than logic circuits. Current Boeing test data on the LM108 and LM101 devices shows input offset current and voltage to be out of specification in the range of 3×10^4 to 10^5 rad (Si). The LM124 and LM139 devices begin to degrade above 10^5 rad (Si). Data for the μA 741 (Reference

TABLE 4-4 TEST CONCEPT FOR RCA CMOS

DEVICE	FUNCTION	PRIORITY
4046	PHASE LOCKED LOOP	AA
4011	NAND GATE	A
4027	JKFF	A
4016	BILATERAL SW	A
4047	ASTABLE MULTIVIB.	B
4013	D FLIP FLOP	C
4001	NOR GATE	C
4030	EXCL OR	C

- MINIMUM SAMPLE SIZE = 5
  PREFERRED SAMPLE SIZE = 10
- IRRADIATE UNDER OPERATING BIAS, TRIGGER AT NOMINAL RATE
- DETERMINE SIGNIFICANT ELECTRICAL PARAMETERS FROM RESPECTIVE DESIGNERS
- TEST AA AND A PRIORITY DEVICES UNLESS LARGE VARIABILITY IN FAILURE THRESHOLD BETWEEN DEVICE TYPES IS NOTED
- IRRADIATE TO FAILURE IN COBALT 60 FACILITY

4.1.2.3 (Continued)

40) shows no change at 10^4 rad (Si), with some degradation at 10^5 rad (Si). Thus, 10^4 rad (Si) is indicated to be a reasonable failure threshold for the linear microcircuits. However, a risk is involved when specific test data are not available for the particular linear microcircuits used. Table 4-5 lists the IUE linear microcircuits. Existing test data for linear microcircuits was found to be limited. Consequently, additional linear microcircuit testing would reduce this risk.

TABLE 4-5 LINEAR BIPOLAR ICs

HA2700	HIGH-PERFORMANCE OPERATIONAL AMPLIFIER
SM105G	VOLTAGE REGULATOR
μA741	FREQUENCY-COMPENSATED OPERATIONAL AMPLIFIER
SM109G-1	5V REGULATOR
μA715	HIGH-SPEED OPERATIONAL AMPLIFIER
LM105	VOLTAGE REGULATOR
LM108A	OPERATIONAL AMPLIFIER
LM101AH/883	OPERATIONAL AMPLIFIER
ICH8500A	JFET OPERATIONAL AMPLIFIER
μA723	PRECISION VOLTAGE REGULATOR
G2700	OPERATIONAL AMPLIFIER
OP747HM	DUAL OPERATIONAL AMPLIFIER
μA709A	HIGH PERFORMANCE OPERATIONAL AMPLIFIER
SM107F-1	OPERATIONAL AMPLIFIER
SM101F-1	OPERATIONAL AMPLIFIER
SE510J	DUAL-DIFFERENTIAL AMPLIFIER
SM101G-1	OPERATIONAL AMPLIFIER

4.1.2.4 Total-Dose Effects on SCR Devices

The Unitrode 2N3028 is the SCR type used in three places in the IUE; the control electronics assembly (relay), the command relay, and the Experiment electronics assembly (LVSW). There is a possible severe problem associated with the use of SCR devices. Most studies of SCRs show thresholds near 10^4 rad (Si) or higher for small changes in parameters (Reference 42). However, some tests (References 42, 43, 44) where an SCR type (2N2323) was irradiated under bias with the SCR in the off state, caused these SCRs to turn on during irradiation at levels near 10^3 rad (Si). Data is insufficient to indicate how widespread this behavior may be. Therefore, it is recommended that the 2N3028 device be irradiated under bias in the off state to determine if they are unusually sensitive.

4.1.3 Displacement Effects

4.1.3.1 Proton Displacement Damage Effects in Bipolar Transistors

The proton displacement damage was calculated for three solar proton levels for the IUE device types known. The proton levels are 3-year fluences based on either a nominal (expected average) or 10 times the nominal yearly fluence (spherical values) to provide a 95 percent probable 3-year environment. Most displacement damage data is obtained by use of a neutron environment. An energy dependent conversion factor has been established to convert proton damage to neutron damage. The equivalent 20-MeV proton levels are converted to displacement damage equivalent neutrons by multiplying by 25. The resulting values are shown following in Table 4-6.

TABLE 4-6 PROTON SENSITIVE TRANSISTORS

TRANSISTOR	f_t/β_o (f_t in MHz)	β/β_o Predicted at: 4.5×10^{10} n/cm^2	1.5×10^{11} n/cm^2	5×10^{11} n/cm^2
2N3350	0.4	>.9	.9	.7
2N2920	0.2	>.9	.8	.55
2N2484	0.086	.85	.65	.4
2N3811	0.33	>.9	.87	.7
2N2854-2	0.3	.9	.85	.6
2N4236	0.07	.82	.6	.3
2N1724/1	0.33	.9	.86	.7
2N2034C	0.05	.77	.5	.25
2N4150	0.37	.9	.87	.7
2N1486	0.034	.7	.45	.2
2N3741	0.07	.82	.6	.3
2N491B	UJT			
2N28/4	0.38	.9	.9	.7

ENVIRONMENT (SPHERICAL SHIELDING)		PROTON	NEUTRON
95%	.400" Al	6×10^9 P/cm^2	1.5×10^{11} n/cm^2
Nominal	.400" Al	1.8×10^9 P/cm^2	4.5×10^{10} n/cm^2
95%	.140" Al	2×10^{10} P/cm^2	5×10^{11} n/cm^2
Nominal	.140" Al	6×10^9 P/cm^2	1.5×10^{11} n/cm^2

4.1.3.1 (Continued)

The transistor degradation is expressed in terms of β/β_0, the ratio of the gain after irradiation to the gain before irradiation. Table 4-6 shows those IUE transistors for which possibly significant degradation is predicted. The gain degradation for at least the 1.5×10^{11} n/cm^2 level should be considered for acceptability, or better the 5×10^{11} n/cm^2 level, since it indicates the predicted degradation in the fully shielded case (0.40 inch Al) for the 95 percent environment. The 0.400 inch case is included to show the relatively small effect of thicker shields.

It should be noted that several transistor types indicate severe degradation for the highest level. The acceptability of this degradation should be confirmed by the subsystem designers.

The 2N49B is a unijunction transistor used in the EEA converter. It is potentially vulnerable to proton displacement damage.

4.1.3.2 Proton-Displacement Effects in Microcircuits

No problem is anticipated with displacement effects in any of the IUE microcircuits. Typical damage thresholds are above 10^{13} n/cm^2, equivalent to 5×10^{11} P/cm^2 (Reference 40). The fully shielded IUE 95 percent proton environment is 2×10^{10} P/cm^2.

4.2 SPECIAL DEVICES

4.2.1 Hall Devices

Hall devices are used in the IUE as mechanism position sensors. The Hall device provided by Bell, Inc., is constructed of aluminum oxide, indium arsenide, polyurethane, copper, and epoxy.

A four-terminal Hall-effect device behaves basically according to the relationship.

$$V = R\ (I \times B)$$

where V is the output voltage, R is the Hall coefficient, I is the control current, and B is the magnetic field. Of these terms, R is the radiation-sensitive parameters. The Hall coefficient is proportional to the inverse of the number of ionized carriers/cm^3. Reference 45 shows carrier density as a function of 4.5-MeV electron fluence. Fluences of the order of 10^{15} 4.5-MeV electronic/cm^2 are required to produce significant changes in the carrier density (approximately 20% at $\emptyset = 10^{15}$ e/cm^2). The effect of such changes on the Hall coefficient was found to change approximately 50 percent (estimatation difficult due to slope of graph) for $\emptyset = 0.5 \times 10^{15}$ el/cm^2.

The Hall device damage mechanism is a result of displacement effects. The displacement damage from the belt electrons is negligible. The displacement equivalent environment for the solar protons is required.

The device is apparently packaged in an approximately 0.1-inch thick epoxy case which gives 0.05 inch on either side of the active element. Assuming the epoxy to have a density of one, this gives 0.13 gms/cm^2 of

4.2.1 (Continued)

shielding. For the IUE mission, this gives an equivalent 20-MeV proton fluence of the order of 3×10^{11} P/cm^2 (20 MeV) using the 95-percent solar proton environment. Such a fluence, based on a $\frac{1}{E}$ cross section, is equivalent to ~1.5×10^{10} P/cm^2 of 1-MeV energy. It has been observed that one 1-MeV proton creates an amount of displacement damage equivalent to ~400 4.5-MeV electrons (Reference 46) in silicon . Thus, if one assumes a similar energy dependence for InAs, the equivalent 4.5-MeV electron fluence for the IUE mission should be ~6×10^{12} (4.5 MeV) e/cm^2. The energy dependence is expected to be similar, but insufficient data is available to confirm this assumption. Therefore, the Hall device should withstand the IUE environment with little adverse effects.

4.2.2 Linear Voltage Displacement Transducer

Discussions with Hewlett - Packard established the internal electronics for the Linear Voltage Displacement Transducer (LVDT) utilizes discrete bipolar transistors, type unavailable, which are placed in an annular configuration around the transformer core. Thus a minimum estimate for the shield thickness is the stainless-steel package (0.55 gm/cm^2) plus the transistor cans (0.21 gm/cm^2). Also, the transducer is sufficiently thick so that the back half-plane can be assumed to be completely blocked. The transducer mounting blocks approximately 70 percent of the solid angle around the transducer, including complete shielding of the transducer ends. Including the blocking of the back half-plane approximately 15 percent of a sphere will be viewed by the transistor chips through 0.76g/cm^{2}Fe. Using the environment curve for Z-22, shown in Section 7.1, the 4π level is 2×10^4 rad (Si)/year, so that 3×10^3 (Si)/year or ~10^4 rad (Si)/year, so that 3×10^3 rad (Si)/year or ~10^4 rad (Si) per mission is accumulated by the transistors.

4.2.2 (Continued)

Therefore, the LVDT is vulnerable only if a very sensitive transistor is used (see bipolar total-dose degradation discussion). If the LVDT is a critical item, it should be tested with active bias in the Cobalt 60 facility.

4.2.3 Mechanism Mounted Electronics

The mechanism-mounted electronics are contained in small packages and consist of 2N2222 transitors, HA2700 amplifiers, diodes, and passive components. Specific test data on these devices show that 5×10^4 rad (Si) electron dose is an appropriate shielding criterion.

Shielding to this electron dose level will allow a proton level of 2×10^{10} P/cm^2. Test data for the 2N2222 and HA2700 amplifiers also show that the corresponding displacement damage is acceptable for these devices.

5.0 SENSOR ANALYSIS

5.1 SENSOR CONSTRUCTION

5.1.1 UV Converter Construction

A cross section of the Proximity Diode is shown in Figure 5-1. The MgF_2 window obtained from Harshaw Chemical has a transmission of >35 percent at 1215 Å. The photocathode is a nicrome layer deposit on the back of the window producing a 15 percent reduction in transmission followed by a layer of Te giving an additional 15 percent reduction in transmission and finally a molecular layer of Cs. The anti-halation layer will reduce the photoelectron energy by 4 KeV. The P11 phosphor is 1 mg/cm^2 of ZnS (Ag) with a mean particle size of 4 to 10 microns and an emission peak at 4460 Å. With a 6-kilovolt bias and 1-watt incident light at 2537 Å the P11 phosphor produces an output of 4 watts. The Proximity Diode is potted with Echobond 24.

5.1.2 SEC Vidicon Construction

The outline of the SEC Vidicon is shown in Figure 5-2. The potentially radiation-sensitive element in the vidicon tube is the KCl target. The material thicknesses surrounding the target have been determined. The front end of the camera module is covered by 1 mm of mu-metal (0.85 g/cm^2), and 1 mm of Aluminum (0.27 g/cm^2). The vidicon wall is 1/8-inch ceramic (0.86 g/cm^2) in the vicinity of the target, 1/32-inch Kovar (0.63) gm/cm^2) adjacent to the ceramic, and 1/16-inch glass (0.42 gm/cm^2) on either side of the Kovar. Interference and damage to the target will be considered.

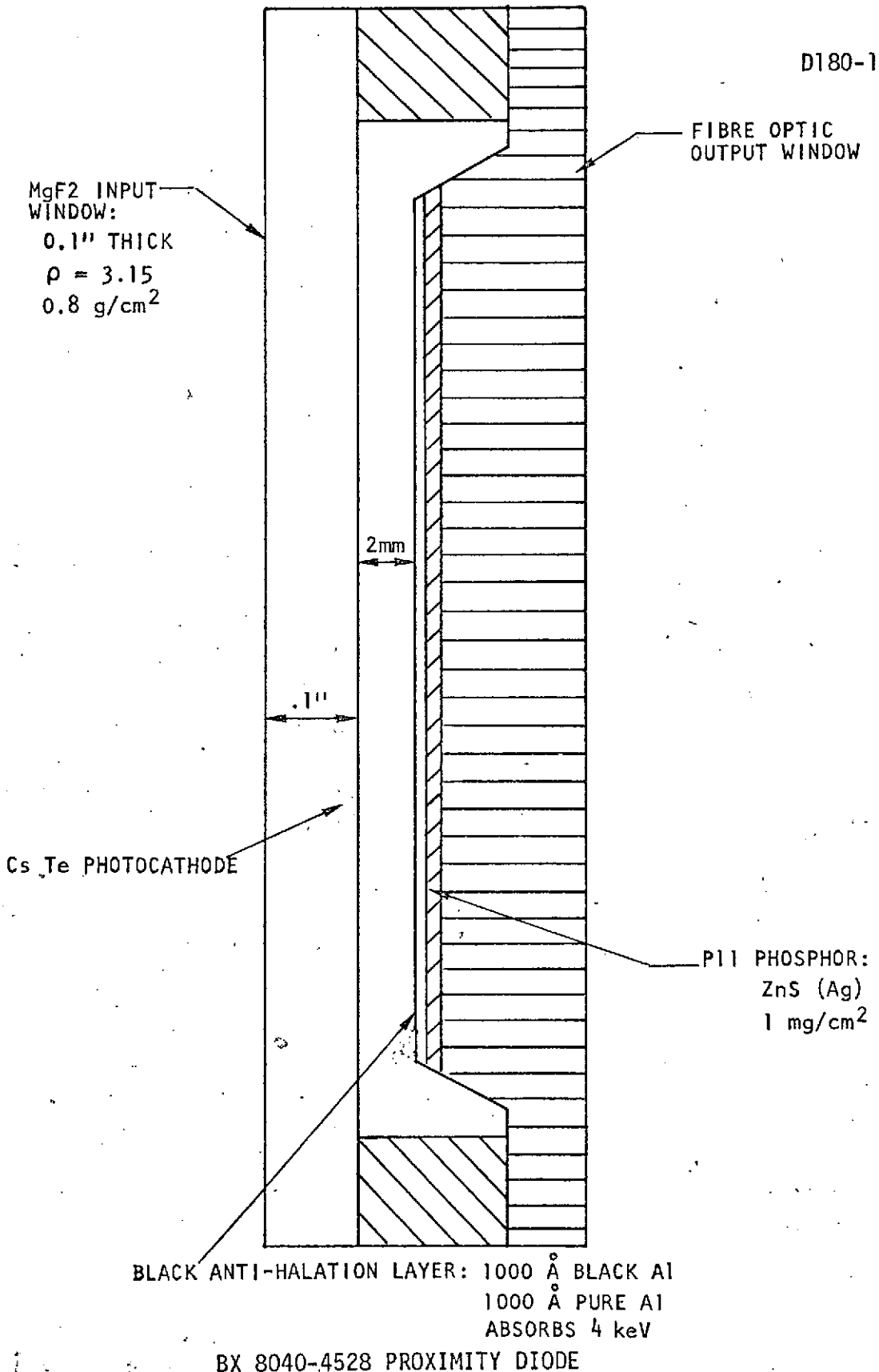

FIGURE 5-1 UV CONVERTER

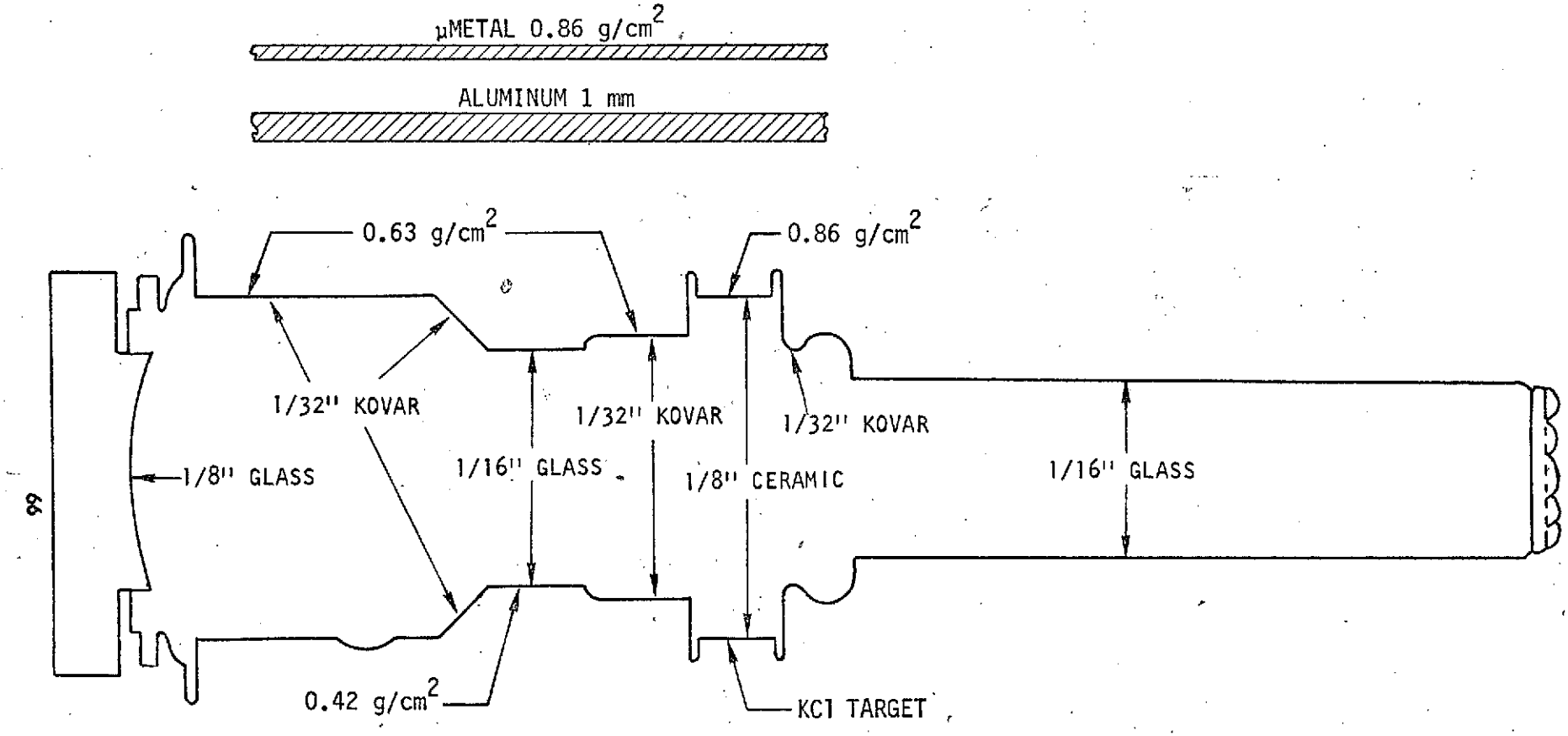

D180-18486-1

FIGURE 5-2 SEC VIDICON TUBE

5.1.3 Fine Error Sensor Construction

The Fine Error Sensor (FES) Head Module consists of an image dissector tube, focusing coils, a mu-metal shield, and some of the associated driving circuitry. It is considered that the material surrounding the dissector tube is sufficiently thick that the only significant radiation flux enters the dissector tube through the optical window. The FES Head Module is mounted on the acquisition deck of the optical unit, and views a front surface mirror, so that interference causing radiation must be scattered into the FES by this mirror.

5.2 DAMAGE EFFECTS

5.2.1 P11 Phosphor Damage

Birks, Reference 47, states that ZnS(Ag) and ZnS(Cu) are damaged identically by alpha particles and that the damage follows the equation

$$I/I_o = \frac{1}{1 + AN}$$

where I_o is the initial fluorescent efficiency
I is the final fluorescent efficiency
A is a damage constant = 4×10^{-14}/particle/cm^2
N is the particle fluence, cm^{-2}

The equation was tested to 10^{13} alpha particles/cm^2, where a fluorescent efficiency of 70 percent was observed. A 5 percent decrease in fluorescent efficiency would result from 1.25×10^{12} alphas/cm^2. Protons or electrons would produce less damage, so that little damage should result from the expected mission fluence of $<10^{12}$ e/cm^2 (through MgF_2 window).

5.2.2 KCl Target Damage

The mechanism of radiation damage in KCl has been studied extensively, References 48 and 48, and the predominant mechanism for producing the largest effect, the production of F centers by radiolysis, is an unusually efficient process. A small amount of radiation triggers the release of energy stored in existing lattice defects, causing long range lattice relaxations. Low energy electrons or even ultraviolet radiation are as effective as more densely ionizing and more energetic particles for causing radiolysis and radiolysis is of the order of 100 times more effective than displacement for producing damage in KCl. Therefore, it could be argued that an electron test of the KCl target is appropriate. Unfortunately, it is not clear that this kind of damage is predominately the cause of the failure of the target to hold charge or the cause of electrical discharges which cause pinholes. Therefore, both proton and electron tests are indicated.

5.2.3 MgF_2 Window Damage

The production of optical absorption bands in MgF_2 by ionizing radiation and neutrons has been studied extensively and the experimental results are described reasonably well in References 50, 51, and 52. A theoretical analysis of the experimental results is given in Reference 53. The results are complicated and can be summarized as follows:

1. The principal absorption is centered at 2600 Å and the absorption bandwidth varies with temperature during exposure and is much broader and more complicated with neutron exposure than with electrons or gammas. The effect of high-energy protons is not discussed, but if one ventures a guess that the additional complexity from neutrons is caused by displacement damage, high-

5.2.3 (Continued)

energy proton damage may be more complicated than that by electrons or gammas. There is also a secondary absorption band produced around 3650 Å by all types of high-energy radiation.

2. The extent of absorption produced at 2500 Å depends on the dose rate, the total dose and the temperature during exposure. No absorption is produced at 150 °K and the absorption increases both with increasing and decreasing temperature. The absorptivity saturates between temperatures of 50 °K, and 200 °K but not outside of this range.

3. The 2500 Å band can be annealed at 200 °K by ultraviolet radiation of the same wavelength, but the residual band is broadened and there is a strong increase in the absorption at 3650 Å. Light of 3500 Å wavelength does not bleach this band.

4. The absorption bands can be thermally annealed at temperatures greater than approximately 400 °K and the time-temperature relationship depends on total dose; the greater the dose, the more rapid the annealing. After annealing at 800 °K there remains a broad absorption band around 3000 Å.

5. Combinations of thermal and radiation annealing are possible. If high absorptivity is produced by radiation with the crystal held at one temperature, then the temperature is changed to one with a lower saturation level and ionizing radiation again applied, the absorption in the 2500 Å band will decrease to the absorptivity saturation level associated with the second temperature.

6. The absorptivity depends on impurities. At low-dose levels impurity (at least Mn) seems to increase the radiation sensitivity and at higher levels to suppress it.

5.2.3 (Continued)

Most of the data on which the above conclusions are based were taken with doses between 10^{15} and 10^{17} MEV cm^{-3}, in the units used in the references, and the observed optical absorption coefficients resulting from these doses were in the range of 10 to 100 cm^{-1}, which is rather strong absorption. Taking the stopping power of MgF_2 to be of the order of 1.5 MeV cm^{-2}/g for electron energies of the order of 1 MeV and the density of MgF_2 to be 3.1 (Reference 54), the conversion of MeV cm^{-3} to electrons/ cm^{-2} = 4.75^{-1} or, in round numbers, 0.2 electrons cm^{-2}/MeV cm^{-3}. Thus an electron fluence of the order of 2×10^{14} e/cm^{-2} would be expected to produce significant absorption in the 2600 Å band. Present spacecraft structure allows a yearly flux of the order of 10^{14} electrons/cm^2 incident on the window. Heath and Sacher, (Reference 55) have reported observing an approximately 60 percent increase in absorption at a fluence of 10^{14} 1 and 2 MeV electrons cm^{-2} and Hass and Hunter, (Reference 56) have reported an approximately 25 percent increase in absorption for a fluence of 10^{15} electrons cm^{-2}. They suggest that the lower sensitivity they observe is due to more pure MgF_2, but in consideration of the complexity of the effect this may not be valid, or at least not a complete explanation. Sacher (Reference 57) reported no change in the transmission of MgF_2 resulting from a total exposure of 8.25×10^{10} protons/cm^{-2} evenly distributed over 3, 3.8 and 4.6 Mev.

In conclusion, it is recommended that in order to have a high degree of certainty that the MgF_2 window will not suffer more than a 10 percent increase in absorption on a 5-year mission, the total electron fluence should be kept below 10^{13} electrons cm^{-2} (at least 0.3 g/cm^2 shielding). This may be considered conservative in consideration of the annealing mentioned above, as well as the uncertainty of the rate

5.2.3 (Continued)

effect at low radiation rates, but the effects of protons are uncertain and were not considered in the above discussions.

5.3 INTERFERENCE EFFECTS

5.3.1 Fluorescence in the MgF_2 Window and the P11 Phosphor

The peak orbital flux at the equator penetrating the 0.1-inch (0.8 g/cm^2) MgF_2 window is of the order of 10^5 electrons/cm^2-sec. An estimate of the ultraviolet photon flux incident on the converter window was obtained as follows. Referring to the SDR, Volume 1, Figure 10.4-4 and Figure 10.4-2, a flux of $F = 10^{-1}$ photons/cm^2-sec Å appears representative of the limiting capability of the long-wavelength high-dispersion spectrograph. Assuming reasonable values of obscuration and optical efficiency, and that the photons in the spectrum are uniformly distributed across the window, the ultraviolet photon flux at the window was calculated to be on the order of 10^4 photons/cm^2-sec. A comparison of this photon flux directly with the above electron flux indicates the possibility of a severe signal-to-noise problem. The effectiveness of the electrons for producing interference is evaluated below.

The P11 phosphor (ZnS (Ag)) is one of the most efficient materials known for producing fluorescence when exposed to ionizing radiation. The fluorescent efficiency is given by Birks (Reference 58) as 3 x 10^4 photons/MeV, or 34 eV/photon. Taking the stopping power to be 1.5 MeV cm^2/g and the P11 thickness as 1 mg/cm^2 results in a calculated fluorescence of 45 photons/electron of the order of 1 MeV in energy. Since the maximum electron flux through the 0.1-inch

5.3.1 (Continued)

MgF_2 window is predicted to be slightly more than 10^5 electrons sec^{-1} cm^{-2}, the fluorescence of the P11 phosphor is then predicted to be at least 4.5×10^6 photons/cm^2/sec in the most intense radiation field expected if no shielding is provided. Taking an ultraviolet to P11 photon gain of 20, this corresponds to an increase in equivalent ultraviolet background of 2.25×10^5 UV photons cm^{-2} sec^{-1} incident. Therefore the predicted P11 electron interference is considerably greater than the signal at limiting sensitivity for peak electron rates.

Sacher, (Reference 51) reported very briefly that MgF_2 "phosphoresced" outside of the visible light range, evidently in the ultraviolet, when simultaneously exposed to ultraviolet and protons (3-4.6 MeV) but no data were given. Fluorescence in the ultraviolet range to which the CsTe photocathode is sensitive could cause objectionable background. It is unlikely that much fluorescent-yield data in the ultraviolet range of interest will be found in the literature because the spectral range of interest for applications such as scintillation counting is outside this ultraviolet range. Thus additional tests on the fluorescence of MgF_2 are recommended. It should be stated that organic materials such as a film of vacuum pump oil or fingerprints might also fluoresce either under ultraviolet radiation or ionizing radiation.

5.3.2 Ĉerenkov Radiation in the Cameras and Fine Error Sensor

The relativistic electrons present in the earth's outer electron belts will produce photons in the window materials of the camera and Fine Error Sensor (FES). To estimate the intensity of the Ĉerenkov radiation the discussion of Reference 60 is used, along with previously

5.3.2 (Continued)

developed electron penetration data for MgF_2 and SiO_2. The photon-production rate for an electron of velocity $v = \beta C$ in a material with an index of refraction, n, is given by

$$I = 1.53 \times 10^{-12} \left(1 - \frac{1}{\beta^2 n^2}\right) dv \text{ photon/cm}$$

The normal to the radiation front makes an angle of

$$\cos \phi = \frac{1}{n\beta}$$

with the particle velocity vector.

For $n = 1.39$, the MgF_2 value, and a relativistic electron, $\beta \sim 1$, $\phi = 44^{\circ}$. The energy-dependent yield function, $(1-1/\beta^2 n^2)$ ranges from 0 at 224 keV, .37 at 723 keV, up to .46 at 2 MeV. Taking an average yield value of .4, based on the shape of the penetrating-electron spectrum, and using a wavelength band of 1200 to 3200Å, the rate of photon production is ~160 photon/cm. The total path length of electrons in the MgF_2 window of the spectrograph camera is estimated from the total energy deposited in the window and from the average electron stopping power in MgF_2. A peak track rate of 6×10^6 cm/cm^2 sec is estimated. This will then result, for an average quantum efficiency of 10 percent in the CsTe photocathode and a photon transmission efficiency of 50 percent, in an electron production rate of 5×10^7 electron/cm^2 sec in the camera. This rate is much greater than the penetrating-electron rate.

The FES, with a quartz window, $n = 1.48$, a larger optical bandwidth, and with exposure to only the scattered electrons would have a peak electron production rate of 5×10^6 electron/cm^2 sec. The transmission

5.3.2 (Continued)

efficiency of photons to the photocathode is difficult to calculate exactly due to the multiple scattering of the electrons and the resulting spread in Čerenkov emission angles, but the transmission efficiency is unlikely to be so small as to cause a major reduction in the interference estimates.

The FES multiplier views the photocathode through an 8 x 8 mil window (4×10^{-4} cm^2). Thus, a peak interference rate of 2000 el/sec is predicted to impinge on the multiplier, compared with the expected signal of 400 el/sec from the photocathode for the dimmest star. The peak electron production rate in the acquisition camera window can be expected to be about the same as in the FES window. Therefore, the FES and camera interference rates are considered possibly severe, should be verified by tests, and special baffles may be necessary.

The penetration of backscattered electrons from the mirror through the FES window was evaluated with the Monte Carlo electron results and found to be less than 10^3 electrons/cm^2 sec at the peak electron environment, thus is insignificant compared to the Čerenkov interference.

5.3.3 KCl Target Interference in SEC Vidicon

The data on page 11-4 of the IUE SDR, Volume I, are used to develop a failure criterion. If a constant flux of 200 electrons/cm^2-sec corresponding to a 5-year cumulative fluence of 3×10^{10} electrons/cm^2 is considered as the maximum acceptable interference rate for a one-hour exposure, then referring to the electron peak penetration rate

5.3.3 (Continued)

chart for L = 5.2 and 200 electrons/cm^2-sec, a total shield of approximately 2.0 g/cm^2 is required. Of course, it should be noted that limiting the peak rate at L - 5.2 to 200 electrons/cm^2-sec by 2.0 g/cm^2 results in a 5-year accumulation of considerably less than 3 x 10^{10} electrons/cm^2. Referring to Section 5.1.2 above, approximately 2g/cm^2 is available. Thus the basic construction of the camera head module appears to provide adequate shielding of the SEC target from penetrating electron flux interference for the L - 5.2 level, which is the worst case. Bremsstrahlung interference is considered negligible.

5.3.4 SEC Preamplifier Noise

Since the SEC preamplifier noise is important to the ultimate sensitivity for the detection of UV photons, the effect of ionizing radiation on the noise of JFET's was considered. Krishnan and Chen, (Reference 61) have concluded that generation - recombination noise is the component of noise most sensitive to increase following electron bombardment. The effect is similar in both n-channel and p-channel devices and is characterized by two time constants, one due to traps in the gate-channel depletion region and the other due to traps in the channel. The effect is most pronounced at low frequencies, but still very significant above 1KHz. "At an electron fluence of 1 x 10^{15} e/cm^2, the minimum noise figure at 600 KHz was increased by a factor of four or five for either type of transistor; the equivalent noise current measured with a 2.2KΩ source resistance at 100 KHz was increased by a factor of about 40 for the p-channel transistor and by a factor of about 60 for the n-type channel transistor; but the changes in gm and I_{DSS} are less than 20 percent of the pre-irradiation value." The transistors tested were Motorola 2N3824 and Texas Instrument 2N3909.

5.3.4 (Continued)

The system performance is preamplifier noise limited for exposures under about 3 hours. However, preamplifier shielding sufficient to protect the electronics from the usual damage mechanisms ($\sim 10^{12} e1/cm^2$) seems adequate to prevent preamplifier noise increase.

5.4 UV CONVERTER AND SEC VIDICON TEST PLAN

The vidicon tests needed are induced noise tests and permanent damage (total dose) tests. The expected electron flux is sufficiently low that it should be possible to complete the noise tests first without subjecting the devices to a significant total dose. Accelerated total dose exposures could then be made on the same devices. The possible noise effects are fluorescence in various optical elements, secondary electron emission, photo and compton electron emission and changes in charge on the storage element (SEC target). The possible total dose effects include reduced optical transmission of some of the optical elements, changes in photo sensitivity of the photo cathodes, and production of pin holes in the SEC target.

The easiest test, if no serious malfunction is encountered, would be to irradiate the entire vidicon tube and UV converter uniformily with an equivalent electron spectrum and observe any changes in readout. It would be valuable, though, to know which element of the assembly produces any changes observed to be caused by ionizing radiation so that additional shielding of that element may be considered. It is, therefore, proposed that several of the elements be exposed separately as shown in Table 5-1.

5.4.1 Electron Flux Effects (Active Noise Test)

It is possible to accomplish the tests for the dose rate effects on the complete assembly by using electrons of selected energies as shown below.

TABLE 5-1 SEC TEST PLAN OUTLINE

5.4.1 ELECTRON FLUX EFFECTS (ACTIVE NOISE TEST)

5.4.1.1 UV CONVERTER

5.4.1.1.1 MgF_2 WINDOW FLUORESCENCE. IRRADIATE WITH ELECTRONS. E_{max} < 1.7 MeV, i.e., P-32, Sr-Y-90 OR ACCELERATOR

5.4.1.1.2 P_{11} FLUORESCENCE. IRRADIATE WITH E_{max} > 1.7 MeV Sr-Y-90 OR ACCELERATOR

5.4.1.2 SEC VIDICON

5.4.1.2.1 FIBER OPTIC WINDOW FLUORESCENCE. IRRADIATE WITH E_{max} < 1.7 MeV P-32, Sr-Y-90 OR ACCELERATOR

5.4.1.2.2 INTERNAL TUBE NOISE. IRRADIATE SEC WITHOUT UV CONVERTER THROUGH FIBER OPTIC WINDOW WITH E_{max} >1.7 MeV, Sr-Y-90 OR ACCELERATOR. IRRADIATE THROUGH SIDE, INCLUDING MAGNETIC SHIELD, WITH E_{min} > 3 MeV

5.4.1.3 ELECTRON SOURCES.
USE INCIDENT FLUX OF 10^8 ELECTRONS/cm^2 SEC IF BETAS ARE USED, OR CORRECT OTHER SPECTRA TO GIVE AT LEAST 10X EXPECTED PENETRATING FLUX

5.4.2 PERMANENT DAMAGE

5.4.2.1 IRRADIATE A MgF_2 WINDOW TO $\geq 10^{14}$ ELECTRONS/cm^2, $\geq$ 1.7 MeV. MEASURE CHANGE IN UV TRANSMISSION EVERY ½ DECADE FROM 10^{10} ELECTRONS/cm^2

5.4.2.2 IRRADIATE A FIBER OPTIC WINDOW TO $\geq 8.4 \times 10^{12}$ ELECTRONS/cm^2, $\geq$ 1.7 MeV. MEASURE CHANGE IN OPTICAL TRANSMISSION 4000 TO 5000 Å EACH ½ DECADE FROM 10^9 ELECTRONS/cm^2.

5.4.2.3 IRRADIATE COMPLETE SEC VIDICON – UV CONVERTER ASSEMBLY, INCLUDING MAGNETIC AND OTHER SHIELDING, TO $\geq 8.4 \times 10^{12}$ ELECTRONS/cm^2, $\geq$ 3 MeV, OR $\geq 10^{14}$ ELECTRONS/cm^2 EQUIVALENT SPACE SPECTRUM. ROTATE WHILE IRRADIATING TO SIMULATE ISOTROPIC FLUENCE. MEASURE CHANGES IN PERFORMANCE AFTER EXPOSURE AS PROOF OF ADEQUATE SHIELDING.

5.4.1.1 UV Converter

5.4.1.1.1 MgF_2 Window Fluorescence

The first exposure should be made to determine the fluorescence of the MgF_2 window. The window would be exposed to electrons with a maximum range just short of the window thickness and at fluxes to at least 10 times the maximum expected, i.e., 10^8 electrons/cm^2 sec. Exposure times should be comparable to the longer times to be used on the mission, e.g., 1 hour to 10 hours, unless appreciable noise background increase is seen earlier.

Electron energies of the order of 0.7 to 1 Mev would be required, depending on the final choice of MgF_2 thickness. The low flux, of 10^8 electronic cm^{-2} sec^{-1}, makes the use of a radioisotope source feasible. More will be said about electron sources later. If the SEC is read out (scanned) after each exposure and the readings compared with the dark, unirradiated, background readings, any increase should be caused by fluorescence in the MgF_2 if the energy of the fluorescence photons is sufficient to produce photo electrons in the CsTe photo cathode.

Many combinations of shields, columnated electron beams, low-level spots of light, etc., are possible if they help determine the extent of a change in the lower detection limit.

5.4.1.1.2 P11 Fluorescence

Having determined the MgF_2 fluorescence, a second group of exposures should be made with electrons with a range greater than the MgF_2 window thickness. The thickness of material between the window and P11 is almost insignificant (as also is the P11) so that an energy of the order of 2 MeV would suffice for the second group of exposures. It would be

5.4.1.1.2 (Continued)

difficult to avoid irradiating the fiber optic window under the thin P11 phosphor, but, because the P11 is known to be a very efficient phosphor, any fluorescence in the underlying materials would be of minor significance. By proceeding as with the MgF_2 test and subtracting any MgF_2 fluorescence using care to calculate an appropriate internal fluence, the increase in lower detection limit caused by P11 fluorescence could be determined.

5.4.1.2 SEC Vidicon

5.4.1.2.1 Fiber Optic Window Fluorescence

It would probably be impractical to accurately determine the fluorescence of the fiber optics by irradiating the assembly through the MgF_2 and P11. The best method would be to irradiate an SEC without an attached UV converter. The electron beam would be normal to the end of the SEC and the energy selected so that the electron range would not exceed the thickness of the window, i.e., <1.7 MeV. Phosphorous 32 would meet this requirement. The SEC fiber optics are the same material as the fiber optics on the UV converter; both are made by Galileo. Determining the fluorescence of one fiber optic will suffice for both.

5.4.1.2.2 Internal Tube Noise

There is some probability that additional noise will result from electrons penetrating the vidicon tube, but this is difficult to assess accurately without a test. Using the data from V1 of the IUE system report, the preamplifier will contribute the equivalent of 156 photo electrons per pixel and the vidicon 1.4×10^{-2} photo electrons/pixel sec. Therefore, the vidicon noise will equal the

5.4.1.2.2 (Continued)

preamplifier noise at approximately 10^4 sec exposure. The preamplifier noise will predominate for exposure times less than 10^4 sec and the noise will significantly increase when equivalent of the order 156 photo electrons per pixel = approximately 1.4×10^7 photo electrons per cm^2 have been generated in the vidicon by high energy electrons. This is equal to 4×10^3 photo electrons/cm^2 sec for one hour. The energy of the electrons with ranges (at normal incidence) just equal to the thickness of the vidicon tube walls plus the magnetic shield is given in Table 5-2, from which it is observed that only electrons with energies exceeding 2.6 MeV penetrate the vidicon tube. The energy spectrum of the penetrating electrons is much higher that that of the accelerated photo electrons. The rate of energy loss per cm of these high energy electrons in the target is at least 10 times less than that of photo electrons from the photo cathode, accelerated through the vidicon electrostatic field, and the thickness (10 - 20μ) of the 1 - 2 percent density KCl target is less than the range of the electrons from either source. Therefore, at least 10 times as many high-energy electrons as photo electrons would be necessary to produce an equivalent noise charge in the target. Secondary electron emissions from the inner surface of the tube would only be a few percent of the incident, high-energy electron flux, and Bremsstrahlung production would also be only a few percent. It is therefore, reasonable to predict that a penetrating electron flux of at least 4×10^4 electrons/cm^2 sec would be necessary to produce a significant increase in vidicon noise by internal mechanisms. From this reasoning, it does not seem that a separate test for orbital electron interference in the SEC is of prime importance.

TABLE 5-2 ELECTRON STOPPING POWER OF SEC VIDICON TUBE AND μ METAL SHIELD

MATERIAL/THICKNESS	THICKNESS g/cm^2	THICKNESS, INCL. μ METAL g/cm^2	STOPPING POWER Mev[1]
Fiberglas Window, 1/8"	0.8	-	1.7
Kovar, 1/32 "	0.6	1.46	2.9
Glass Wall, 1/16"	0.4	1.26	2.6
Ceramic, 1/8"	0.8	1.66	3.3
MgF_2 Window 0.1"	0.8	-	1.7
MgF_2 + 2 Fiberglas Windows	2.4	-	4.7

Calculated from $R(g/cm^2) = .542E\ (Mev) - .133$

5.4.1.3 Electron Sources

The electron flux to which the SEC vidicon should be tested is 10^8 particles/cm^2 sec. It is inconvenient to generate such a low current beam with an accelerator, but a radioisotope source of this strength is very convenient to work with. Easily procured radioisotopes which emit only beta radiation in the energy range of interest are given in Table 5-3.

The proton dose to the fiber optics will be similar to the electron dose, and the proton dose penetrating the magnetic shield and SEC-Vidicon tube walls will be approximately 5 times the electron dose. We are, therefore, recommending that the fiber optic window and the inside of the SEC-Vidicon be tested to 50 times the 95 percent proton dose to include any uncertainty in the relative effectiveness of protons to electrons. Alternately, the fiber optics and the complete SEC-Vidicon, UV converter could be tested with proton radiation, using either $\geq 1.6 \times 10^{11}$ protons/cm^2 with energies of 60 MeV, or an equivalent 20 MeV penetrating spectrum.

The tests recommended consist of determining the change in optical absorption of the MgF_2 window and the fiber optic windows in the optical range of interest, and a proof of design test on the complete assembly of SEC, UV converter, magnetic shield, and a simulated shadow shield to reduce the radiation incident on the window end of the assembly to that expected in the satellite. This test will also serve as a test on the KCl target, but with the reservation that the target will be scanned of the order of 10^6 times and irradiated with the flood lamp nearly equal number of times during the mission. It is difficult to say whether this would enhance or heal the damage. It is assumed that an acclerated rate of exposure, necessitated by practical

TABLE 5-3 ISOTOPE SOURCES

ISOTOPE	E_{MAX3} Mev	HALFLIFE	RANGE, gm cm^{-2}
Cl-36	0.7	10^6 y	0.246
P-32	1.7	14d	0.788
S_r-Y90	0.6, 2.3	28 y	1.11

5.4.1.3 (Continued)

considerations, will produce at least as much change as the same dose at a lower rate would. Some indication of the rate of annealing, given some initial damage, could be obtained by remeasuring the response of the windows and the assembly at various times after exposure.

It may be preferrable to irradiate a vidicon tube passively or in an electrically simplified test fixture, and return it to NASA for electrical testing. Care should be taken in the case of passive irradiation and in the design of the test fixture to prevent the production of unrealistic electrical stress on the target.

It would also be possible to perform optical tests on the windows at a facility different from the irradiation facility, but that would be less convenience because several cycles of irradiation and testing are recommended.

Some data on the transmission of the fiber optic window after exposure of 5×10^5 rad to 10^6 rad was transmitted to us from Galileo Electro-optics Corporation, from which Table 5-4 was constructed. The type of radiation source was not given, however.

Radioisotope source strengths needed are in the 10 millicurie range, and are easy to procure in the form of very thin deposits covered with a thin window to prevent contamination and backed by sufficient low Z material to absorb all the betas and facilitate handling. The beta energy spectrum has some similarity to the trapped electron spectrum, so would produce a similar depth dose.

TABLE 5-4 PERCENT TRANSMISSION, FIBER OPTIC WINDOW

DOSE	4000Å	4250Å	4500Å	4750Å	5000Å	5250Å	5500Å
5×10^5 R	0.93	0.97	0.95	0.95	0.96	0.98	0.97
1×10^6 R	0.91	0.94	0.95	0.95	0.96	0.98	0.97

5.4.1.3 (Continued)

The 0.1 inch MgF_2 window will stop all electrons $\leq$1.72 MeV, therefore, a P-32 source with a small additional absorber would be a good choice to irradiate the window and Sr-Y-90 betas would penetrate the window and irradiate the P11 phosphor. (Ytrium -90 alone would be adequate except for inconveniently short half life of 64 h). Alternately, Sr-Y-90 could be used for both tests by first using an abosrber to reduce the electron range to just less than the MgF_2 window thickness and then removing the absorber to irradiate the P11 phosphor.

Chlorine -36 was included in the list of radioisotopes because, although the beta range is less than half the thickness of MgF_2, the long half life would make it a more convenient source than P-32 for testing the window fluorescence. Also, the Sr-90 betas from a Sr-Y-90 source have a spectrum similar to Cl -36 and a Cl-36 source could be used to obtain a correction factor for the Sr-90 contribution to the window fluorescence in the test for P-11 fluorescence.

The selection of suggested radioisotopes was limited to isotopes which do not emit gamma radiation. However, the gamma interaction probably is only a few percent that for betas, and the selection of isotopes could be extended if those which emit both betas and gamma were considered.

5.4.2 Permanent Damage (Total Dose)

Electron radiation was specified for the active noise tests because trapped proton energies are too low to penetrate the satellite skin and it is assumed that scientific data will not be taken during large solar flares. The flare protons will contribute to the total dose,

5.4.2 (Continued)

however, and when considering whether or not a total dose test should be made with protons, electrons or both it was necessary to consider relative rad dose of each kind of particle and the relative damage per rad caused by each kind of particle.

5.4.2.1 MgF_2 Window

The belt electron dose will exceed the 95 percent proton dose for areas shielded with less than approximately 1.2 gm/cm^2 and the proton dose will exceed the electron dose for shielding greater than 1.2 g/cm^2. If it is assumed that approximately 0.5 g/cm^2 shielding will be added to protect the MgF_2 from a total mission dose of greater than 10^{13} electrons/cm^2, the electron dose to the MgF_2 will be approximately 5 times the proton dose. An electron test to 10^{14} electrons/cm^2 should cover the uncertainties reasonably well.

5.4.2.2. Fiber Optic Windows

The electron range in the fiber optic on the SEC Vidicon is also 1.7 MeV and the same sources can be used to test the fiber optic for fluorescence and to irradiate the inside of the tube through the fiber optic window.

5.4.2.3 SEC-Vidicon - UV Converter Assembly

The minimum energy electron which will penetrate the vidicon plus the magnetic shield was tabulated above. There is not an available radio-isotope with sufficient beta energy to test the adequacy of the self-shielding of the tube and magnetic shield. Therefore, an

5.4.2.3 (Continued)

accelerator source is required if this test is to be made. The current of a dc accelerator such as a Van de Graf or dynamitron can be reduced to low levels by various combinations of running at low filament current, using a filament with low thermionic emission, spreading the beam with lenses, such as magnetic quadrapoles, and scattering the beam with a thin foil. If scattering is used, it will be necessary to place the vidicon some distance from the scatterer to obtain the desired reduction in flux. In addition it will be necessary to account for the change in energy spectrum caused by both the scattering foil and the intervening air.

A linear accelerator is a possible alternate to a dc accelerator. The required low average electronic flux can be obtained by a combination of short pulse width and low pulse repetition rate, probably in conjunction with magnetic lenses and scattering. The minimum energy of many linacs is approximately 5 MeV and the maximum energy is typically 25 to 50 MeV. This opens several options of using a higher energy electron beam plus scattering to obtain an electron spectrum more representative of belt electrons than could be obtained from a dc accelerator with a maximum energy of a few MeV.

6.0 PREVIOUS SATELLITE EXPERIENCE

6.1 SPACECRAFT CHARGING EFFECTS

Reference 62 discussed anomalous behaviour in subsystems of several different spacecraft in synchronous orbit, particularly ATS-5.

Flight data and laboratory simulations indicate that portions of the spacecraft surface charge to many kilovolts under space electron bombardment, and discharge by arcs or corona. The consequent electromagnetic pulse can couple into cables and cause interference in subsystems. Also degradation of the thermal blanket can occur from removal of the metalization by the arc discharge.

A number of recommendations are made for spacecraft design practices in the reference.

6.2 S^3 MOSDAM EXPERIMENT

Several MOS device types, the GI M2009, AMI SC1304, and the RCA CD4007A were flown on the S^3 satellite (Reference 63) as an experiment designed to measure MOS degradation as a result of space radiation. The data were obtained to permit evaluation of the extent of rate effects, if any.

The dose-depth profiles for the S^3 electron and proton environments are shown in Figures 6-1 and 6-2. The internal environment level from the dose-depth profiles for spherical shielding for the semiconductor chips is shown in Table 6-1, using spacecraft configuration data provided by Wannemacher. MOS test data from several sources have been compiled in Table 6-2 to indicate the magnitude and variability of MOS response. The RCA CMOS data, except for the 4041A, are for the early, less vulnerable devices, to be comparable to the devices used in MOSDAM. The particular CMOS laboratory data used to compare with the MOSDAM data seem representative. The pseudo control group laboratory data are shown in Table 6-3. The MOSDAM data for which comparable laboratory data was avilable are shown in Table 6-4. Table 6-5 compares the MOSDAM data with the laboratory data. Values of dose ratio greater than one would indicate long-term annealing. Values of voltage ratios less than one would indicate long-term annealing. Thus, some long-term annealing may have occurred. However, the ratios observed are of the magnitude of environment prediction errors, moreover, the magnitudes of the ratios do not appear sufficiently large or consistent to provide anything but an additional, possibly undependable, safety factor.

Several contacts were made in the industry concerning long-term annealing. These contacts were M. Simon (RTI), B. D. Shafer (Sandia),

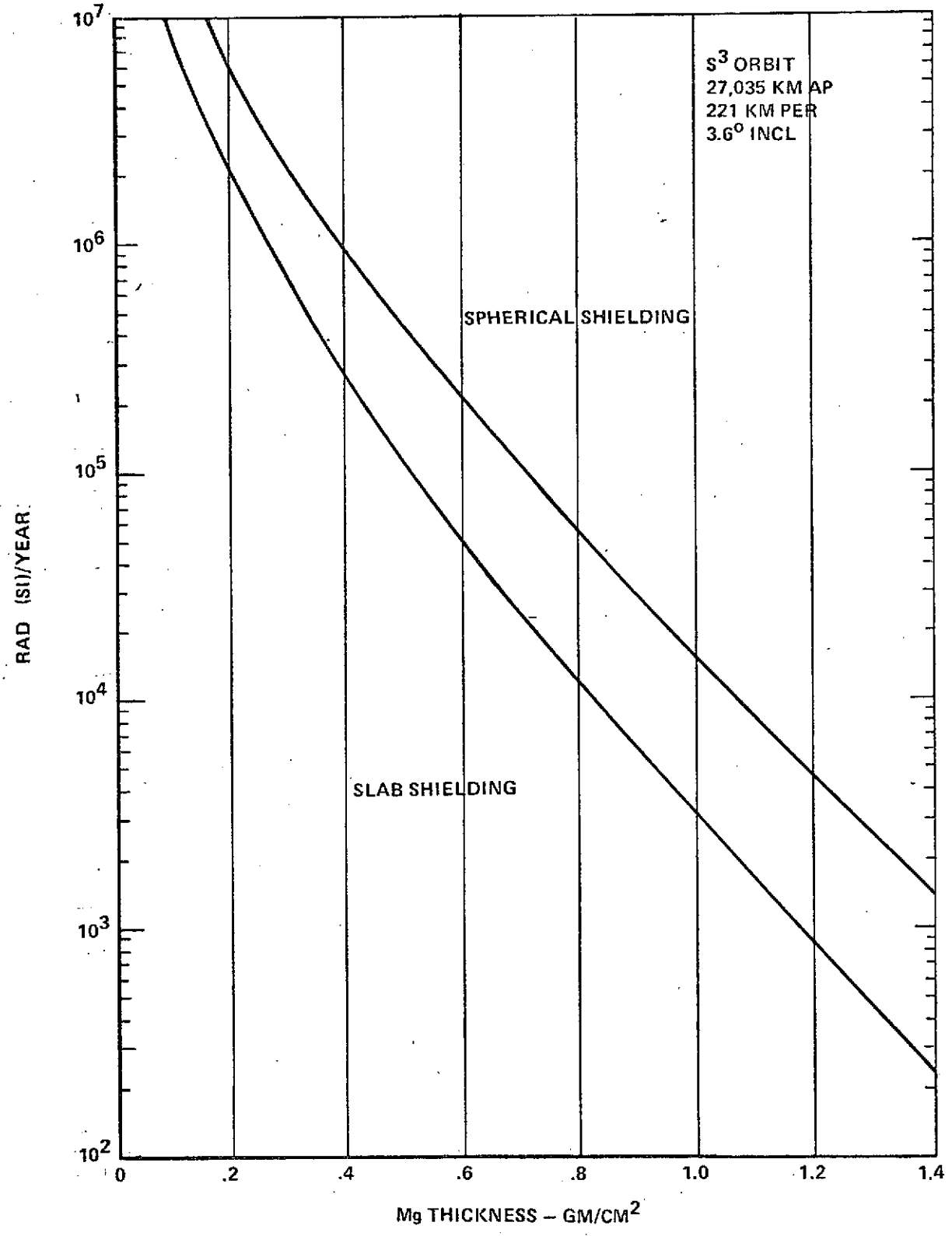

FIGURE 6-1 S^3 TRAPPED ELECTRON YEARLY DOSE

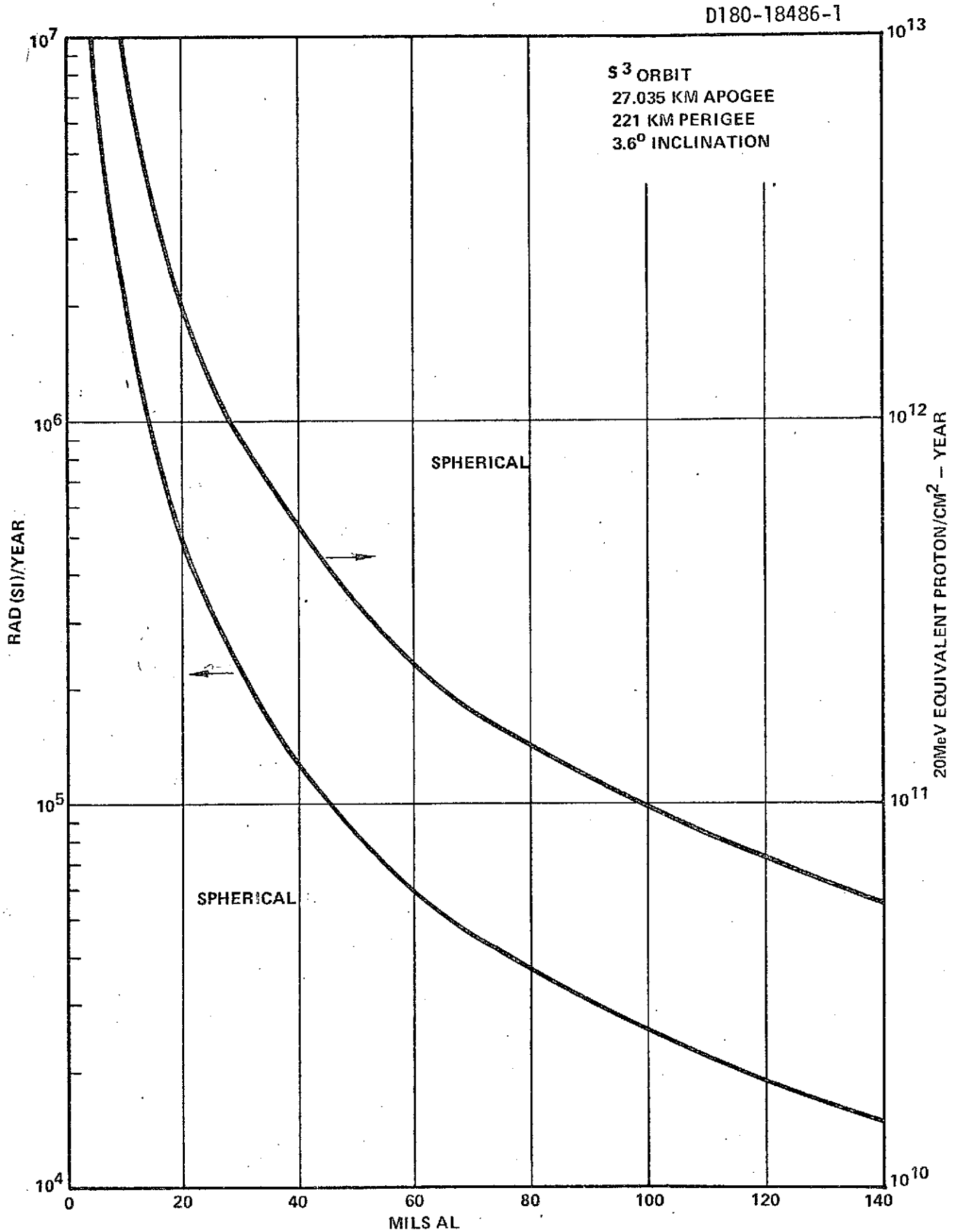

FIGURE 6-2 S^3 TRAPPED PROTON YEARLY ENVIRONMENT

TABLE 6-1 INTERNAL ENVIRONMENT MOSDAM EXPERIMENT

SIDE	ITEM	INDIVIDUAL		COMPOSITE		DOSE PER THICKNESS			DOSE PER ITEM	TOTAL
		g/cm^2	$\Omega/4\pi$	g/cm^2	$\Omega/4\pi$	PROTON	ELECTRON	TOTAL		
OUTSIDE	HOUSING, COMPONENT	.206	.4	.892	.4	2×10^4	3×10^4	5×10^4	2.0×10^4	4.6×10^4 RAD (Si)/YR = 126 RAD (Si)/DAY
	HOUSING, SPACECRAFT	.206	.4							
	CIRCUIT BOARD	.274	.4							
	PIECE PART PACKAGE	.206	1							
BOTTOM	HOUSING, COMPONENT	.206	.2	.686	.2	3×10^4	10^5	1.3×10^5	2.6×10^4	
	CIRCUIT BOARD	.274	.2							
	PIECE PART PACKAGE	.206	1							
TOP	SPACECRAFT	∞	.4	–	–	–	–	–	–	

TABLE 6-2. COMPARISON OF MOS LABORATORY DATA

WITH MOSDAM		V_T							
		N-CHANNEL				P-CHANNEL			
		10^5 RAD		10^6 RAD		10^5 RAD		10^6 RAD	
SOURCE (See Notes)	DEVICE	BIAS		BIAS		BIAS		BIAS	
		0 V	10 V	0 V	10 V	0 V	-10 V	0 V	-10 V
REF. 64	4001A	** 0.45	1.6	+0.85	TOO LARGE	** 0.55	0.2	2.6	0.75
REF. 64	4007	0.5	2.9	1.0	4.7	0.85	8.2	1.8	5.7
REF. 65 *	4007	0.5	1.6	+0.6	TOO LARGE	0.3	~0	1.2	1.0
REF. 66 *	4007	0.6	2.7	+0.6	TOO LARGE	0.4	~0.2	2.5	0.9
REF. 67	4007A	+0.4	1.9	+2.0	2.0	1.4	0.5	4.6	2.5
REF. 67	4007	0.3	1.5	0.2	1.6	0.2	6.3	0.75	7.0
REF. 68	4007	---	---	---	---	0.4	5.6	---	---
REF. 69	4041A	~2.0	~8.2	---	---	~2.0	~3.0 AT 5.6 x 10^4 RAD ~3.7 V	---	---
REF. 70	AMI PMOS TEST DEVICE	---	---	---	---	---		---	---

NOTES ON COMPARISON OF MOS DATA

1 The data from Ref. 64 through 68 compare the variations in Laboratory test data for the type of devices used in the MOSDAM experiment. The intent is to determine a pseudo control group for the MOSDAM experiment.

2 The data from Reference 69 shows the increased degradation of the "New A" series.

3 Reference 70 provides additional PMOS test data.

*PROBABLY "A" SERIES
**COMPARED WITH MOSDAM

TABLE 6-3 LABORATORY DATA – PSEUDO CONTROL GROUP FOR MOSDAM

DEVICE	CHANNEL	BIAS VOLTS	DOSE FOR ΔV_T = 1/2V	ΔV_T FOR 10^5 RAD
CD4001A (REFERENCE 64)	P	0	8×10^4	0.55V
	N	0	1×10^5	0.45V
AMI1304 (REFERENCE 64)	P	0	1.4×10^4	1.3
	P	-10	1.8×10^4	1.1

TABLE 6-4 MOSDAM DATA

DEVICE	CHANNEL	BIAS VOLTS	TIME FOR ΔV_T = 1/2 V DAYS	DOSE RAD FOR ΔV_T = T/2 V	ΔV_T FOR 10^5 RAD
CD4007A (Ref 64)	P	0	330	4.16×10^4	0.6
	N	0	650	8.19×10^4	0.21
AMI1304 (Ref 64)	P	0	270	3.4×10^4	0.8
	P	-12	230	2.9×10^4	1.0

TABLE 6-5 MOSDAM COMPARISON WITH LAB DATA (1)

DEVICE	CHANNEL	BIAS VOLTS	DOSE RATIO, $\left(\frac{\text{MOSDAM DOSE}}{\text{LAB DOSE}}\right)$ FOR $V_T = 1/2$	VOLTAGE RATIO, $\left(\frac{V_T \text{ MOSDAM}}{V_T \text{ LAB}}\right)$ FOR 10^5 RAD(Si)
CD 4001A (REFERENCE 64) (2) (3)	P	0	0.52	~1
	N	0	0.82	0.47
AMI 1304 (REFERENCE 64) (3)	P	0	2.43	0.62
	P	-10	1.6	~1

NOTES ON MOSDAM COMPARISON WITH LAB DATA

(1) The ambient temperatures during irradiations in the MOSDAM and the lab experiments were found to be nearly equal.

(2) Danchenko's data on CD4001A are compared to MOSDAM CD4007A data since both types of devices were made not far apart in 1971. There are no lab data available on CD4007A devices for the same period. However, the radiation hardness of CD4001A and CD4007A devices is presumably the same, due to identical oxide processing techniques.

(3) The time delay between radiations and measurements is not indicated in Danchenko's report. If the short term (0-few hrs.) annealing was not negligible, the amount of damage was underestimated.

6.2 (Continued)

H. Sanders (Sandia), L. Palkuti (NRL), and R. Burghard (Sandia). The general consensus was that long-term annealing did occur, however, opinion on its extent ranged from small to very significant. The relevant data base was small, however.

6.3 COMSAT RADIATION PROTECTION

Space radiation protection has been incorporated into the COMSAT satellites. Discussions were held with COMSAT and Hughes personnel. A summary of the techniques used is given below.

- Radiation hardening is started at the design stage.
- Radiation test data on every piece part flown is obtained by using existing data or performing additional tests.
- In general, piece part radiation screening is done by sample testing on device lots.
- 100% radiation screening of piece parts by applying 5-10% of expected radiation level without annealing is done when budget permits.
- Irradiate and anneal is not favored because of expense and concern over reliability impact.
- Detailed dose distribution calculations within spacecraft boxes are performed.
- Use of MOS is minimized, and where used, MOS is spot shielded. Recent RCA MOS are shielded to 10^3 rad (Si).
- Weight problem is solved with powerful boosters.
- For the one satellite failure observed, which occurred after four years, no screening was done, but MOSFETS were shielded.

7.0 DETAILED SHIELDING CALCULATIONS

7.1 SHIELDING MATERIAL SELECTION

It is desired to select (choose among alternate z values) a shield material that provides a specified internal environment with minimum weight. Competing physical processes (electron dose and bremsstrahlung dose) result in a complex relationship between the optimum material and the desired internal total dose.

The electron dose alone is most effectively shielded by materials of high z, as they produce increased scatter in the material. For electron-dose reduction alone, high z material is then best. However, increasing z leads to increased bremsstrahlung production. This results in the electron plus bremsstrahlung depth-dose curves decreasing in slope at greater thicknesses. Depth-dose curves for z = 13, 22, 52, and 92 are shown in Figure 7-1. The dose curves actually cross over at various thicknesses, with, for example, uranium (z=92) crossing the aluminum curve at 1.15 g/cm^2, or 5.8 x 10^3 rad/year. The solar proton-attenuation curve is only weakly effected by changes in material. The optimum material will then depend on the internal dose level required, and the weight savings possible will also depend on the internal dose level and resultant optimum z material.

Choosing a required internal dose level, for example 1.7 X 10^3 rad/year, determining the required thickness for each z from Figure 7-1, and then plotting z versus thickness, then repeating for several required internal levels, results in the curves of Figure 7-2. The value of z for minimum weight then can be seen for a particular internal-environment requirement.

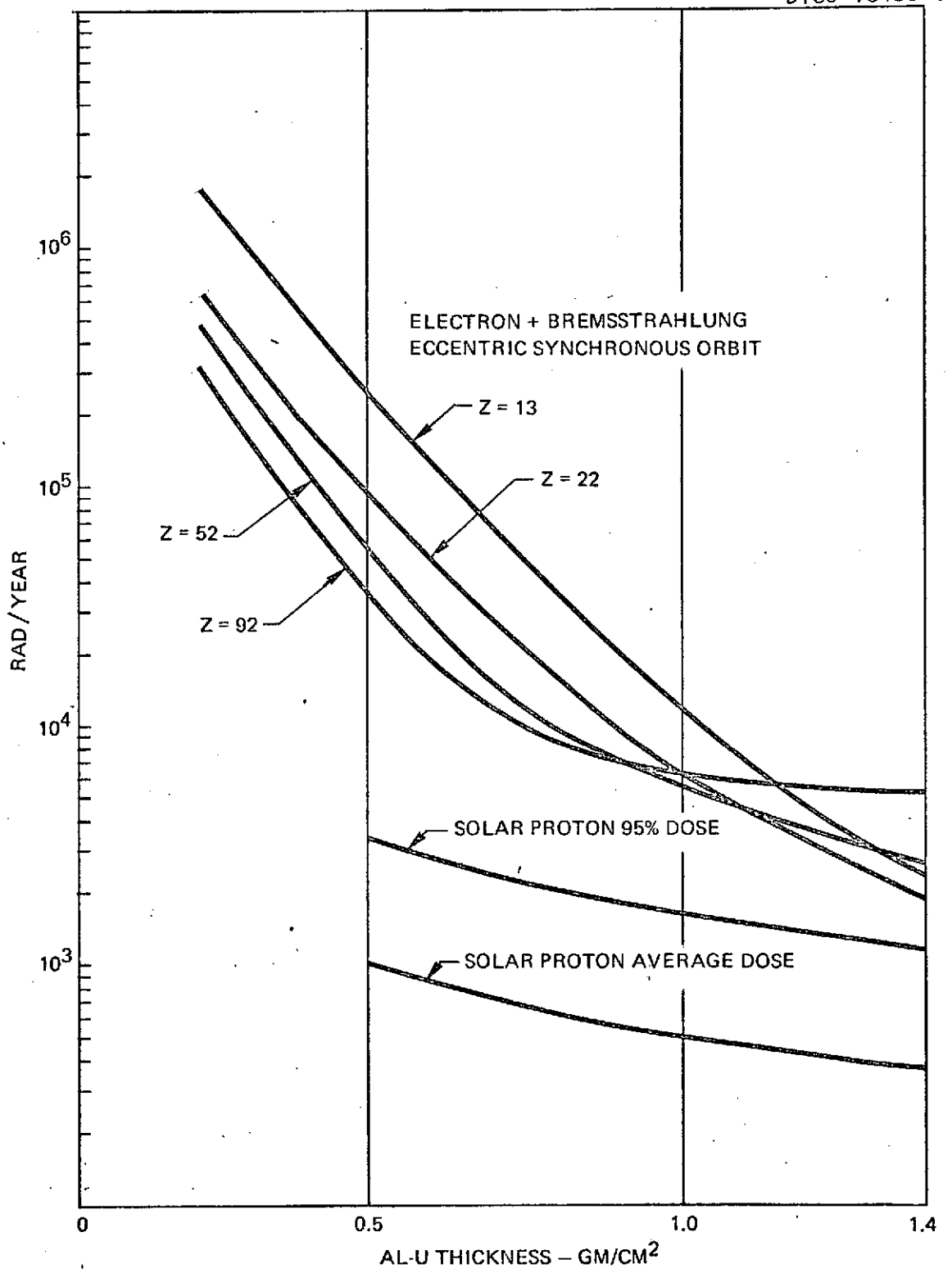

FIGURE 7-1 TOTAL ELECTRON AND BREMSSTRAHLUNG DOSE FOR DIFFERENT MATERIALS Z = 13 TO Z = 92

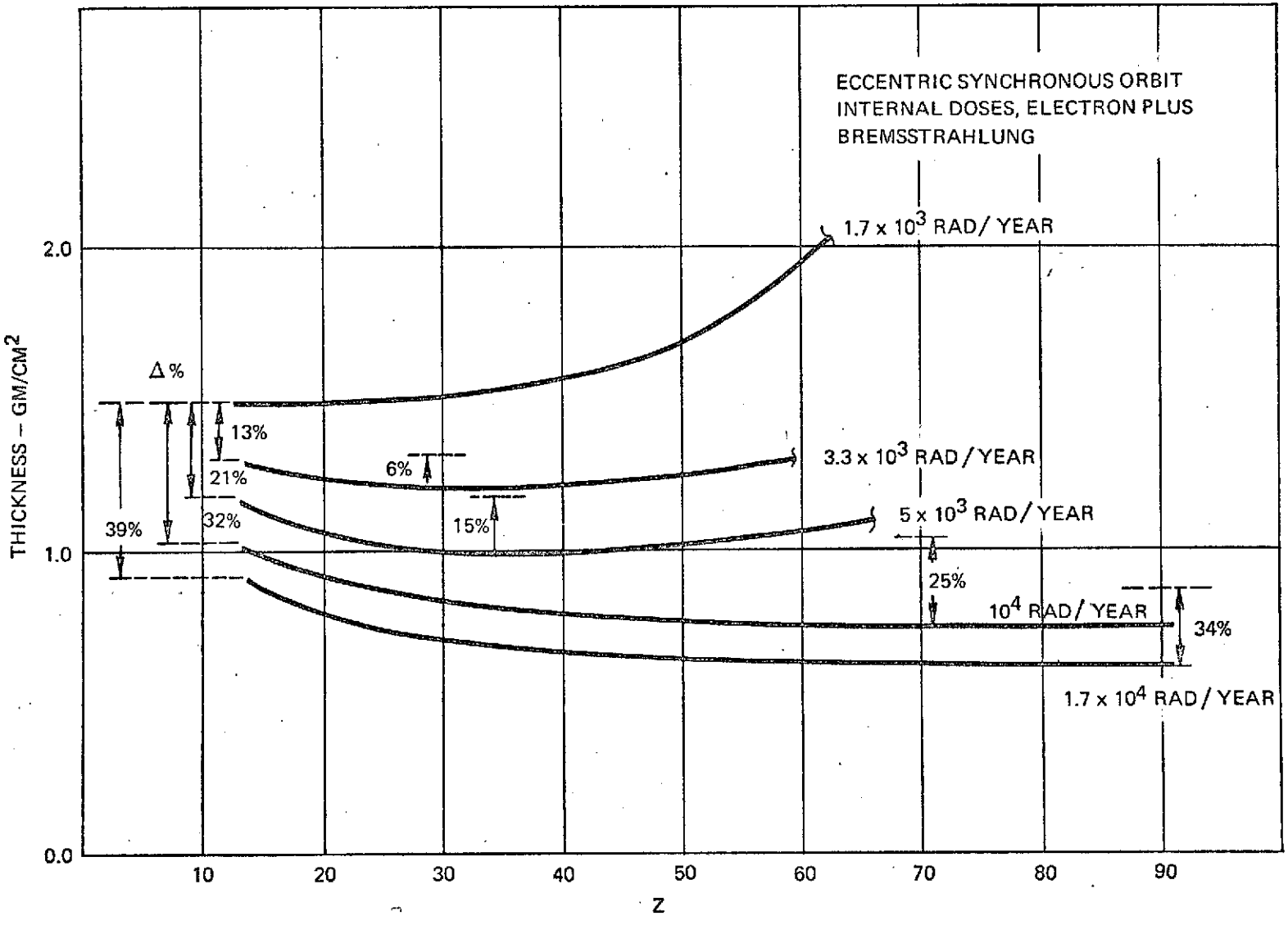

FIGURE 7-2 REQUIRED THICKNESS AS A FUNCTION OF INTERNAL DOSE AND MATERIAL

7.1 (Continued)

For low dose levels (1.7 X 10^3 R/Yr) aluminum is optimum, while for higher levels increasing z materials are optimum. The percent weight saving possible for different criteria levels with aluminum are shown at the left side of Figure 7-2, while the percent weight savings over aluminum obtainable by choosing the optimum material are shown on the right side of Figure 7-2. These results are given for the electron and bremsstrahlung dose only.

Choosing the optimum z for each internal dose level from Figure 7-2, and plotting optimum z versus dose, the optimum z shield without solar proton dose curve in Figure 7-3. The result of adding solar proton 95 percent dose is shown. Figure 7-3 also shows the material thicknesses required for an aluminum shield to reduce both the electron plus bremsstrahlung dose to a given level, and also to reduce the total radiation environment; electron dose, bremsstrahlung dose, and solar proton dose, to a given level. Note that for higher criteria dose levels (> 10^4 rad/year) high z materials offer weight savings above 20 percent, but as the criteria dose is lowered the optimum material z and the possible weight saving are both reduced.

It is important to note that the detailed shield weight calculations are keyed to criteria of 5 X 10^3, 10^4, and 5 X 10^4 rad (Si) of transmitted electron dose plus nominal proton dose. Bremsstrahlung dose and the 95% solar proton dose are not included. Referring to Figure 7-3, which includes bremsstrahlung, a level of 1.7 X 10^3 rad (Si)/yr (5 X 10^3 rad (Si) mission) corresponds to 1.5 gm/cm^2, then adding the 95% solar proton criteria dose, 3.3 X 10^3 rad (Si)/yr or 10^4 rad (Si)/mission results. MOS failures and some bipolar transistor failures are expected in the neighborhood of 10^4 rad (Si).

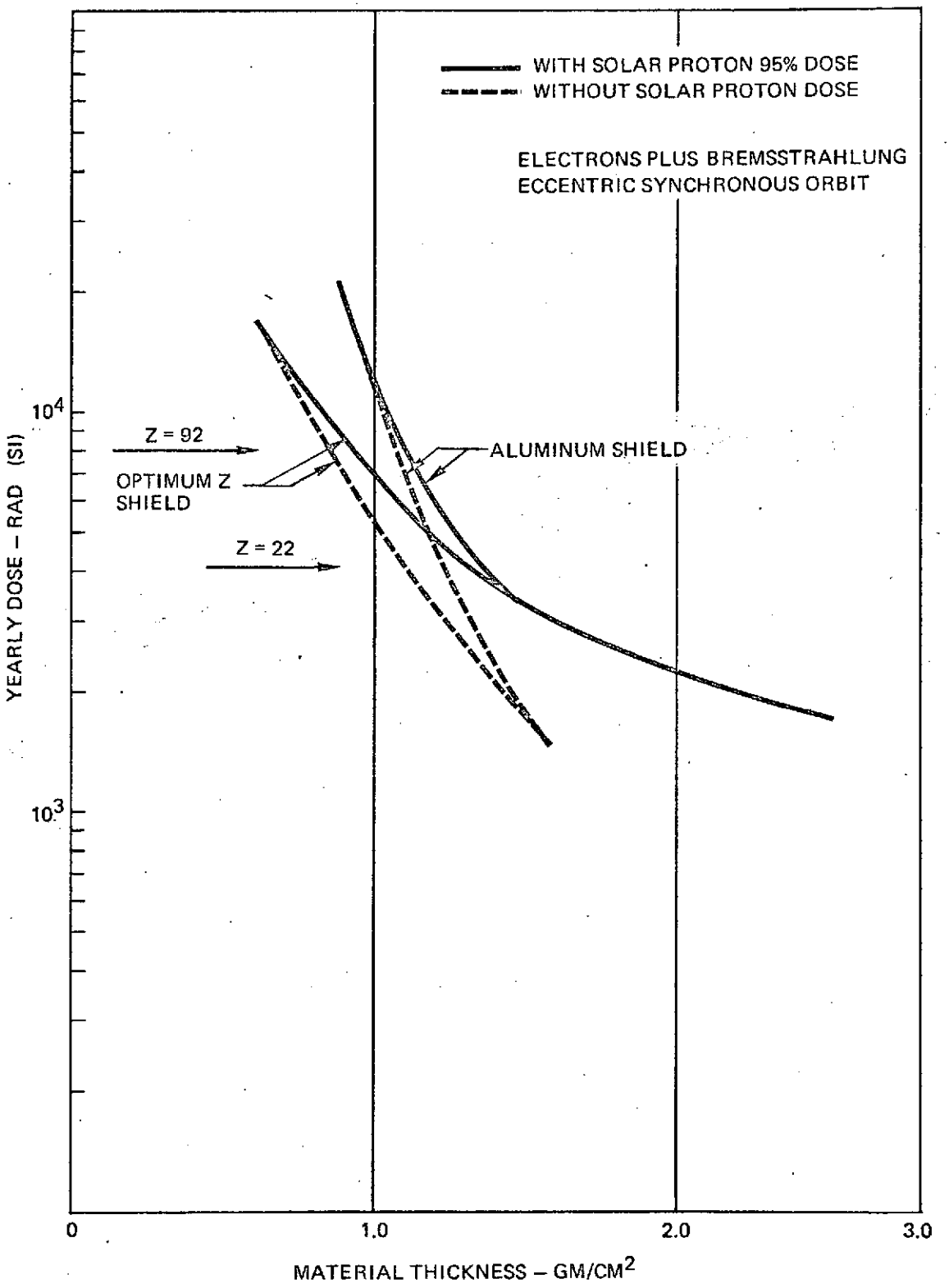

FIGURE 7-3 SHIELDING REQUIREMENTS FOR VARIOUS MATERIALS

7.1 (Continued)

The basic safety factors are: 1) the 95 percent solar proton criteria is about three times a predicted mean value, 2) the possibility of long-term annealing of the semiconductor damage, and 3) slight conservatism in the shielding calculations as a result of using the spherical shielding values.

These safety factors are balanced by the significant possibilities of the existence of unusually radiation sensitive components or small circuit design margins in critical applications which are undetected because of the limited scope of this study, as well as uncertainties in predicted belt environment levels. Thus the shielding thicknesses corresponding to 5×10^3 rad (Si) electron dose are recommended for all system components except those for which specific data permits setting higher levels (e.g., mechanism electronics, computer central processor module (CPM), etc.). For this criteria aluminum is the best shield. However, if decreased weight and consequent greater risk is necessary, the data in Figures 7-1 through 7-3 permit choice of optimum shield material for any desired internal environment criterion.

7.2 SHIELDING CALCULATION METHOD

7.2.1 Solid Angle Calculation Method

Determination of shielding for the IUE was calculated considering both the material immediately surrounding sensitive piece parts and adjacent, nontouching masses which provide some additional protection (shadow shielding). To determine the effect of any object providing shadow shielding, its effective thickness and the solid angle obscured by the object as viewed from some desired dose point must be known. The method used for calculating solid angles is developed below for a rectangular obscuring surface.

As shown below, the dimensions of the obscuring surface are l and m. The dose point P is a perpendicular distance C from one corner x of the surface. The vector $\vec{r}$ is the directed distance to an element of surface area $\vec{ds}$.

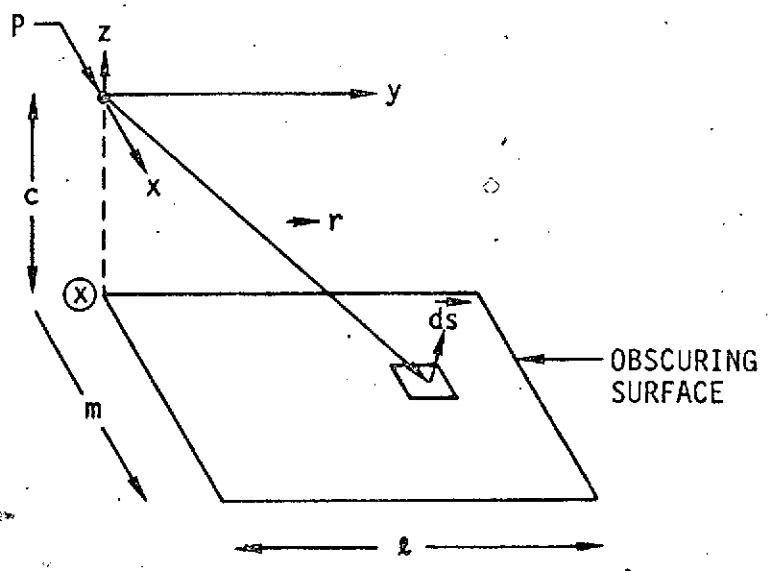

7.2.1 (Continued)

A general expression for solid angle Ω is

$$\Omega = \int \frac{\vec{r} \cdot \vec{ds}}{r^3}$$

Then, developing the expression for Ω for the rectangular surface viewed from P,

$$\vec{r} = \vec{xi} + \vec{yj} + \vec{ck}$$

$$\vec{ds} = \vec{k}\, dxdy$$

$$r = (x^2 + y^2 + c^2)^{\frac{1}{2}}$$

$$\Omega = c \int_{y=0}^{y=\ell} \int_{x=0}^{x=m} \frac{dx\, dy}{(x^2 + y^2 + c^2)^{3/2}}$$

This expression was integrated to closed form:

$$\Omega = c\ell \int_{x=0}^{m} \frac{dx}{(x^2 + c^2)(x^2 + c^2 + \ell^2)^{\frac{1}{2}}}$$

$$= \tan^{-1} \left[\frac{m\ell}{c(m^2 + \ell^2 + c^2)^{\frac{1}{2}}} \right]$$

7.2.1 (Continued)

The above formulation gives the solid angle obscured by a rectangular slab at a point a perpendicular distance c away from one corner of the slab. Similar approaches were used to calculate the solid angles of off axis discs, etc.

In some cases, it is desired to calculate the solid angle obscured by a rectangular slab for a dose point at any arbitrary position with respect to the rectangular surface.

The approach is to add (or subtract) additional rectangles until the dose point is on a line perpendicular to the corner of a new rectangle in such a manner that the solid angle of the composite rectangle and the additional rectangles can be calculated by the above formulation, then separating the desired solid angle. For example:

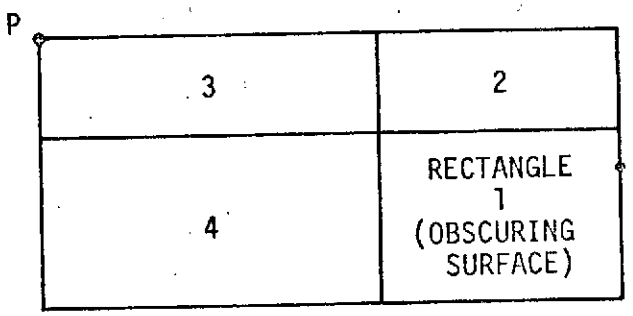

POINT P IS A DISTANCE c ABOVE PLANE OF RECTANGLES.

$$\text{THEN } \Omega_{\Sigma} = \Omega_1 + 2 + 3 + 4 = \Omega_1 + \Omega_3 + 4 + \Omega_2 + 3 - \Omega_3$$

$$\text{THUS } \Omega_1 = \Omega_{\Sigma} + \Omega_3 - \Omega_2 + 3 - \Omega_3 + 4$$

So that Ω_{Σ} is broken into elements, all of which can be calculated by the previous formulation, and then Ω_1 can be expressed in terms of known solid angles.

7.2.1 (Continued)

To illustrate this method and to indicate the capability of obscuring objects to provide shielding, an example solid angle shielding calculation is performed below.

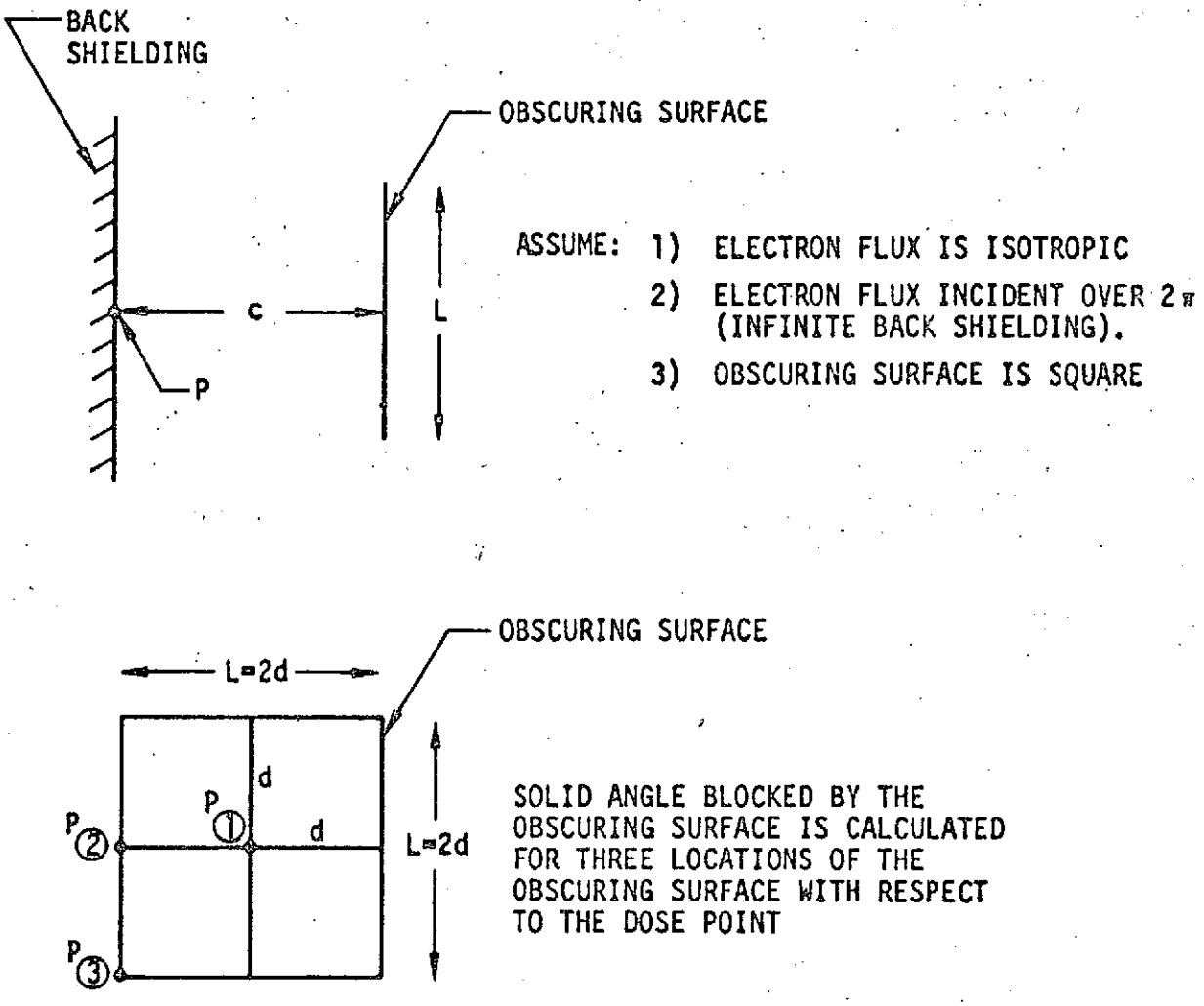

7.2.1 (Continued)

For dose point P at 1

$$\ell = d$$
$$m = d$$

so that

$$\Omega = 4 \tan^{-1} \frac{d^2}{c(2d^2 + c^2)^{\frac{1}{2}}}$$

The solid angle blocked by the obscuring surface was calculated for several separation distances c, which are expressed as fractions of the length of the side of the obscuring surface as c = 0.05L, 0.1L, 0.5L, and L.

For c = 0.05L = 0.1d

$$r = 4 \tan^{-1} \frac{1}{0.1(2.01)^{\frac{1}{2}}} = 5.72$$

then $$\frac{\Omega}{2\pi} = 0.91$$

which shows that 91 percent of the half-space is blocked by the obscuring surface at point 1 for c = 0.05L. Since it has been assumed for these examples that the rear half space is completely blocked, then only .09 percent of the sphere is unobscured.

7.2.1 (Continued)

For dose point 2

$$\ell = 2d, \; m = d$$

$$\Omega = 2 \tan^{-1} \frac{2d^2}{c(5d^2 + c^2)^{\frac{1}{2}}}$$

then for $c = .05L = .1d$

$$\Omega = 2 \tan^{-1} \frac{2}{.1(5.01)^{\frac{1}{2}}} = 2.7$$

$$\frac{\Omega}{2\pi} = .43$$

For dose point 3

$$\ell = L = m$$

$$\Omega = \tan^{-1} \frac{L^2}{c(2L^2 + c^2)^{\frac{1}{2}}}$$

then for $c = .05L$

$$\Omega = \tan^{-1} \frac{1}{.05(2.0025)^{\frac{1}{2}}} = 1.5$$

$$\frac{\Omega}{2\pi} = .24$$

The above calculations are repeated for the other values of c, and the results are given in Table 7-1.

TABLE 7-1 SHADOW SHIELDING EXAMPLE

	$\frac{\Omega}{2\pi}$			
LOC. \ C =	0.05L	0.1L	0.5L	L
①	0.91	0.82	0.33	0.13
②	0.43	0.43	0.22	0.10
③	0.24	0.23	0.15	0.08

7.2.1 (Continued)

The ratios $\Omega/2\pi$ or in some cases $\Omega/4\pi$ are the shielding factors for obscuring surfaces. Such factors are used in the detailed shielding calculations.

The fraction of unobscured solid angle for the above examples can be calculated by:

$$\text{Open Fraction} = 1 - \frac{\Omega}{2\pi}$$

The open fractions determined from the shielding factors in Table 7-1 have been plotted in Figure 7-4. Figure 7-4 illustrates that a dose point must be quite close to the obscuring surface to provide significant shielding.

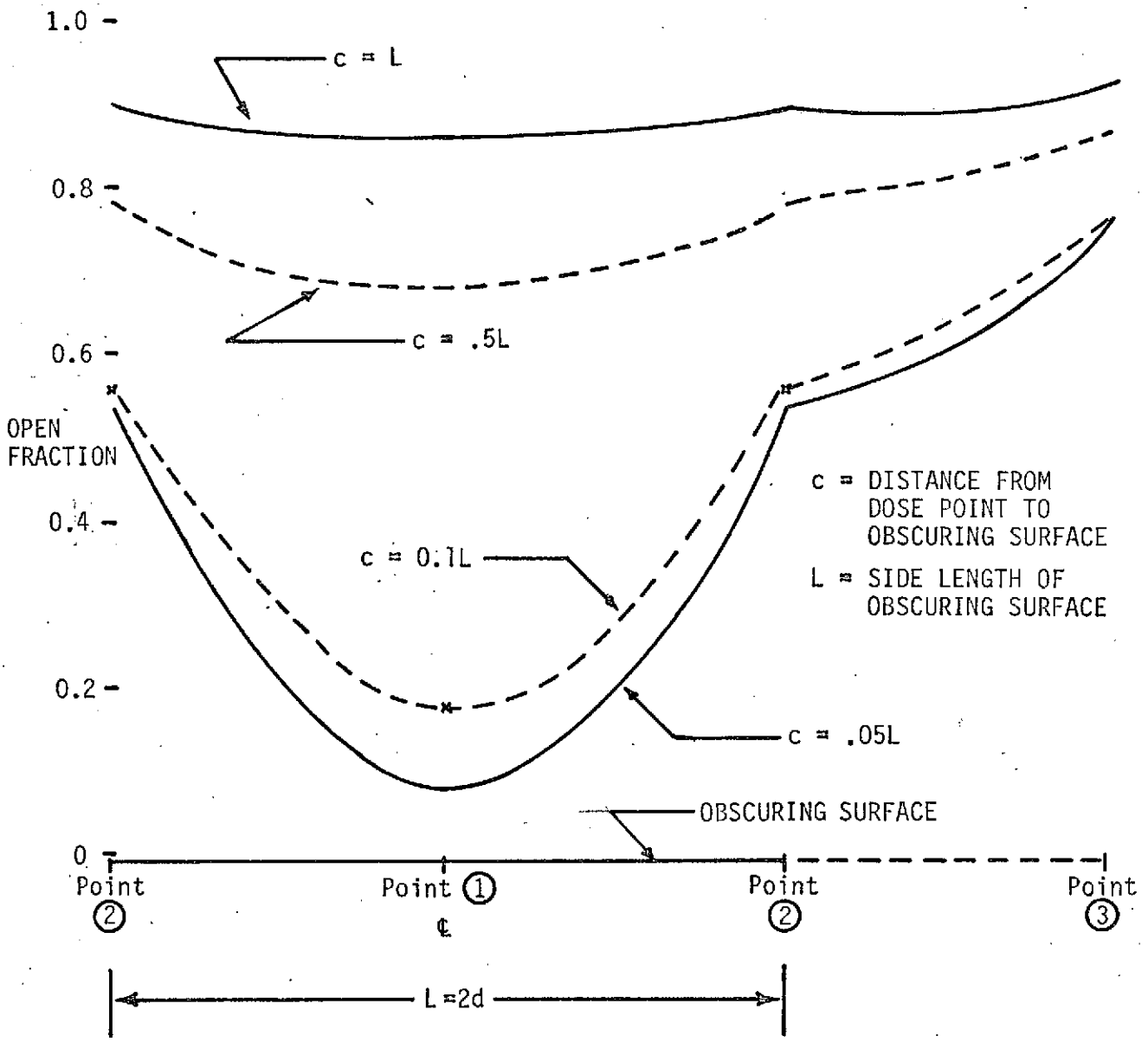

FIGURE 7-4 SHADOW SHIELDING EXAMPLE

7.2.2 Shield Thickness Calculations

The method used to perform the shielding calculations for this study considers both the shielding provided by the surrounding material (piece-part package, housing, and platform) and the shadowing provided by nearby objects. Simplifying assumptions were made to provide tractability.

The spherical values for the electron dose-depth curve were used, since the component sides were not wide enough for the slab values to be pertinent, and since the spherical values were better near component corners. For a dose point just inside each component side, calculations were made for the one-half space (2 Π steradians) just outside that side. This calculation assumed that one-half the dose reaches the dose point through the considered side, and that one-half the dose reaches the dose point from all of the other sides. This assumption is valid for a uniformly shielded box. The overall procedure, including shadow shielding, results in a uniformly shielded box. An additional refinement is made in that one octant behind the dose point is assumed to be completely blocked. In the shadow-shielding calculations, the solid angle Ω, subtended by each significant shadowing object was calculated for each component side. These solid angles determined the shielding factors $\frac{\Omega}{2\Pi}$.

The material thicknesses on each side of the sensitive piece parts separating them from the external environment were identified, tabulated, and summed. To distinguish the sides of each component, a directional system similar to cylindrical coordinates was defined. Each component side was designated by the direction it faces. In this system sides of components that primarily face the longitudinal axis of the spacecraft are termed "inside", sides facing away, "outside",

7.2.2 (Continued)

sides facing the telescope direction of the axis are termed "top", sides facing the apogee motor direction "bottom", and "left" and "right" sides face directions of left and right rotation about the axis.

To illustrate the overall method, consider the internal environment calculation for the inside of the VHF Transponder (#1). Referring to Table 7-2, the item column lists the significant shields. The housing is given as 31 mils Al (0.212 gm/cm^2); the piece-part package is assumed to be equivalent to 30 mils Al, and values are given for the main platform, upper platform, spectrograph cover, and echelle deck.

Individual shielding factors are given for each item. With the exception of the housing and piece-part package, these factors are independent (nonoverlapping). The composite column gives the total shielding occupied by each fraction of solid angle. For example, the main platform provides 0.343 g/cm^2 over 43 percent of the half space, to which is added 0.212 g/cm^2 for the housing and 0.206 g/cm^2 for the piece-part package, for a total of 0.761 g/cm^2 over 43 percent of the half space. The same procedure is used for the upper platform, the spectrograph cover, and the echelle deck. All the shadow shielders occupy 72 percent of half space, leaving 28 percent for the combination of housing and piece-part package of 0.418 g/cm^2. The dose through 0.418 g/cm^2 is 5.6 X 10^5 rad (Si), Figure 7-5, for a three-year mission, using one half the spherical shielding value (for half space). Then multiplying by 0.28, the dose contributed by that fraction of the half space is 1.57 X 10^5 rad (Si). Similar calculations are performed for the remaining items. The sum of 2.17 X 10^5 rad (Si) is the dose

TABLE 7-2 INTERNAL ENVIRONMENT VHF TRANSPONDER NO. 1

COMPONENT/SIDE	ITEM	INDIVIDUAL g/cm²	INDIVIDUAL Ω/2π	COMPOSITE g/cm²	COMPOSITE Ω/2π	DOSE PER THICKNESS	DOSE PER ITEM	SUM rad(Si)
OUTSIDE	HOUSING	.212	1.0	.418	?	5.6×10^5	?	S Band Transmitter design not available
	PIECE-PART PACKAGE	.206	1.0	—		—	—	
	S-BAND TRANSMITTER	∞	?	∞	?	0	0	?
INSIDE	HOUSING	.212	1.0	.418	.28	5.6×10^5	1.57×10^5	
	PIECE-PART PACKAGE	.206	1.0	—	—	—	—	
	MAIN PLATFORM	.343	.43	.761	.43	6.8×10^4	2.92×10^4	
	UPPER PLATFORM	.219	.04	.637	.04	1.45×10^5	5.8×10^3	
	SPECTRO COVER	.206	.16	.624	.16	1.55×10^5	2.48×10^4	
	ECHELLE DECK	∞	.09	> ∞	.09	0	0	2.17×10^5
RIGHT	HOUSING	.212	1.0	.418	1.0	5.6×10^5	5.6×10^5	
	PIECE-PART PACKAGE	.206	1.0	—	—	—	—	5.6×10^5
LEFT	HOUSING	.212	1.0	.418	1.0	5.6×10^5	5.6×10^5	
	PIECE-PART PACKAGE	.206	1.0	—	—	—		5.6×10^5
TOP	HOUSING	.212	1.0	.418	.86	5.6×10^5	4.82×10^5	
	PIECE-PART PACKAGE	.206	1.0	—	—	—		
	UPPER PLATFORM	.219	.14	.637	.14	1.45×10^5	2.03×10^4	5.02×10^5
BOTTOM	HOUSING	.212	1.0	.761	1.0	6.8×10^4	6.8×10^4	
	PIECE-PART PACKAGE	.206	1.0	—	—	—		
	MAIN PLATFORM	.343	1.0	—	—	—		6.8×10^4

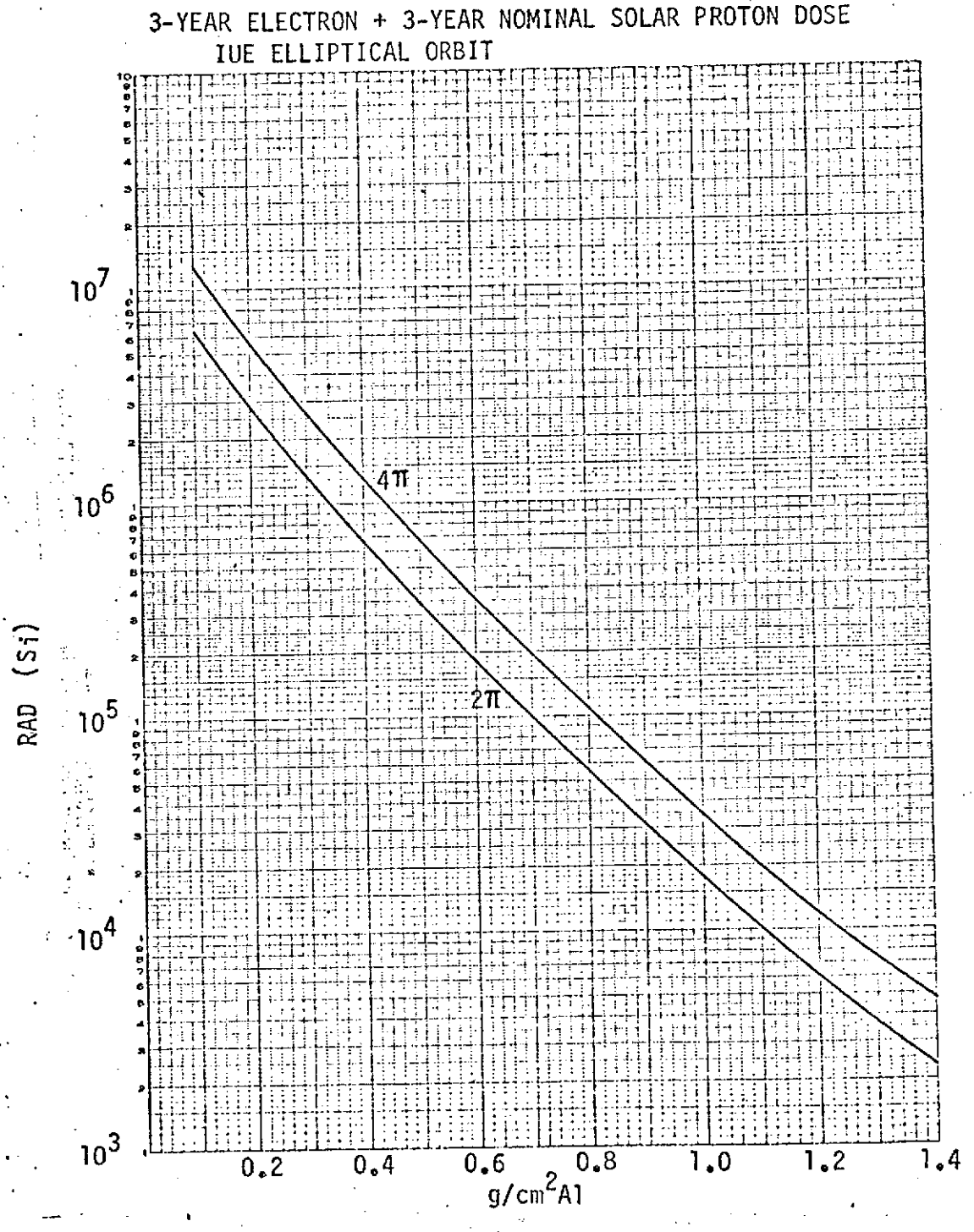

FIGURE 7-5 DOSE DEPTH PROFILE FOR ALUMINUM SHIELDING CALCULATIONS

7.2.2 (Continued)

at the dose point through one side only. The allowable dose for that side, 2.86 X 10^3 rad (Si), is one half the required internal environment, 5 X 10^5 rad (Si), increased by a small factor to account for the blocking rear octant previously discussed. Then, to obtain the additional shielding required, refer to the dose-depth curve for one-half the spherical values for a three-year mission, obtain an equivalent thickness of 0.57 g/cm^2 for 2.17 X 10^5 rad (Si), and a required thickness of 1.35 g/cm^2 for 2.86 X 10^3 rad (Si). Thus the additional shielding required for the inside is 0.78 g/cm^2 for an internal environment of 5 X 10^3 rad (Si). This value is converted to weight in the additional shielding column of Table 7-3. It is important to note that the required 0.78 g/cm^2 can be obtained in several ways (such as piece-part placements, consideration of existing flanges in an equipment stack, spot shielding, etc., other than simply adding a 115 mil aluminum plate. Consequently the given shield weight as herein calculated may be reducible in specific cases, while maintaining the required total shielding.

The procedure of obtaining an equivalent shield thickness of 0.57 g/cm^2 for the sum dose of 2.17 X 10^5 rad (Si) is permissible because the depth-dose profile is approximately linear, in the thickness region of interest, on semilog paper. Thus an additional shield slab on a component side will reduce the contribution at the dose from each shadow shield by the same proportion.

Reductions in shield weight as a result of connector cut-outs have been incorporated into the weight calculations.

TABLE 7-3 ADDITIONAL SHIELDING VHF TRANSPONDER NO. 1

COMPONENT/SIDE	EXISTING HOUSING THICKNESS MILS Al	ADDITIONAL SHIELDING, ALUMINUM							
		5×10^3 RAD(Si)				10^4 RAD(Si)			
		gm/cm^2	MILS Al	AREA (in^2)	WEIGHT(lb)	gm/cm^2	MILS Al	AREA(in^2)	WEIGHT(lb)
OUTSIDE	31	.928	135	22	.289	.803	115	22	.246
INSIDE	31	.779	115	22	.246	.654	95	22	.203
RIGHT	31	.928	135	40	.526	.803	115	40	.448
LEFT	31	.928	135	24	.315	.803	115	24	.269
TOP	31	.909	130	40	.51	.745	115	48	.45
BOTTOM	31	.587	85	40	.33	.461	65	48	.25
TOTAL					2.22				1.87

NO SOLID ANGLE SHIELDING FROM S BAND TRANSMITTERS IS ASSUMED

TABLE 7-3 ADDITIONAL SHIELDING VHF TRANSPONDER NO. 1 (CONTINUED)

COMPONENT/SIDE	EXISTING HOUSING THICKNESS MILS Al	ADDITIONAL SHIELDING, ALUMINUM							
		5×10^4 RAD(Si)							
		gm/cm^2	MILS Al	AREA (in^2)	WEIGHT(lb)	gm/cm^2	MILS Al	AREA(in^2)	WEIGHT(lb)
OUTSIDE*	31	.49	70	22	.150				
INSIDE	31	.35	50	22	.107				
RIGHT	31	.49	70	40	.273				
LEFT	31	.49	70	24	.164				
TOP	31	.48	70	40	.273				
BOTTOM	31	.15	20	40	.078				
TOTAL					1.045				

* NO SOLID ANGLE SHIELDING FROM S-BAND TRANSMITTERS IS ASSUMED

7.2.2 (Continued)

The remaining sides of the VHF Transponder were done similarly. Additional calculations were done for 10^4 rad (Si) and 5 X 10^4 rad (Si) of electron dose.

7.3 WEIGHT SUMMARY

Using the techniques of Section 7.2, the shield thicknesses for the remaining components and component stacks were calculated. The results are given in the Supplement to this report. The consequent shield weights are summarized in Table 7-4. These are values for aluminum. Section 7.1 provides data for conversion to other materials, if needed.

7.4 STREAMING

The extent of streaming of belt electrons through a small crack in the side of a box can be calculated using the solid-angle formula.

Defining the length of the crack as 2ℓ, the width of the crack as m, and the distance from the crack to the dose point as c, the solid angle of the crack is:

$$\Omega = 2 \tan^{-1} \left[\frac{m\ell}{c(m^2+\ell^2+c^2)^{\frac{1}{2}}} \right]$$

Assuming that the piece-part packages provide 0.21 g/cm^2 shielding, a transistor chip otherwise unshielded would receive 5 X 10^6 rad (Si) in three years. Then assuming that the piece-part is completely shielded by the housing except for the crack, the streaming dose D_s is found by:

TABLE 7-4 WEIGHT SUMMARY

SUBSYSTEM/COMPONENT	SUMMARY OF ADDITIONAL WEIGHT					
	$5x10^3$ RAD(Si)		10^4 RAD(Si)		$5x10^4$ RAD(Si)	
	COMPONENT WEIGHT	STACK WEIGHT	COMPONENT WEIGHT	STACK WEIGHT	COMPONENT WEIGHT	STACK WEIGHT
COMMUNICATIONS SUBSYSTEM:						
S BAND TRANSMITTER #1 (a)						
S BAND TRANSMITTER #2 (a)						
VHF TRANSPONDER #1 (a)	2.22		1.87		1.05	
VHF TRANSPONDER #2 (a)	2.2		1.86		1.04	
COMMAND SUBSYSTEM:						
COMMAND RELAY	2.10		1.79			
COMMAND DECODER #1	1.27		1.11			
COMMAND DECODER #2	1.97	5.3	1.71	4.6		
DATA HANDLING SUBSYSTEM:						
MULTIPLEXER:						
CONVERTER (PRIME)	0.80		0.64			
CONVERTER (BACKUP)	0.37		0.31			
DATAPLEXER(PRIME)	0.95		0.83			
DATAPLEXER(BACKUP)	0.95		0.84			
SUBPLEXER #1	0.51		0.44			
SUBPLEXER #2	0.51		0.45			
SUBPLEXER #3	0.85		0.75			
SUBPLEXER #4	0.85	5.8	0.75	5.0		

TABLE 7-4 WEIGHT SUMMARY (CONTINUED)

SUBSYSTEM/COMPONENT	SUMMARY OF ADDITIONAL WEIGHT					
	$5x10^3$ RAD(Si)		10^4 RAD(Si)		$5x10^4$ RAD(Si)	
	COMPONENT WEIGHT	STACK WEIGHT	COMPONENT WEIGHT	STACK WEIGHT	COMPONENT WEIGHT	STACK WEIGHT
COMPUTER:						
POWER CONVERTER #1 (a)	0.99		0.82		0.31	
POWER CONVERTER #2 (a)	0.53		0.46		0.25	
CPM #1 (c)	0.59		0.5		0.30	
CPM #2 (c)	1.44		1.22		0.74	
		3.6		3.0		1.8
MEMORY: (a)						
MEMORY #1 (a)	1.48		1.21		0.53	
MEMORY #2 (a)	1.06		0.90		0.50	
MEMORY #3 (a)	1.88		1.64		0.83	
		4.0		3.8		2.03
POWER SUBSYSTEM:						
POWER MODULES (2TOT) (a)	3.22		2.68		1.27	
MISSION ADAPTOR	3.57		3.09		—	
		6.97		5.77		
STABILIZATION & CONTROLS SUBSYSTEM:						
IRA SENSOR CAP						
IRA ELECTRONICS (b)	7.22		6.45			
NUTATION SENSOR ASSY:	NR					
CONTROL ELECTRONICS ASSY	4.02		3.50			
WHEEL DRIVE ASSY	1.42		1.11			

TABLE 7-4 WEIGHT SUMMARY (CONTINUED)

SUBSYSTEM/COMPONENT	SUMMARY OF ADDITIONAL WEIGHT					
	$5x10^3$ RAD(Si)		10^4 RAD(Si)		$5x10^4$ RAD(Si)	
	COMPONENT WEIGHT	STACK WEIGHT	COMPONENT WEIGHT	STACK WEIGHT	COMPONENT WEIGHT	STACK WEIGHT
SUN SENSORS AND PAS	N/R					
SUN SENSOR & PAS ELECTRONICS	2.72		2.40			
SCIENTIFIC INSTRUMENT SUBSYSTEM:						
EXP. MECH MOUNTED ELECTRONICS:					.16	
MODE SELECT MECH EL (a)			.24			
SHUTTER MECH EL (a)			.22		.12	
FOCUS MECH EL.						
EXPERIMENT ELECTRONICS ASSY	5.1		4.42			
CAMERA ELECTRONICS BOX	4.23		3.14			
ACQUISITION CHM (2 TOTAL)	1.85		1.51			
SPECTROGRAPH CHM (4 TOTAL)	3.84		3.12			
FES HM (a,b)	0.92		0.80		.55	
FES ELECTRONICS (b)	1.27		1.09			
SUN SHUTTER SENSOR						

NOTES:

(a) ALL BIPOLAR

(b) ASSUMES ZERO EXISTING HOUSING THICKNESS

(c) TTL ONLY

7.4 (Continued)

$$D_s = \frac{\Omega}{4\pi} \times 5 \times 10^6 \text{ rad (Si)}$$

The results are plotted in Figure 7-6.

This procedure overestimates the streaming dose, since the collimating effect of the crack is not considered. Also, the effect of the crack length is negligible nearby. However, it is evident that crack widths of 0.002 inches or less are desirable to keep the streaming dose to a fraction of the allowable internal environment.

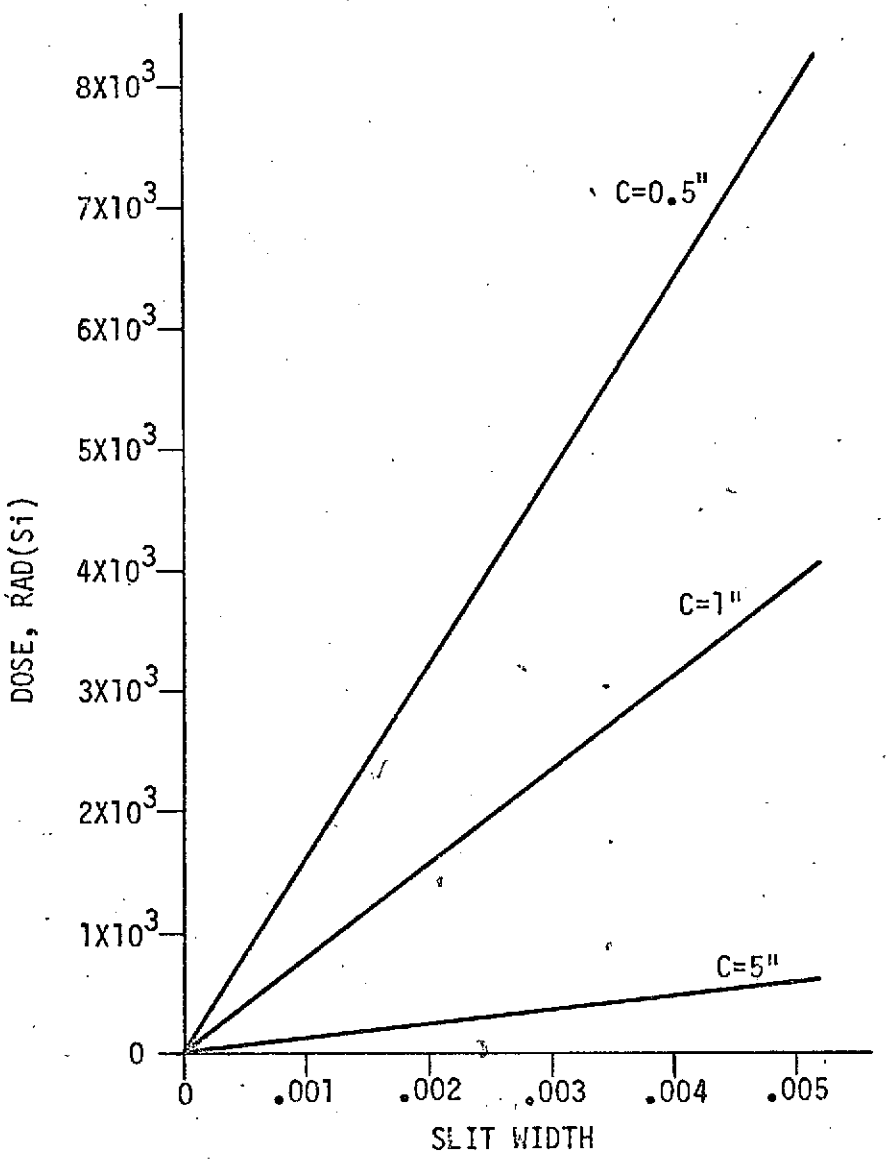

FIGURE 7-6 STREAMING DOSE IN THREE YEARS

8.0 SUMMARY AND CONCLUSIONS

8.1 PROGRAM SUMMARY

The energetic electrons and protons of the earth's radiation belts, and solar protons comprise the penetrating radiation environment of principal concern for the IUE spacecraft. This environment is sufficiently severe to cause a significant possibility of interference, degradation, or failure for unprotected or sensitive items. Hence, the IUE radiation and shielding study was conducted to assess radiation degradation on all IUE parts and materials, identify and plan necessary radiation tests, and determine shielding requirements for radiation sensitive parts and materials.

The inputs used for this program were the spacecraft description, design information, and trajectory definition. The following tasks were performed: the radiation environment levels were defined in terms suitable for vulnerability analysis; screening was performed to identify those materials and components that are not significantly degraded by the radiation environment; the remaining materials and components were analyzed in greater detail. The performance of detailed circuit analysis was not within the scope of this program.

The classes of items receiving emphasis were semiconductor devices, optical sensors, and materials. The IUE semiconductors were organized by subsystem and component into categories and problem areas identified. The optical sensors were analyzed for degradation of critical elements and interference. The IUE materials were classified by generic-material failure threshold and the application and location of the materials was examined to permit identification of problem areas.

8.1 (Continued)

The failure thresholds for generic categories of piece-parts and materials were used as a basis for the establishment of permissable internal-environment levels for the associated spacecraft component.

Potential exceptions to the categorization were defined to the extent possible.

The existing shielding was determined, and the additional shielding required to provide the required internal environment was calculated.

8.2 RESULTS

8.2.1 Materials Analysis

No materials (excluding optics) were considered significantly susceptible except for acrylics (adhesives), teflon, and the hydrazine tank diaphragm. The acrylics and teflon are considered possibly susceptible only if operated under a large, long-term mechanical load where cracking, separation, or crumbling could cause a critical failure. The hydrazine tank diaphragm is probably not susceptible, but its function is sufficiently critical to merit test if small changes in its parameters are important to its function. In addition, the heat dump resistor adhesive may merit testing in a radiation environment.

The absorptance of the metallized FEP teflon thermal blanket may increase to a value as large as 0.20. The hydrazine decomposition from radiation is small.

Severe darkening for several optical glasses has been reported for dose levels equivalent to that expected on IUE. Cerium stabilized

8.2.1 (Continued)

glasses are significantly less vulnerable. There is large variability in vulnerability between different compositions of glass. The specific glass composition in particular applications is not very accessible. In conjunction with the requirements for protection against interference in the optical sensors as well as darkening of the transmission optics, shielding may be required. Radiation tests of the particular glasses used in IUE will determine if the damage threshold for darkening is significantly above 10^4 rad (Si).

8.2.2 Semiconductor Analysis

The assessment of the IUE electronics is based on piece-parts vulnerability. Piece-part types have been categorized according to the types of construction which bear some relationship to their general response to radiation. Wide variability in radiation response within part types reduces accuracy of such a categorization. The intent of such a categorization is to permit establishment of reasonable lower limits on environment levels likely to cause failure for each piece-part category. Hence the categories of piece-parts used in particular system components provide the basis for setting reasonable values for the vulnerability threshold of those components.

Detailed circuit analysis to determine specific margins and electrical-failure criteria for each circuit application of the piece-parts is out of the scope of this analysis effort. This effort involved no test performance.

A "sure-safe" dose level for semiconductors would be less than 10^3 rad (Si). Such a level is impractical for IUE, particularly when the 95

8.2.2 (Continued)

percent solar proton dose is considered. However, only a small fraction of device types have such a low failure threshold.

The choice of the failure threshold of 10^4 rad (Si) for bipolar transistors, bipolar linear integrated circuits, and digital MOS integrated circuits is supported by the available data. However, a small but not negligible risk is taken by the assumption of this threshold level without the performance of at least sample radiation testing on the particular IUE device types in these categories.

Bipolar digital ICs of the general type used on IUE have failure thresholds in excess of 10^7 rad (Si).

The SCR and UJT devices require testing. Displacement damage (from protons) for the individual bipolar types has been predicted, and a few types are indicated for which damage may be significant.

Displacement damage is not considered to be significant for the remaining device categories for the IUE environment.

The LVDT (Linear Voltage Displacement Transducer), the Hall devices, and the Mechanism Electronics were examined. The Hall devices were not vulnerable. The existing LVDT structure was found to provide shielding to 10^4 rad (Si).

8.2.3 Sensor Analyses

Damage and interference effects were examined in the MgF2 window, the P11 phospher and the fiber optic window of the UV converter tube, the KCℓ target and window of the SEC vidicon for the spectrograph and acquisition cameras, and the Fine Error Sensor.

8.2.3 (Continued)

Essentially no damage is expected to the P11 phospher. The darkening in the MgF2 window without additional shielding is probably significant. Insufficient data was found to establish the dominant damage mechanism for the KCℓ target. The major source of interference was found to be Čerenkov radiation produced in the transmission optics. This interference is likely to be significant.

Tests to resolve the sensor radiation response uncertainties are recommended. A detailed test plan for the sensors was prepared. The results of the sensor tests will permit the design of appropriate shields and baffles for the sensors.

8.2.4 Other Spacecraft Experience

Spacecraft charging effects from space radiation have been shown to cause significant interference for certain spacecraft design configurations.

The S^3 MOSDAM experiment was analyzed to evaluate the possibility that long-term annealing may reduce the vulnerability of spacecraft electronics. However, the indications of annealing that were found are insufficiently large or consistent to permit annealing to be considered of significant benefit.

The COMSAT program was found to include a reasonably thorough radiation effects design and test approach.

8.2.5 Detailed Shielding Calculations

The method used to perform the shielding calculations for this study considers both the shielding provided by the immediately surrounding material and the shadowing provided by nearby objects, with suitable simplifying assumptions.

The failure thresholds for generic categories of piece-parts and materials were used as a basis for the establishment of permissable internal-environment levels for the associated component. The existing shielding was determined, and the additional shielding required to provide several different selected internal environments were calculated.

The dose depth profile used for the shielding calculations was the 3-year belt electron dose plus the 3-year nominal solar proton dose The additional shielding thicknesses were calculated for levels from this dose depth profile of 5×10^3 rad (Si), 10^4 rad (Si), and 5×10^4 rad (Si).

Shield thicknesses for each side of every component or component stack were calculated.

The shielding thicknesses corresponding to 5×10^3 rad (Si) dose are recommended for all system components except those for which specific data permits setting higher levels. This shielding level allows for a small additional bremsstrahlung dose and the possibility of solar proton dose in excess of the nominal level. Adding in bremsstrahlung and using the 95 percent proton dose, the total dose is $<10^4$ rad (Si). The semiconductor threshold has been established as $>10^4$ rad (Si).

8.2.5 (Continued)

An investigation of shield material choices was made, and aluminum was determined to be best for the recommended internal environment level. If decreased weight and consequent greater risk is necessary, sufficient data are provided to permit the choice of the optimum shield material for any desired internal environment.

The basic safety factors in the choice of an internal environment are: 1) the solar proton criteria is approximately a 95 percent upper limit; and is about three times a predicted mean value, 2) the possibility of long-term annealing of the semiconductor damage, and 3) slight conservatism in the shielding calculations as a result of using the spherical shielding values.

These safety factors are balanced by the significant possibilities of the existence of unusually radiation-sensitive components or small circuit design margins in critical applications which are undetected because of the limited scope of this study, as well as uncertainties in predicted belt environment levels.

The additional shielding thicknesses for 5×10^3 rad (Si) are in the neighborhood of 0.125-inch Al. If the shielding is done by adding shielding external to each component or component stack, the additional shield weight is approximately 60 pounds. Consequently, detailed consideration of specific piece-part vulnerability for particular applications, shielding provided by existing internal structure in components, and the addition of spot shielding are recommended to provide significant weight savings.

8.2.5 (Continued)

Calculations of the dose accumulated from electrons streaming through a narrow crack were made. The results indicate that tight tolerance must be maintained on mating surfaces of components in a component stack to preserve shielding integrity.

9.0 REFERENCES

1. System Design Report for International Ultraviolet Explorer, Goddard Space Flight Center, September 1973.

2. F. A. Carr, Impact of Eccentric Synchronous Orbit, Memo, Goddard Space Flight Center, May 1974.

3. G. Singley and J. Vette, The AE-4 Model of the Outer Radiation Zone Electron Environment, NSSDC 72-06, August 1972.

4. J. H. King, Solar Proton Fluences as Observed During 1966-1972 and as Predicted for 1977-1983 Space Missions, X-601-73-324, NASA Goddard Space Flight Center, October 1973.

5. S. B. Curtis, et al, Study of Radiation Hazards to Man on Extended Near Earth Missions, NASA CR-1469, 1969.

6. W. R. Webber, Sunspot Number and Solar Cosmic Ray Prediction for Cycle 20 (1965-1975) with Preliminary Estimates for Cycle 21, Boeing Document D2-113522-1, May 1967.

7. Introduction to Space Sciences, Second Edition, Edited by W. N. Hess and G. D. Mead, Gordon and Breach Science Publishers, New York (1968).

8. Paul Hahn, RSIC Computer Code Collection - Space Radiation Environment Shielding System (SPARES), CCC-148, AS-2807, ORNL RSIC, 1969.

9.0 (Continued)

9. E. G. Stassinopoulous and C. Z. Greychy, UNIFLUX: A Unified Orbital Flux Integration and Analysis System, to be published.

10. J. Baicker, et al, Applied Physics Letters, 2, 104, 1963.

11. John B. Rittenhouse and Jack B. Singletary, Space Materials Handbook, AFML-TR-68-205, July 1968.

12. J. F. Kircher and R. E. Bowman, Effects of Radiation on Materials and Components, Reinhold, N.Y., 1964.

13. Progress in Ceramic Science, V4. J. E. Burke, ed. Pergamon Press (1966).

14. J. H. Kleinpeter, W. J. Clare, Effects of Ionizing Radiation on Stabilized Photo Optics, Battelle N.W. Lab., Richmond, Washington. BNWL 1137 (Oct. 1969), N70-22768 3/14.

15. J. R. Webster, Radiation Effects on Fiber-Optic Light Guides, Optical Spectra, p. 59-61. Jly/Aug 1968.

16. J. E. Brady and T. R. Heaton, Radiation Problems Associated with Skylab, Martin-Marietta Corp., Denver Div., p. 748-755.

17. J. R. Malitson, M. J. Dodge, M. E. Gonshery, Effects of Space Radiations on Refractive Properties Optical Glasses, Proc. Ann. Corp. on Photographic Sci. & Engn. p. 75-77 (May 1966).

9.0 (Continued)

18. James B. Heaney, Suitability of Metalized FEP Teflon as a Spacecraft Thermal Control Surface, SAE/ASME/AIAA Life Support and Environmental Conference, July 12-14, 1971, San Francisco, Cal. (paper 71-Av-35)

19. TRW Systems Group, TRW Inc., Report Number 8526. 16-72-159, 28 Aug. 1972.

20. John Schutt, Chairman, Helios Qualification Committee, Memorandum, Jan 19, 1972.

21. Richard H. Hoffman, Spaceflight Performance of Silver Coated FEP Teflon as a Thermal Control Surface on the IMP-1 Spacecraft, Goddard Space Flight Center, Greenbelt, Md., Apr. 1974 (x-762-73-113).

22. J. F. Kircher, J. L. McFarling, et al., Final Report on Radiation Effects on Stored Liquid Propellants on Spacecraft with Auxiliary RTG or Nuclear Power Sources (Battelle, Columbus) NASA Contract NAS7-577, May 31, 1968.

23. J. F. Kircher, R. E. Best, J. E. Rollins, Final Report on Liquid Propellants (Battelle, Columbus) NASA Contract NAS7-722, February 2, 1970.

24. L. L. Hanks and D. J. Hamman, Radiation Effects Design Handbook, Section 1, "Semiconductor Diodes," NASA CR-1785, July 1971.

9.0 (Continued)

25. R. A. Burghard, and C. W. Gwyn, Radiation Failure Modes in CMOS Integrated Circuits, IEEE Transactions on Nuclear Science, Vol. NS-20, December 1973 pp. 300-5.

26. Hosea D. White, Jr. and Donald C. Lokerson, The Evolution of IMP Spacecraft MOSFET Data Systems, IEEE Transactions on Nuclear Science, Vol. NS-18 #1 pp. 233-6.

27. W. Schambeck, Effects of Ionizing Radiation on Low-Threshold CMOS Integrated Circuits, Presented at the IEEE Annual Conference on Nuclear and Space Radiation Effects, July 24-27, 1972.

28. W. J. Poch and A. G. Holmes-Siedle, The Long-Term Effects of Radiation on Complementary MOS Logic Networks, IEEE Transactions on Nuclear Science, Vol. NS-17 #6, December 1970, pp. 33-40.

29. Roy O. Lange, Space Radiation Challenges the MOSFET, IEEE Symposium on Electromagnetic Capability, Seattle, Wash., July 23-25, 1968. pp. 360-80.

30. D. Hampel and K. J. Prost, Transient Radiation Tests on RCA COS/MOS Circuits, RCA Digital Integrated Circuits Application Note ICAN-6604, September 1971, pp. 15-16.

31. V. Danchenko, Radiation Damage in MOS Integrated Circuits, Goddard Space Flight Center Report, X-711-71-410, Part I, September 1971.

9.0 (Continued)

32. Louis L. Sivo, Radiation Hardened MOS and CMOS Technology for Application in Military and Space Systems, Boeing Document D180-17911-1, January 1974.

33. D. H. Habing and B. D. Schafer, Room Temperature Annealing of Ionization - Induced Damage in CMOS Circuits, IEEE Transactions on Nuclear Science, Vol. NS-20, December 1973, pp. 307-13.

34. J. C. Rouanet, J. L. Giraud, Y. Gervais Lafond, Effects of 600 MeV Protons on M.O.S. Transistors, IEEE Transactions on Nuclear Science, Vol. NS-16 #5, pp. 106-8.

35. W. Poch and A. G. Holmes-Siedle, Permanent Radiation Effects in Complementary-Symmetry MOS Integrated Circuits, IEEE Transactions on Nuclear Science, Vol. NS-16, #6, December 1969, pp. 227-32.

36. K. H. Zaininger and A. G. Holmes-Siedle, A Survey of Radiation Effects in Metal-Insulator-Semiconductor Devices, RCA Review, June 1967, pp. 208-39.

37. G. Ezzard, Radiation Effects on COS/MOS Devices, RCA Digital Integrated Circuits Application Note ICAN-6604, September 1971, pp. 1-6.

38. V. Danchenko, Private Communication, NASA Goddard Space Flight Center. March 1974.

39. J. Novello, Radiation Test of RCA COS/MOS Logic for IUE Orbit, Memo: NASA Goddard Space Flight Center, June 1973.

9.0 (Continued)

40. W. E. Horne, Literature Search and Radiation Study on Electronic Parts, Final Report, JPL Contract #952565, May 1970.

41. D. J. Hamman, Space Radiation Effects in Integrated Circuits, IEEE Transactions on Nuclear Science, Vol. NS-13, #6, 1966.

42. W. E. Horne, Data Search for Information Pertaining to Low-Dose Turnon of SCR Devices in Gamma Environments, The Boeing Company, Memorandum 2-5372-0010-159, May 26, 1970.

43. P. P. Measel, Total Gamma Dose Effects on Several Types of Semiconductor Devices, The Boeing Company, Memorandum 2-7911-00-882, August 1967.

44. J. A. Folsum, unpublished research at The Boeing Company, 1969.

45. L. W. Aukerman, Electron Irradiation of Indium Arsenide, Phys. Rev., Volume 115, No. 5, P1133, September 1959.

46. R. R. Brown and W. E. Horne, Space Radiation Equivalence for Effects on Transistors, Final Report, NASA CR-814, July 1967.

47. J. B. Birks, The Theory and Practice of Scintillation Counting, N.Y., The MacMillan Co., 1964, p. 573-574.

48. E. Sonder and W. A. Sibley, Defect Creation by Radiation in Polar Crystals, in Defects in Solids Eds., J. H. Crawford and L. Slifkin, Plenum Press, N.Y., 1971.

9.0 (Continued)

49. W. A. Sibley, Radiation Damage in Oxides and Other Materials, IEEE Transactions on Nuclear Science, N.Y., 18, #6, P273-80, December 1971.

50. W. A. Sibley, IEEE Transactions on Nuclear Science NS-18, No. 6, P273-80, December 1971.

51. J. L. Kolopus, J. T. Lewis, W. P. Unruh and L. G. Nelson, J. Phys, C (London) 4 3007-14 December 1971.

52. M. R. Buckton and D. J. Pooley, Phys. (London) 5 1553-62, July 1972.

53. W. P. Unruh, L. G. Nelson, J. T. Lewis and J. L. Kolopus, J. Phys. C (London) 4 2992-3006, December 1971.

54. H. E. Swanson, et al, NBS Circular,539, P.33, 1955.

55. D. F. Heath and P. A. Sacher, App. Opt. 5 937-43, June 1966.

56. G. Hass and W. R. Hunter, App. Opt. 9 2101-7, September 1970.

57. P. A. Sacher, Report No. X-622-67-416, p.3, Goddard Space Center.

58. J. B. Birks, The Theory on Practice of Scintillation Counting, The MacMillan Company, New York, 1964.

59. Paul A. Sacher, Report X-622-67-416, p.3, Goddard Space Flight Center, August 1967.

9.0 (Continued)

60. W. E. Mott and R. B. Sutton, Scintillation and Cerenkov Counters, Handbuch Per Physik, Volume 45, Springer Verlag, 1958.

61. I. N. Krishnan and T. M. Chen, Solid State Electronics, 16, pp. 1233-40 (1973).

62. R. W. Fredricks and F. L. Scarf, Observations of Spacecraft Charging Effects in Energetic Plasma Regions, Photon and Particle Interactions with Surfaces in Space, p. 277-308, D. Reidel Co., 1973.

63. H. E. Wannemacher and R. G. Martin, Space Radiation Effects on MOSFETS from Circuits Flown on S^3 (1971-96A-SSS-1), Informal Memo, NASA Goddard.

64. V. Danchenko, Radiation Damage in MOS Integrated Circuits, Part I, G. S. F. C. X-711-71-410, September 1971.

65. R. A. Burghard and C. W. Cwyn, Radiation Failure Modes in CMOS Integrated Circuits, IEEE Transactions on Nuclear Science, NS-20, 300, December 1973.

66. E. E. King, et al., The Effects of Ionizing Radiation on Various CMOS Integrated Circuit Structures, IEEE Transactions on Nuclear Science, NS-19.

67. W. Schambeck, Effects of Ionizing Radiation on Low Threshold CMOS Integrated Circuits, Presented at IEEE Conf. on Nuclear Space Physics, July 1973.

9.0 (Continued)

68. W. Poch and A. G. Holmes-Siedle, Permanent Radiation Effects in Complementary-Symmetry MOS Integrated Circuits, IEEE Transactions on Nuclear Science, NS-16, 227, December 1969.

69. Recent, as yet unreported data by R. A. Burghard of Sandia, April 1974.

70. Private Communication, D. Lokerson to L. Sivo, April 17, 1974.